The Internet of Humans: Optimal Resource Allocation and Wireless Channel Prediction

Yizhou Yang

A thesis submitted for the degree of

Doctor of Philosophy

The Australian National University

May 2021

© by Yizhou Yang 2020

All Rights Reserved

Except where otherwise indicated, this thesis is my own original work. This thesis has not been submitted by me in whole or part for a degree or diploma in any university or other tertiary education institution. The content of this thesis is mainly based on my publications listed below:

- **Y. Yang**, D. Smith, "Wireless body area networks: Energy-efficient, provably socially-efficient, transmit power control," *2017 IEEE International Conference on Communications (ICC)*, Paris, 2017, pp. 1-6.

- **Y. Yang**, D. B. Smith and S. Seneviratne, "Deep Learning Channel Prediction for Transmit Power Control in Wireless Body Area Networks," *ICC 2019 - 2019 IEEE International Conference on Communications (ICC)*, Shanghai, China, 2019, pp. 1-6.

- **Y. Yang**, D. Smith, "Robust wireless body area networks coexistence: A game theoretic approach to time-division MAC," *arXiv preprint arXiv:1808.10094*.

- **Y. Yang**, D. Smith, J. Rajasegaran, S. Seneviratne, "Power Control for Body Area Networks: Accurate Channel Prediction by Lightweight Deep Learning," *IEEE Internet of Things Journal*, 2020

- **Y. Yang**, D. Smith, "A Game-Theoretic Approach to Joint PHY/MAC Resource Allocation in Body Area Networks," *IEEE Journal of Biomedical and Health Informatics*, (under review)

- **Y. Yang**, D. Smith, "Towards Explainable AI for Body Area Networks: A Parametric Analysis of Deep Learning Enabled Channel Prediction," *IEEE Transactions on Wireless Communications*, (in preparation)

Yizhou Yang

7 May 2021

To my beloved parents, Chunhong and Mingjie.

Acknowledgments

I would like to extend my greatest appreciation to each of the following people for their great help and assistance throughout my PhD study. Firstly, I would like to thank Dr David Smith, my esteemed supervisor, for his invaluable supervision, support, patience and understanding over the past years, who has been keeping supportive, while allowing me the freedom and respect to pursue various new ideas. Without his scientific advice, endorsement and insightful advice, it would not have been possible for me to complete this thesis. I am also grateful to my Chair of Panel Dr Xiangyun Zhou from Australian National University (ANU), whose support means a lot to me. Especially, his help in my research schedules and many administrative issues is greatly appreciated. I also would like to express my thanks to my advisor Dr Leif Hanlen, a few words from whom could always bring me back to the correct path.

It is my great fortune to have had a chance to collaborate with Dr Suranga Seneviratne, who is always inspiring and informative. I would also like to express my deep appreciation to my dearest colleagues and friends at ANU/-Data 61, especially Samiya, Hongtao, Yan, Tong and Weixuan, for their encouragement and support. Further, my gratitude extend to my lovely friends: Maoyuan, Shaobai, Tao, Xiaoyu, Yuan, Zhengkun and ZiAng, who are greatly supportive and understanding. Particularly, I would like to thank Yue Cao. Time, as always, marches on, but it is a true blessing to once have had you stay with me in my joys and sorrows. At last, I would like to deliver my im-

measurable gratitude to my parents for their dear fostering to shape my life with optimism and passion by always offering me the best of them, including their unconditional love, rock steady support and understanding. Despite difficulties in life, they have always directed me to get ahead and not give up.

Abstract

Recent advances in information and communications technologies (ICT) have accelerated the realization of the Internet of Humans (IoH). Among the many IoH applications, Wireless Body Area Networks (BANs) are a remarkable solution that are revolutionising the health care industry. However, many challenges must be addressed, including: a) unavoidable inter-BAN interference severely degrading system performance. b) The non-stationarity and atypical dynamics of BAN channels make it extremely challenging to apply predictive transmit power control that improves the energy efficiency of the network. In this context, this thesis investigates the use of intelligent and adaptive resource allocation algorithms and effective channel prediction to achieve reliable, energy-efficient communications in BAN-enabled IoH.

Firstly, we investigate the problem of co-channel interference amongst co-existing BANs by proposing a socially optimal finite repeated non-cooperative transmit power control game. The proposed method improves throughput, reduces overall power consumption and suppress interference. The game is shown to have a unique Nash equilibrium. We also prove that the aggregate outcome of the game is socially efficient across all players at the unique Nash equilibrium, given reasonable constraints for both static and slowly time-varying channels.

Secondly, we address the problem of overlapping transmissions among non-coordinated BANs with multiple access schemes through intelligent link resource allocation methods. We present two non-cooperative games, employed with a time-division multiple access (TDMA) based MAC layer scheme

that has a novel back-off mechanism. The Link Adaptation game jointly adjusts the sensor node's transmit power and data rate, which provides robust transmission under strong inter-BAN interference. Moreover, by adaptively tuning contention windows size an alternative game, namely a Contention Window game is developed, which significantly reduces latency. The uniqueness and existence of the games' Nash Equilibrium (NE) over the action space are proved using discrete concavity. The NE solution is further analysed and shown to be socially efficient.

Motivated by the emergence of deep learning technology, we address the challenge of long-term channel predictions in BANs by using neural networks. Specifically, we propose Long Short-term Memory (LSTM)-based neural network (NN) prediction methods that provide long-term accurate channel gain prediction of up to 2s over non-stationary BAN on-body channels. An incremental learning scheme, which provides continuous and robust predictions, is also developed. We also propose a lightweight NN predictor, namely 'LiteLSTM', that has a compact structure and higher computational efficiency. When implemented on hand-held devices, 'LiteLSTM' remains functional with comparable performance.

Finally, we explore the theoretical connections between BAN on-body channels' characteristics and the performance of NN-based power control. To analyse wide-sense stationarity (WSS) characteristics, different stationarity tests are performed for a range of window lengths for on-body channels. Following from this, we develop test benches for NN-based methods at corresponding window lengths using empirical channel measurements. It is observed that WSS characteristics of the BAN on-body channels have a significant impact on the performance of NN-based methods.

Contents

List of Figures

List of Tables

Chapter 1

Introduction

1.1 Motivation and Scope

In recent years, the phenomenon of an ageing population is creating a significant impact on the socio-economic structure of society [1], which challenges the current healthcare system. This raises an ever-growing need for sustainable solutions to support health promotion and illness prevention throughout life spans, especially in old age.

Internet of Things (IoT) is emerging as an effective tool to aid this socio-technical struggle [2]. The IoT market for healthcare is poised to grow 56% each year through 2019 [3], reaching $15 billion from $4 billion in 2014 [4]. According to PwC [5], 86% clinicians believe that such mobile technology will become important to physicians for patient health management over the next few years. Many see IoT as key factors in reducing the cost and increasing the reach of healthcare [6, 2], which contributes to the development of a more human-centric Internet, namely the Internet of Humans (IoH). With the recent advances made in wireless and electronics technology, IoH promises to increase not only the quality of healthcare but also patient accessibility, while achieving all this at a lower cost per patient.

To achieve this, it is important for IoH to have the capability of collection and optimisation of physiological data from sensors placed on humans, gen-

erally with wearable technology. As wearable technologies advance for the monitoring of human health, recently envisioned Wireless Body Area Networks (BANs) have great potential for continuous patient monitoring in ambulatory settings as well as for the early detection of abnormal conditions and supervised rehabilitation. The applications of BANs span a wide area, such as remote medical systems, ubiquitous healthcare, sport, fitness, entertainment, and the military [7].

Meanwhile, to support a variety of applications, excellent Quality of Service is required in terms of reliability, data rate, latency and energy consumption, etc.. BAN nodes may operate on non-rechargeable batteries of small size and low-power capacity for several months or even few years, in particular, for those nodes implanted in the human body. Thus, limited by the size of the battery and also specific absorption rate (SAR), the transmission power consumption are stringently restricted [8]. Mobility also has to be supported as the nodes are positioned on different parts of the body that move with regard to each other. Nonetheless, with a rapid increase in active devices, when a large number of sensors of different BANs coexisting in close proximity access the same channel at the same time BANs will suffer unavoidable inter-BAN interference due to no central coordinator amongst networks [7]. To address these issues, it is very important to distribute the limited radio resources in an optimised manner to support the Quality of Service (QoS) requirement of varies IoH applications. Although most resource allocation schemes mainly focus on Medium Access Control (MAC) layer, cross-layered methods need to be investigated for more effective operations.

At the same time, given the complicated deployment environments and peculiar channel characteristics with relatively large path loss in BAN chan-

nels [9, 10], it is more challenging to maintain robust transmission under dynamic BAN scenarios, which is the focus of this thesis. Previous studies [11] reveal that accurate prediction of the future wireless channel status can benefit the performance of power control schemes, even when prediction accuracy is low. The dynamic behaviour of BAN wireless channels poses the challenge to forecasting tasks using traditional prediction methods, such as [12] or computational intelligence methodologies such as artificial neural networks (ANN) and machine learning methods [13]. To address such challenges, recurrent neural networks (RNN) that have been used in various prediction tasks [14] will be exploited to provide better performance in BAN channel predictions. Meanwhile, due to the high complexity of neural networks (NN), it is often very challenging to interpret their action and results. It is because, although neural networks are parametric, the large number of parameters inside such networks makes them nearly non-parametric, such that the link between the input and the results are hard to model. This is the main reason why neural networks are always considered as "black boxes". Therefore, characterisation and modelling of the non-stationarity of BAN channel is important to support autonomous predictive resource allocation for future BAN .

1.2 Hypothesis, Key Research Questions and Answers

The summarised research challenges for BANs in IoH leads to the following hypothesis and key research questions that are answered by this thesis:

How can resource allocation be performed in a self-adaptive and intelligent manner to accurately predict BAN channel dynamics — in order to achieve reliable, energy-efficient and scalable communications — for BAN enabled IoH applications.

In this context, this thesis aims to answer the following questions:

Q1 How can game-theoretic transmit power control improve the overall QoS of the system while guaranteeing social optimal outcomes from best responses of co-existing players/networks?

Q2 How can the limited radio resources among co-existing BANs be allocated autonomously and intelligently to improve uncoordinated communications?

Q3 What are the benefits of using adaptive cross-layer optimisation approaches in inter-BAN interference management? Are they able to maintain high social efficiency?

Q4 How to solve the long-existing challenge in long-term channel prediction for BAN channels in order to further increase energy efficiency?

Q5 How much performance improvement does NN based predictive transmit power control provide compared with traditional methods?

Q6 Is it feasible to implement NN based methods on a mobile device without compromising computational complexity?

Q7 To what extent do the non-stationary, shadow fading radio channels affect the performance of the NN predictor?

The research work to be presented in this thesis answers these questions. In summary, the proposed work provides improved energy efficiency, mitigated co-channel interference, accurate channel prediction and optimised radio resource allocation for BAN applications in realistic scenarios as shown in Figure 1.1. The performance of proposed solutions is evaluated using empirical BAN channel measurements, with experimental analysis. In brief, to be fully described in the remainder of this thesis, the research questions are answered as follows:

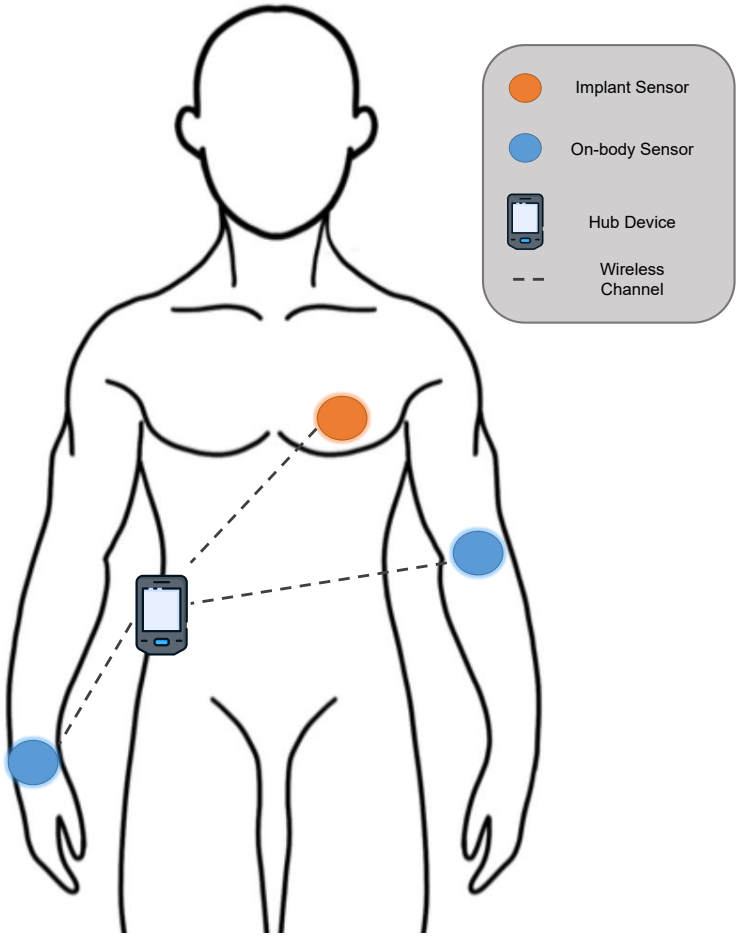

Figure 1.1: A BAN system with on-body and implanted sensors

- The socially optimal non-cooperative game-based method with a novel utility function suppresses interference level and improve energy efficiency. Evaluated by using a realistic channel model, the game is shown to be very energy-efficient, significantly reducing power consumption and improving packet delivery ratio (PDR) with respect to other potential schemes, consuming 67% less circuit power than transmitting constantly at 0 dBm.

- Cross-layered adaptive optimisation methods not only improve the energy efficiency of BAN communication in realistic scenarios but also provide higher QoS, in terms of latency, PDR and throughput.

- A long-term on-body channel prediction method based on LSTM networks is presented, which can provide up to 2s ahead BAN channel prediction. It is an incremental learning scheme, where the NN model is fine-tuned in each training episode via recent channel samples. This allows the NN model to capture the dynamics of streaming data and make robust predictions

- When the predicted channel gain is applied with transmit power control and compared with traditional methods, the circuit power consumption of BAN is reduced by up to 45% and the reliability of communications is increased by nearly 50%.

- With reduced computational complexity, it is feasible for 'LiteLSTM' to conduct training in an online manner when implemented on hand-held devices. Meanwhile, the performance degradation is relatively small.

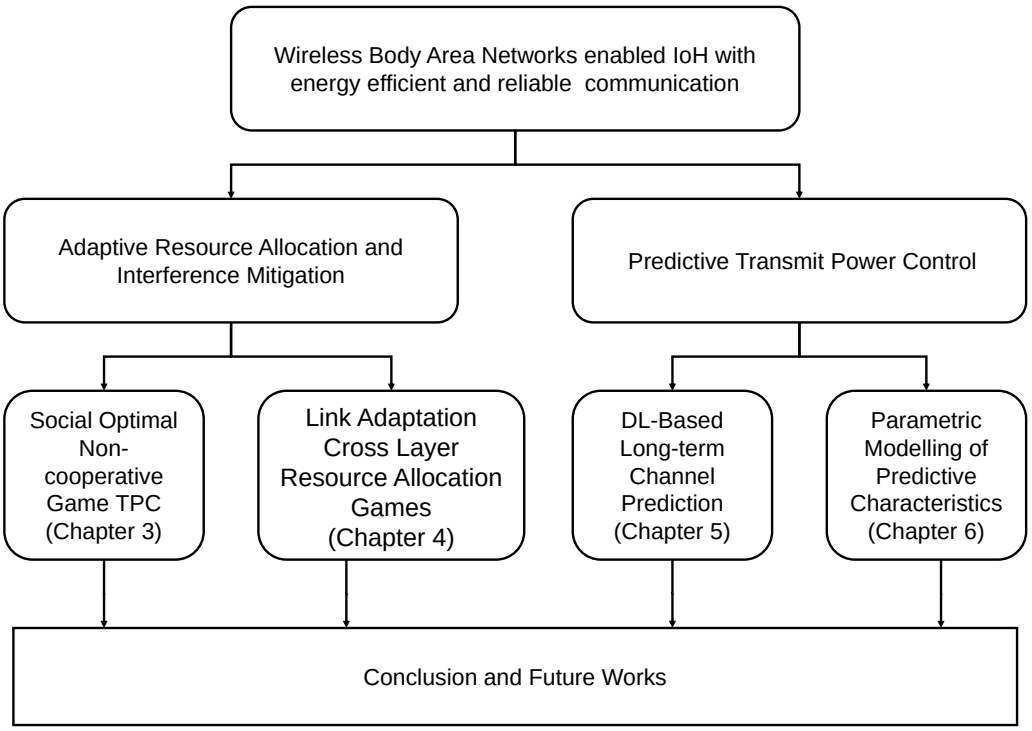

Figure 1.2: Thesis's Outline

1.3 Thesis Outline

The technical contributions of this thesis are detailed in four chapters, which address the hypothesis outlined above. The structure of these chapters is summarised in Figure 1.2.

Chapter 2: Chapter 2 presents a literature reviewdetailing relevant research to this thesis. Current issues and challenges in BANs are analysed and addressed. Related prior standards for BANs are firstly reviewed. Up-to-date comparative studies are presented of relevant literature to this thesis including literature on interference mitigation schemes, transmit power control (TPC) and channel prediction.

Chapter 3: In this chapter, we propose a socially optimal finite repeated non-cooperative transmit power control game, in order to mitigate radio interference amongst coexisting BANs, improve throughput and reduce power consumption. The game is shown to have a unique Nash equilibrium. When reasonable constraints are given, it is proven that the outcome of the game is socially efficient across all players at the unique Nash equilibrium. Using a realistic channel model, the game is shown to outperforms other methods. The key results are listed as follows:

- Compared with 0 dBm constant transmit power SOG has 3% greater probability that PDR can reach the target of 0.9 with 23 dB less transmit power.

- The proposed method is extremely energy efficient by significantly reducing circuit power usage, consuming 17% less circuit power than Sample-and-Hold and 67% less than constant transmission at 0 dBm.

Chapter 4: To achieve smart-resources allocation among coexisting BANs, two novel non-cooperative games are proposed that jointly adjust the BAN sensor node's transmit power and data rate, employed with a time-division multiple access (TDMA) based MAC layer scheme that has a novel back-off mechanism. The link adaptation game (LAG) tuning the transmit power and the data rate at the same time using a non-cooperative game. Another game namely contention window game (CWG) that adaptively tunes contention windows size as an alternative game solution is also developed, which significantly reduces the latency.

The uniqueness and existence of the games' Nash Equilibrium (NE) over the action space are proven using discrete concavity. Both proposed games

provide robust transmission under strong inter-BAN interference, but are demonstrated to be applicable to different scenarios, and shown to be socially efficient.

Chapter 5: In Chapter 5, neural networks that are the backbone of deep learning (DL) are used to make long-term BAN on-body channel prediction to optimise radio resource allocation in terms of transmit power. A realistic test bench demonstrates that the proposed long short term memory (LSTM) based channel predictor provide higher accuracy compared with traditional prediction methods. The incremental learning scheme is also introduced to guarantee the robustness of the predictor. In addition, in order to suit the needs of mobile implementation for typical BAN use case scenarios, a light-weighted DL predictor namely 'LiteLSTM' is developed from the original LSTM channel predictor. 'LiteLSTM' significantly reduces the computational costs and maintaing similar prediction accuracy. Most importantly, due to the reduced complexity, the incremental learning scheme is supported when 'LiteLSTM' is implemented on mobile hand-sets. The key outcomes with experimental measurements are as follows:

- The proposed LSTM predictor provided ups to 2s of channel prediction ahead with 50% NMSE reduction compared to the benchmark.

- When mapped to a suitable power control algorithm, LSTM-based methods provide noticeable improvements in reliability (achieving 1.2% outage reduction on average) and power consumption (up to 25% circuit power saving) in comparison to other predictive power control methods.

- With respect to the number of time steps T, 'LiteLSTM' is considered

to be linear in time. Therefore theoretically, compared with traditional methods, the overhead of 'LiteLSTM' is not significantly increased.

Chapter 6: The novel application of DL methods in BAN channel resource allocation raises the challenge how to interpret their operation and outcomes. Therefore, in this chapter, we address the relationship between the characteristics of the BAN channels and the performance of the DL channel predictor. Using the null hypothesis significance testing (NHTS), the predictability attributes of the BAN channels are characterised in terms of the probability of stationarity then extended to the concept of Wide Sense Stationary (WSS). By parametric modelling via extensive experiments, the relationship between the performance metric of 'LiteLSTM' and on-body BAN channels is analysed.

Chapter 7: The final chapter provides some concluding remarks upon the findings of this thesis, as well as providing some possible directions for future research.

Chapter 2

Background and Related Work

In recent years, the world has seen continued rapid growth in the number of elderly persons. According to [15], nowadays, 8.5 % of people worldwide are at least 65 years old, which is expected to balloon to nearly 17 percent by 2050 — 1.6 billion people over 65 by 2050. In Australia, according to the Australian Institute of Health and Welfare, the Australian population is ageing, with older Australians a growing proportion of the total population [16]. In 2017, 15% of Australians (3.8 million) were aged 65 and over; this proportion is projected to grow steadily over the coming decades. Meanwhile, traditional health-care system is inefficient in dealing with chronic diseases [17]. As a result, the ageing population has led to a dramatic rise in demand for health-care services, as the health of older persons typically deteriorates with increasing age. Motivated by the social goals of achieving better health care at lower costs, IoH will revolutionize medical practice in the future.

In this chapter, firstly the current standards are introduced. Then the state-of-art of interference mitigation schemes, transmit power controls and BAN radio resource allocation are discussed. Lastly, the learning-based channel prediction studies are reviewed, as learning techniques haven't been largely used in wireless body-area communication.

2.1 BAN Standards:

For a successful realization of any BAN that is able to address the requirements of IoH applications, it is important to provide communications which is not yet fully described by existing wireless standards. The aim of BAN enabled IoH technology is to provide a broad range of data rates at much lower power consumption than current standards. However, most established standards are designed to cover much lager distances. With the explicit assumption of covering only a relatively small distance around the human body, BAN standards should provide a broad range of data rates at much lower power consumption than current standards. Some standards have been adapted for healthcare applications like Bluetooth (IEEE 802.15.1) [18] or ZigBee (IEEE 802.15.4) [19] protocols etc.. Although theses standards are well documented and have been adopted for commercialized applications, they are mainly designed for networks flexible topologies and larger communication ranges.

2.1.1 IEEE 802.15.6 Standard

In 2007, IEEE 802.15.6 ((IEEE 802.15 Task Group 6 [20]) was proposed to support a wide range of data rates, to consume less energy, and to provide reliable BAN communication surrounding the human body, and it was completed and published in 2012. Frequency bands in BANs have to comply with applicable medical and communication regulatory authorities. The IEEE 802.15.6 provides an overview of the frequency band regulation for BANs as shown in Figure 2.1. The Medical Implant Communications Service (MICS) band is a licensed band used for implant communication and has the same frequency range (402-405 MHz) in most countries. Wireless Medical Teleme-

try Services (WMTS) is a licensed band used for medical telemetry system. Both MICS and WMTS bandwidths do not support high data rate applications. The Industrial, Scientific and Medical (ISM) band supports high data rate applications and is available worldwide. However, there are high chances of interference as many wireless devices including IEEE 802.1 and IEEE 802.15.4 operate at ISM band. Detailed descriptions of MAC and PHY layers specification of BAN application are provided in IEEE 802.15.6. The basic requirements of IEEE 802.15.6 are summarizes as follows:

- Bit rates in the range of 10 kBps to 10 MBps should be supported via the BAN links.
- Packet Delivery Rate (PDR) should be larger than 90% for a 256 octet payload for more than 95% of the best-performing links.
- Up to 256 nodes should be supported by each BAN.
- Reliability, jitter and latency should be supported for specific BAN applications. For instance, medical applications and non-medical of BANs require latency to be less than 125 ms and less than 250 ms, respectively; whilst jitter should be less than 50 ms;
- BAN nodes should allow reliable communication in case of mobility scenarios for both on-body and in-body communications.
- Up to 10 randomly distributed co-located BAN networks should be supported in a $6 \times 6\text{m}^2$ area.

Apart from the IEEE standard, other popular standards are also introduced in this section, such as "SmartBAN", Bluetooth Low Energy (BLE) and etc., which will be summarized as follows.

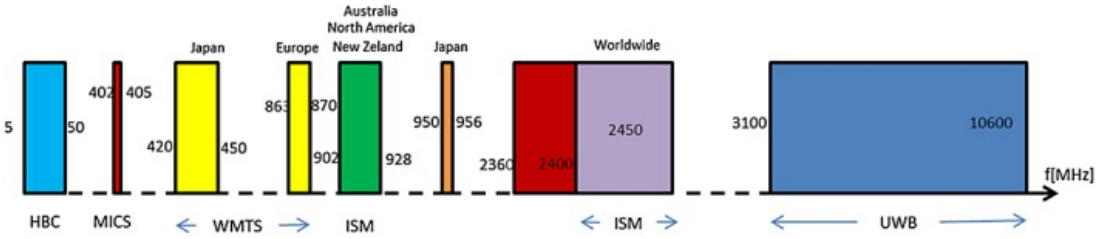

Figure 2.1: Available bands for BAN in different country/regions

2.1.2 "SmartBan" Standard

Recently, European Telecommunication Standards Institute Technical Committee (ETSI TC) drafted a new standard for BAN applications – namely "SmartBAN" [21]. The goal of the "SmartBAN" is to define a standard for low power devices and networks to be used in short range links supporting, e.g., healthcare, wellness and sport relating BAN applications operating around a human body. Both on-body links and links to implanted devices are supported. The system architecture of "SmartBAN" is shown in Figure 2.2. The concept of "SmartBAN" is based on the heterogeneous multi-radio approach. Within this end-to-end system, "SmartBAN" devices is allowed to be connected by using other existing radio standards, e.g., Bluetooth, Zigbee, BLE and etc.. Since the hub/master can act as a relay or bridge between devices operating with different radio standards.

Compared with IEEE 802.15.6, "SmartBAN" specifies low-power, low-complexity PHY and MAC layers with lighter data presentation formats. Two different channels: the control channel and the data channel are used in "SmartBAN". The hub/master transmits control beacons that contains network parameters using the control channel, and management and control transmissions occupy the data channel. This mechanism provides fast chan-

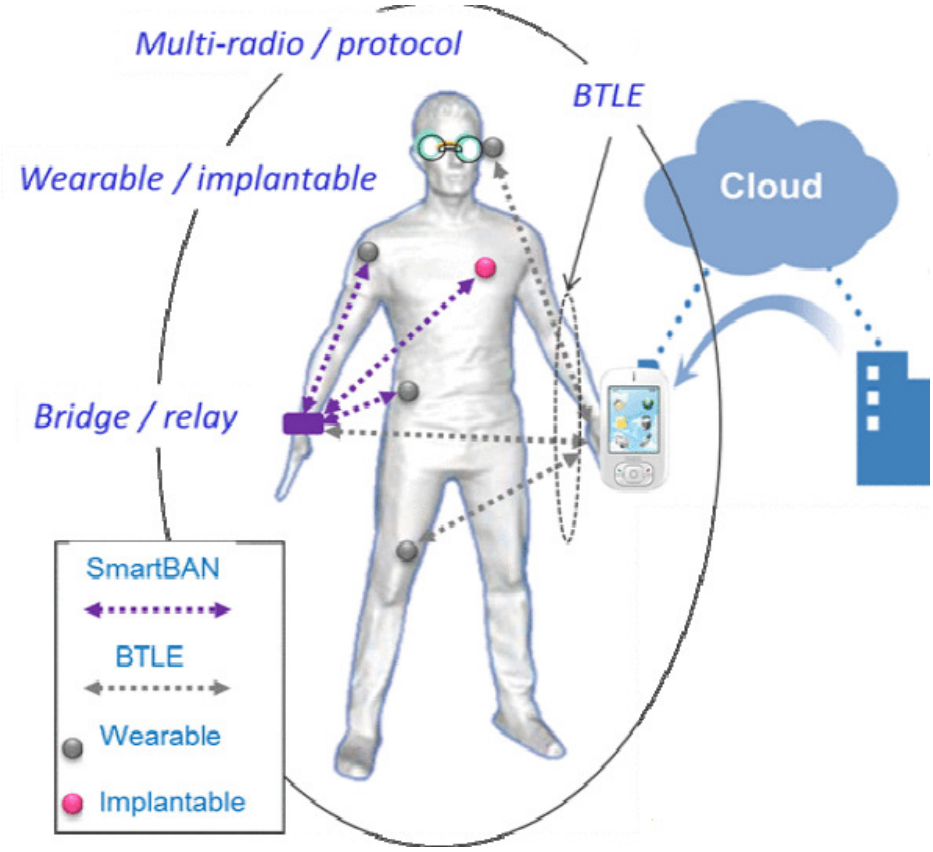

Figure 2.2: System architecture of "SmartBAN"

nel acquisition and easy hub to hub communication, which increase the usability of the network [22].

2.1.3 Bluetooth Low Energy:

Bluetooth Low Energy (BLE) is the main feature introduced by the Bluetooth 4.0 specification, which supports both the legacy BR/EDR (Basic Rate/Enhanced Data Rate) controller and the new LE (Low Energy) controller. BLE has a different topology to Bluetooth. The typical topology of Bluetooth is illustrated in Figure 2.3. BLE network (which is called a piconet) is composed of one master and one or more slaves, and is based on a star topology.

Each slaves communicate on a separate physical channel with the hub/-

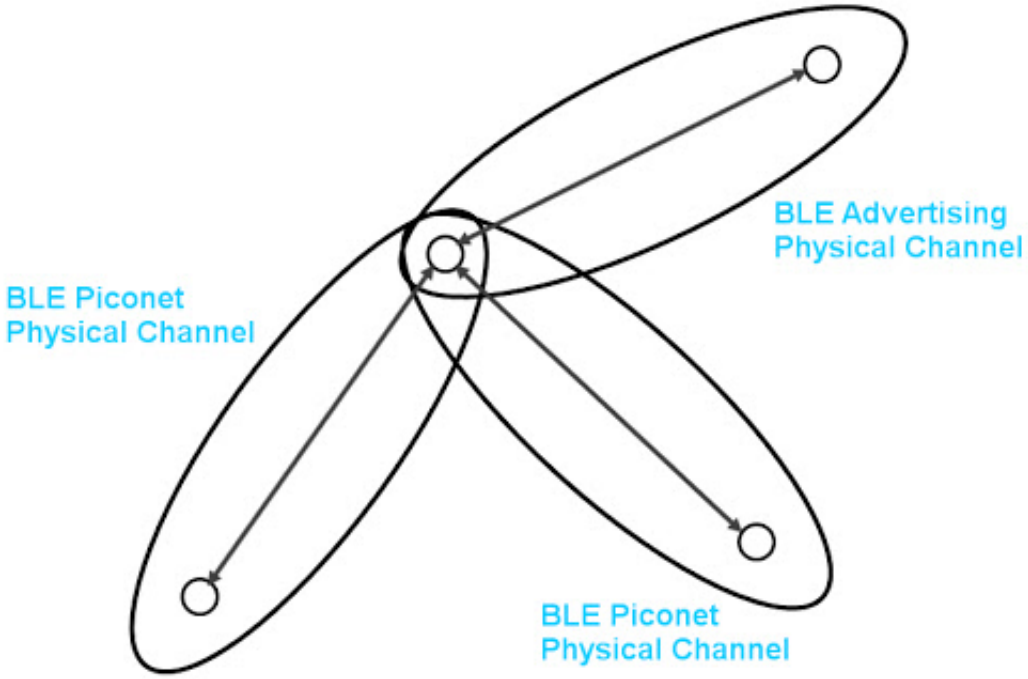

Figure 2.3: Bluetooth LE Star-bus Topology

master. Unlike a classic Bluetooth network/piconet, where all slaves listen for incoming connections and therefore need to be on constant standby, a BLE slave invites connections and so is in total control of when to consume power. The Bluetooth LE enables dual-mode implementations to reuse the Bluetooth RF part and to guarantee ultra low power consumption for devices with embedded stand-alone implementation of the Bluetooth LE specification. The Bluetooth LE has a physical layer bit rate of 1 Mbps and may achieve a link distance of around 10 meters. Bluetooth LE consumes only 10% of the power consumed by Bluetooth. It can save energy and extend battery life by sleeping and waking up when it needs to send data.

2.2 Existing Issues:

This section identifies current existing challenges that hinder the development of BAN in IoH scenarios.

2.2.1 Mobility:

Different from other RF-based Wireless Sensor Networks, BAN sensors are either placed on the human body or implanted in the human body. Thus the body movement and change in human posture exhibit high mobility in sensor nodes. This may bring the shadowing effect that makes the wireless channel between the sensor nodes and the hub to suffer considerably in a highly variable way [23]. Despite this, RF is the only practical communication solution for future BAN-based IoH, as the non-RF communication– Human Body Communication– has relatively low communication range [24]. However, in order to maintain stable connectivity under high mobility, extra transmit power is used by battery-constrained BAN sensors, which raises a critical problem in energy management. Most importantly, as a simple postural change may lead to a long period of outage, such mobility can therefore bring life-threatening risks to human wearers.

2.2.2 Power Constraints:

For BAN enabled IoH applications, sensors are used to monitor or control medical conditions of the human wearer, such as diabetes, coronary care, etc.. However, one of the crucial issues in using these sensors is the battery lifetime [25]. Because **a)** the longevity of a BAN depends heavily on the battery life cycle of the sensors nodes, **b)** and the battery sizes should be small to guarantee

miniature size of the sensors. Moreover, without employing complicate medical procedures, the in-body sensor battery can not be replaced or recharged. Therefore, it is expected that the lifespan of a battery powered sensor should last for 10 to 15 years. Such requirement places a strict energy constraint on BAN networks, as the sensor should limits its power consumption but also maintain a long duration of operation with high connectivity.

2.2.3 Network Coexisting:

As one of the narrowband carrier frequencies for BAN (IEEE 802.15.6 [20]), the ISM unlicensed band is much more crowded because of legacy use by various communication systems, e.g. WiFi hubs, Bluetooth-enabled devices, cordless phones. As Forbes predicted, the market size of smart wearable device will be doubled by 2022, with more than 233 million unit sales [26]. The number of people using wireless sensors device will also be surging [4], thus the co-existence of different wireless systems is more likely to become unavoidable. Meanwhile, with the advent of BANs, the probability of multiple BAN users co-located in each other's vicinity will also increase. For instance, in a hospital foyer or waiting area, neighbouring BANs operating in the same frequency bands are likely to significantly increase the homogeneous interference level amongst networks.

2.2.4 MAC Layer:

Body movement leads to density and topology changes that make the sensor nodes move into or out of communication coverage of each other. Therefore, MAC layer protocol designs for BANs should be able to guarantee the reliabil-

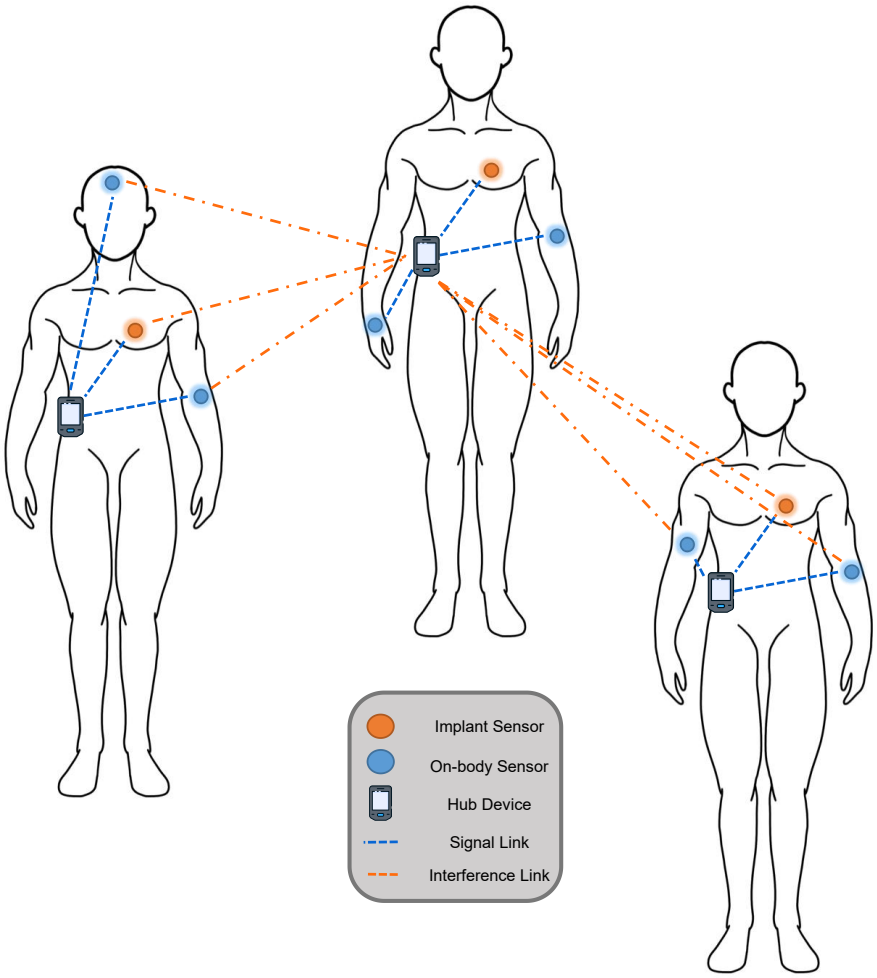

Figure 2.4: The scenario of multiple BANs co-located

ity of the system despite mobility. In addition, MAC protocols must support the energy efficiency requirements of BAN applications, prolong sensor lifetime, allow flexible duty cycling and save energy by periodically switching the radio on/off. However, the MAC protocols proposed thus far for BANs do not provide efficient network throughput and delay performance at varying traffic, and the synchronization of duty cycles of their sensors with variant traffic characteristics and power requirements remains a challenge [27]. Traditional MAC protocols mainly focus on improving bandwidth utilization,

throughput, and latency. However, they lack energy conserving mechanisms, which is one of the most strict needs for BANs.

2.3 Existing Research:

2.3.1 Interference Mitigation:

With the popularisation of e-healthcare systems, it is inevitable that inter-BAN interference will become a problem. Avoidance and mitigation of channel interference have been extensively researched in wireless communication literature. Advanced signal processing using interference cancellation techniques [28, 29] has also been proposed to minimise the impact of interference. However, these methods require knowledge of the channel condition between BANs, which is infeasible for BANs operation due to the lack of a central coordinator. In addition, high complexity makes the implementation of interference cancellation impractical. Co-channel interference mitigation scheme among BANs was first addressed in [30], by focusing on the probability density function of the total interference. Several pioneer works on inter-BAN interference issues mainly focus on physical layer analysis and solutions, e.g.,[31, 32], which aim to reduce the interference level by minimise the sensors transmit power. Meanwhile, to provide higher spatial reuse, node-level interference has also been studied in [33] and [34]. This method maintains a low interference level and adds no complexity to the sensors. [35] propose a distributed two-hop incomplete coloring (DTIC) algorithm that adopts a game-theoretic approach. DTIC exploits two-hop information to enable high channel reuse among two-hop neighbours.

Cooperative communication schemes were also widely studied, e.g.,[36,

37, 38]. Assuming that the intra-BAN and inter-BAN transmission are scheduled by a TDMA scheme, [37] proposed and analysed the performance of a decode-and-forward cooperative communication scheme for BANs, where the BAN-of-interest communicates cooperatively via two relays when multiple BANs coexist in the same area. Using packet reception rate as design criteria, a distributed cooperative scheduling scheme that considers single-BAN scheduling as an assignment problem and multi-BAN concurrent scheduling as a game is proposed in [39]. In [40], Cui et al. proposed a joint relay selection and power control scheme (JRP) that takes into account transmission reliability. The proposed protocol achieved a good trade-off between reliability and energy consumption.

Time-Slotted Channel Hopping (TSCH) that uses time synchronization to achieve low-power operation and channel hopping to enable high reliability has been applied in IoT applications [41, 42]. A scheduling and interference mitigation scheme in TSCH using Latin rectangles is used in [42], which prevents scheduling nodes from channels that are already allocated. For BAN applications, [43] use a game-based channel selection mechanism that adopts a finite repeated potential game. Two proposed learning algorithms, Stochastic Learning Algorithm (SLA) and Stochastic Estimator Learning Algorithm (SELA) outperform the random channel selection specified in the IEEE 802.15.6 standard.

2.3.2 Transmit Power Control

As the sensors in BAN systems mainly rely on battery power, prolonging the lifetime of these nodes are of prime importance. However, most proposed BAN standards adopt pre-defined or fixed transmit powers (Typically less

than 0dBm as regulated by FCC), which promotes energy wastage. Meanwhile, inefficient use of transmit power might result in packet loss that leads to power wastage and increase in delay. Most importantly, when critical packets are lost, a patients' life may also be threatened. In this regard, transmit power control that is able to adjust the output power according to the unique changing nature of BAN will play an important role in future developments of IoH technology. Also, transmit power control methods are potentially able to suppress intra-BAN interference or inter-interference among coexisting BANs [31] [44]. It should be noted that transmit power control methods are often implemented for BAN on-body channels, which use narrow-band communications. Because, as shown in Figure 2.1, most BAN applications operate at unlicensed Industrial Scientific and Medical (ISM) radio bands that are centred at 2.45 GHz. In this section, a various number of transmit power control methods have been studied in the literature will be discussed.

2.3.2.1 Non-Game-theoretic Transmit Power Control

Many techniques involve transmission power control that is based on a centralised [45] and partially distributed [46] approach. These techniques are proved to be effective for stable topology networks with fewer power constraints [47].

In realistic BAN scenarios, only using low transmit power may leads to reduction of reliability [48], which may eventually increase the transmission delay and energy wastage due to the re-transmissions of undelivered packets. In addition, low transmit power will make receivers constantly operate near their sensitivity (normally between -85dBm and -93dBm), which increases the packet loss as small channel fluctuationds will make the RSSI go below the Rx

sensitivity. Therefore, it is important to make sure that power control methods are robust to large BAN channel attenuations. In this regard, reactive-based power control mechanisms that are able to "respond" to the wireless channels have been addressed in literature. This mechanism rely on a “margin” that is sometimes referred to as a target range or threshold. The “margin” is used to update the transmit power, resulting in a lower probability of packet loss and higher signal stability. Notably that, for this type of mechanism, it is assumes that unlike the source nodes, the coordinator is not energy constrained. This means that, the basic operation of this close-looped principle is demonstrated in Figure 2.5.

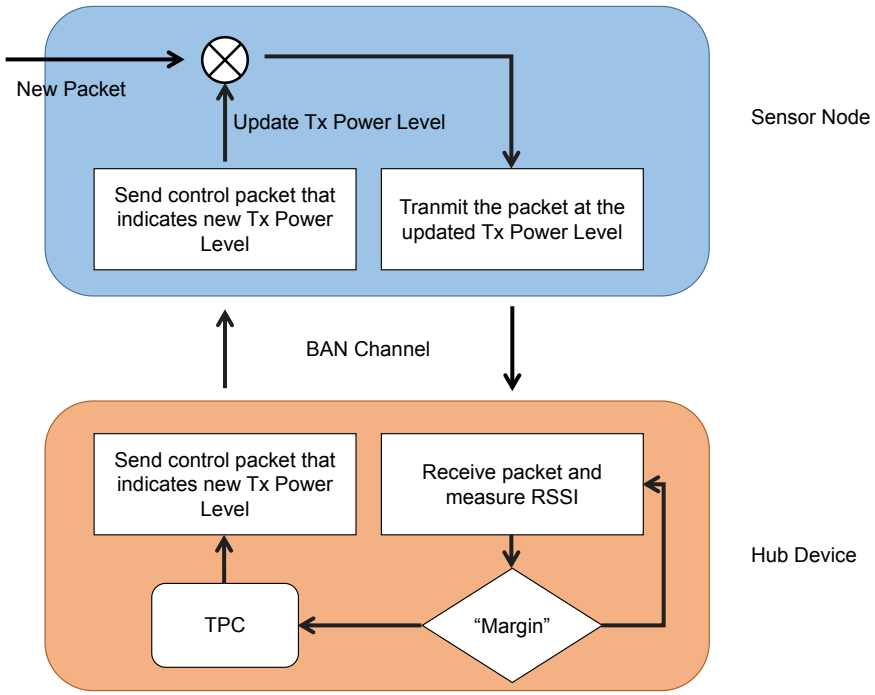

Figure 2.5: Flow Chart of Closed-Loop Mechanism.

The upper and lower bound of the “margin” can be tuned dynamically

in order to adapt to the time-varying nature of the wireless channel. The classic reactive approaches are: *Binary* [49], *Linear* [50] and *Dynamic* [51]. Figure 2.6 demonstrate the basic concept of these methods. a) *Binary*: Binary approach was firstly proposed in [49], it exponentially changes the transmit power. Compared with the target "margin", if the measured RSSI is higher, then the transmit power for next transmission is set as the midpoint between the previous transmit power and the minimum transmit power (normally at -30dBm). If the measured RSSI is lower than target "margin", then the transmit power for next transmission is set as the midpoint between the current transmit power and the maximum transmit power (normally at 0dBm). This method reaches the optimal transmit power faster than others, thus reducing the rate of exchange control packets. However, when the channel is oscillating, it is impossible for the binary approach to find an optimal transmit power, and the transmit power is updated exponentially, which makes the method extremely inefficient. [52] b) *Linear*: The linear algorithm [50] gradually changes the transmit power (one power level at the time) based on the previous RSSI. The optimal transmit power is the transmit power value for which the current RSSI value falls within the target "margin". Because the RSSIs can be continuously placed within the Target "Margin" so that the linear approach operates more efficiently in a dynamic environment, providing higher packet delivery rate and a low outage probability. c) *Dynamic*: The dynamic algorithm assigns the optimal transmit power based on the knowledge of link characteristics, which can be express by a primary equation. The primary equation shows that for a specific link, when the postural position changes, the new RSSI value can be written as linear equation of current power level. The equation's slope and constant are obtained based on two col-

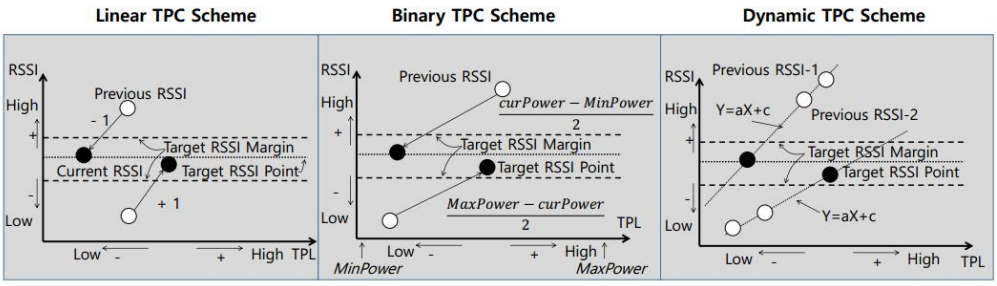

Figure 2.6: Linear, Binary, and Dynamic Transmit Power Control Schemes

lected RSSI values. After the slope and constant of the equation are decided, the TPL can be adjusted dynamically by using this feedback mechanism at runtime without any pre-stored information.

To better cope with unstable BAN channel dynamics, [52] proposed a hybrid transmit power control algorithm that considers both stable and dynamic scenarios. It uses the Binary approach in stable environments and the Linear approach in dynamic environments. The decision of which algorithm to use is made in real time and the Hybrid algorithm evaluates the current-channel environment based on changing RSSI values. [53] uses reinforcement learning with approximation to learn from the environment and improve BANs performance. Due to small scale fading, the target RSSI ranges are important for TPCs that adopt a reactive based TPL control mechanism. More studies about the most suitable TPL's upper and lower values based on node location, user movement and surrounding environment are required since these factors clearly influence the magnitude of the small-scale fading and traffic overhead. Thus, pre-defined upper and lower values of the TPL margin might not be recommended in BANs, since in different scenarios, different nodes locations and user movements may leads to different fading properties which result in different transmission outage probabilities [54].

The posture and movement of BAN users have the most significant influence on channel quality. Several researchers have explored different techniques to recognize posture and/or movement [51, 55]. The inertial sensor-based TPC solutions rely on hardware to determine the posture and/or activity of the user in order to estimate the current channel quality or predict it at near future instants. Different solutions have been addressed in literature to either estimate [56] or anticipate channel quality accordingly to user posture and movement [57, 58].

2.3.2.2 Game-theoretic Transmit Power Control

As a useful tool in analyzing the interactions of decision makers, game theory has been widely used by economists to investigate the actions of economic agents in a market. In ecent years, game theory control schemes have been shown to be beneficial in wireless network's quality of service (QoS) Game-theoretic power control, incorporating pricing factors in utility functions, e.g., [59, 60], has been shown to improve QoS in wireless networks. Due to the general lack of a central coordinator in BANs, transmit power control must be distributed across BANs. In recent studies, BANs have been modelled as rational players competing for resources in non-cooperative power control games, e.g., [61, 62, 31, 63].

An important aspect for overall coexistence of BANs is the social efficiency, which refers to the maximisation of aggregated utilities. Lack of social efficiency may result in overall power wastage and unfairness among BANs. However, in general, social optimality has rarely been achieved due to imperfect information among BANs [64]. Although, in large-scale cellular networks and ad-hoc networks, some socially optimal algorithms have been proposed,

e.g., [65], where centralised coordination and some global knowledge are required, which is infeasible for BANs. Other socially-efficient methods referred to as distributed, e.g., [66], require some global knowledge and are only socially efficient for static channels after a large number of iterations.

2.3.2.3 Predictive Transmit Power Control

In order to deal with such dynamic channel characterization of the BAN channel, prediction-based power control schemes [11] have been proposed to enhance BAN communications. A novel energy-efficient adaptive power control algorithm is proposed [67], which can adaptively adjust transmit power level. However, this method introduces a large proportion of packet losses. [68] propose a practical transmission power control protocol based on both short and long-term link-state estimation. A very similar algorithm was also proposed by [69] where a non-static threshold ~~parameter TRH~~ is updated. To this a value is added, which represents the channel quality variation (standard variation of n RSSI samples).

2.3.3 Resource Allocation

As previously explained, to successfully deploy BANs that can perform long-term and continuous IoH applications, it is critical that the wearable and implanted devices are small, lightweight and energy efficient. Resource allocation protocols, when applied in BANs, must take topology and link changes, as well as the dynamic traffic, into account. If carefully designed, these protocols may work efficiently under the high level of interference and mobility conditions. Up to now, most research in resource allocation for BANs focus on intelligent MAC protocol design. It is because, although the IEEE

802.15.6 standard has been endorsed by the biomedical industry, such a standard doesn't provide complete specifications of the MAC layer protocol. Thus the MAC still remains a challenging issue for the future development of BANs as MAC protocols plays an important role in dealing with packet delivery ratio and latency [70, 27, 7]. Recently, several MAC layer protocols that seek to solve inter-BAN interference problems [71, 72, 33] have been proposed. The work in [71] uses cooperative schemes to suppress inter-BAN interference, where a random incomplete coloring (RIC) algorithm is proposed to realize a fast and high spatial-reuse for inter-BAN scheduling. In [72], a mixed graph coloring is used for interference mitigation among BANs, where the proposed method pairs every two BANs into a cluster and uses cooperative scheduling between the pairs in each cluster to reduce interference. Node-level scheduling is considered in [33] to increase spatial reuse. However, these methods only work for fixed topologies in the network. To better cope with the required flexibility in BAN implementations, in [73, 74, 75], collision avoidance techniques, such as beacon rescheduling, channel sensing and adaptive sleeping are used to improve the overall QoS performance for interfering BANs. Many energy efficient MAC protocols have been proposed, such as [76, 77]. In B-MAC [78], the sender needs to broadcast a long preamble to be detected by the right receiver to reduce power consumption, but this, however, incurs unnecessary transmission overhead. [79] proposes A Traffic Load Aware Sensor (ATLAS) MAC design, in which the traffic load is estimated into four different classes. According to the traffic load estimation, a different superframe mode is used. A traffic Priority and Load Adaptive MAC (PLA-MAC) is proposed in [80], where traffic is differentiated into four classes on the basis of data type and data rate of the sensor nodes. The prioritization among

sensor nodes is done through prioritized random back-off. [81] evaluates energy efficient MAC protocols in terms of wake-up radio. To interleave BAN sensors active period through contention or negotiation, Two Master Nodes Cooperative Protocol (TMNCP) is proposed in [82].

2.3.3.1 Link Adaptation

In comparison to transmission power control schemes, resource allocation methods tuning some other parameters, such as transmission rate, packet size and so on, have proven to be more effective. Research interests in this area are emerging and some centralized methods [83] have been proposed in recent studies. As for distributed algorithms, game theoretic approaches are widely used. For cellular networks, [84] game theoretic schemes with multiple discrete code rates or modulation schemes are proposed, which is also known as link adaptation [85]. The mobile terminals update power and rate by optimising the Utility Function to obtain a Nash Equilibrium. This idea is further extended for wireless Ad hoc networks in [86], a simple utility function only depending on Signal to Interference and Noise Ratio (SINR) and pricing is used. However, for BANs, there has been limited literature on this subject. [87] proposed a transmission rate adaptation policy for BANs to improve the QoS by solving a convex optimisation problem, but only dynamic postures in BANs channels are considered.

2.3.4 Learning-based Prediction Schemes

Communications reliability is vital for wireless body area networks (BANs), while minimizing transmit radio power is crucial for BAN sensor radios lifetime. Thus, efficient radio transmit power control is very important for BANs ,

which needs to be enabled by effective radio channel prediction [11]. As most traditional prediction methods are discussed in subsection 2.3.2.3, therefore, only learning-based prediction studies are reviewed in this subsection.

Box and Jenkins [12], in the late 70s, made an important work in studying applications composed of mathematical linear models. These models represent Autoregressive (AR) and Moving Averages (MA) processes, and most existing literature on long-term channel prediction for typical radio networks often adopts AR predictive methods [88] or weighted alternate-least-squares technique modeling [89].

However, the narrowband on-body BAN channel is typically non-stationary [90], and traditional long-term prediction methods may not be applicable. Recently, learning methods using different types of Artificial Neural Networks (ANN) have been successfully adopted in time series related forecasting/predicting tasks [91, 92, 93, 94]. The ANNs provide novel mathematical representations of the non-linearity in time-series and thus improve the prediction accuracy. ANN proposals in the literature [95] are based on a non-linear autoregressive structure. However, the dynamic behavior of most of the wireless channels restrict the NN from properly modelling channel characteristics, which poses the challenge to using ANN-based methods in wireless channel prediction tasks.

For signal processing, deep learning approaches, typically employing recurrent neural networks (RNNs) with long short-term memory (LSTM) [96], have been used in numerous applications [97] with better prediction than machine learning methods. Due to its ability to capture long-term dependencies, LSTM models have shown superior results in speech recognition [98, 99], and sentiment analysis [100].

2.4 Concluding Remarks

In this chapter, to better motivate our research on perform resource allocation in BANs and predict BAN channel dynamics, a contextual review of the literature has been provided. The current communications standards for BANs were reviewed firstly. The current issues in BAN research have also been highlighted, which further motivates the innovative contribution of this thesis to be given in the following chapters. Moreover, the state-of-art literature were reviewed and discussed. These techniques are categorized as interference mitigation, transmit power control, link adaptation and channel prediction methods.

From this chapter the conclusion can be reached that existing resource allocation techniques do not completely address QoS requirements and achieve desired performance for IoH applications. Moreover, most existing approaches can not be implemented in an autonomous manner and the fairness of the systems is hard to guarantee. In addition, at the current stage, traditional methods are not able to grasp the channel dynamics of BAN channels and provide highly accurate channel prediction, which would benefit the overall performance for BANs. Such research challenges, made clear from this chapter, are addressed in proceeding chapters of this thesis.

Chapter 3

Energy-Efficient, Provably Socially-Efficient, Transmit Power Control

3.1 Introduction

To make sure body area networks, providing long-term reliable low-power communications for IoH applications, it is paramount to achieve high PDR, as minor errors in communications could be life-threatening to the wearer. It is often necessary to have several BANs operating in each other's vicinity in different environments, for example, hospitals, nursing homes and age care centres. However, it is not feasible to coordinate the BANs due to unpredictable human movement [101]. The lack of central coordinator raises the issue of co-channel interference that causes packet loss and leads to energy wastage among closely-located, coexisting BANs. Additionally, BAN channels are generally non-stationary and BAN sensors, with small size and limited battery capacity, are required to consume ultra-low power. Therefore, practical algorithms that can improve communication reliability, and mitigate interference across non-coordinated, coexisting BANs are of great importance.

In recent studies, BANs have been modelled as rational players compet-

ing for resources in non-cooperative power-control games, e.g., [64, 31]. Obviously, by using larger transmit power, a self-interested player (BAN) can achieve a better utility outcome if the other BANs keep their transmit powers unchanged. However, because of the strong interference experienced, if every player in the range does so, it will worsen the social welfare that is the aggregation of all player's utilities, which will ultimately result in overall power wastage and unfairness amongst BANs. Here, in this chapter, we aim to distribute spectral resources for non-cooperative BANs fairly and effectively to increase energy efficiency and reliability, without global knowledge.

3.2 System Model

We consider the absence of a centralised controller amongst multiple co-located BANs. The system model is shown in Figure 2.4, each BAN adopts a star topology with one coordinator (or hub). Since time division multiple access (TDMA) is more reliable and power efficient when compared with contention-based access methods [72, 102]. Therefore, TDMA is adopted for every BAN, so that in a single BAN, intra-network transmission collisions are avoided. It should be noted that, because there is no global coordinator among multiple BANs, the TDMA scheme used here is slightly varied from traditional TDMA [102], given no prior channel information.

As illustrated in Figure 2.4, each BAN suffers inter-BAN interference received from other simultaneously transmitting BANs, thus the signal-to-noise-plus-interference ratio (SINR) of the i_{th} BAN at time τ, $\gamma_i(\tau)$ is defined as:

$$\gamma_i(\tau) = \frac{|h_i^i|^2 p_i(\tau)}{\sigma^2 + \sum_{j=1, j\neq i}^{m} p_j(\tau)|h_j^i|^2}, \tag{3.1}$$

where σ^2 denotes additive gaussian white noise. $|h_i^i|$ is the on-body channel gain between the sensor and hub in i_{th} BAN, and $|h_j^i|$ the inter-BAN channel gain from the sensor in j_{th} BAN to the hub in i_{th} BAN. Meanwhile, the $p_i(\tau)$ and $p_j(\tau)$ are the transmit powers of sensors at time τ in i_{th} and j_{th} BAN respectively.

Accurate modelling of the packet delivery ratio (PDR) for the BAN is a key foundation of the success implementation of the non-cooperative power control mechanism here. According to IEEE 802.15.6 Standard [20], cyclic error-correcting codes BCH (31,19) and DPSK/BPSK modulations with a packet length of 256 bytes are applied.[1] The BCH(31,19) coding gives about 2dB coding gain over the uncoded scheme when implemented. Considering the 2dB channel coding gain, the relationship between PDR and the SINR can be expressed as:

$$PDR = \exp\left(-\left(\frac{1}{\gamma a_c}\right)^{b_c}\right) = \exp\left(a\gamma^b\right), \tag{3.2}$$

where the value of parameter a_c and b_c is determined by the modulation type, packet size and data rate. With a root-mean-square error of the approximation less than 0.006, the value of a_c and b_c are estimated with respect to fitting the DPSK and BPSK modulation as in [64]. For DPSK modulation $a_c = 0.23, b_c = 7.409$, and for BPSK modulation $a_c = 0.293, b_c = 6.358$.

3.3 The Social-Optimal Power Control Game

Each BAN is modeled as a self-interested and rational player competing for resources (shared channel) in the proposed non-cooperative game: $G =$

[1] The BCH (31,19) code is a shortened code derived from a BCH (63, 51) code.

$\{\mathcal{N}, \mathbf{P}, U\}$, $\mathcal{N} = \{1, 2, ..., N\}$ is a set of players, i is the index of the player in $\mathcal{N}$. $\mathbf{P}$ is the pure strategy space, for each player i and $\mathbf{P}_i$ is a finite set of discrete transmit powers from P_i^{min} to P_i^{max}. The global strategy space $\mathbf{P}$ is given by the Cartesian product of all players' strategy space $\mathbf{P} = \mathbf{P}_1 \times \mathbf{P}_2 \times ... \times \mathbf{P}_n$. And $\mathbf{P}_{-\boldsymbol{i}}$ represents all other player strategies except for player i. In order to minimise the transmit power and maximise the packet delivery ratio (PDR) at the same time, the utility function $U(\cdot)$ is defined in terms of the current transmit power and packet delivery ratio as:

$$U\left(p_i, pdr_i\right) = -C \cdot p_i^w + \log\left(1 + pdr_i^v\right), \tag{3.3}$$

where p_i and pdr_i are the i_{th} players transmit power and PDR respectively. The current PDR of the i_{th} BAN changes according to the current transmit power of the i_{th} player and all other players (sensors) $-\boldsymbol{i}$. The exponents $w > 0$ and $v > 0$ can be adjusted according to the communications scenario. The pricing factor $C > 0$ adjusts the trade-off between PDR and transmit power, to enable each player to best maximise their utility. At the end of the each stage, the BAN updates its transmit power for the next time slot to maximise the utility function: $p_i(\tau + 1) = \arg\max(U(p_i(\tau), pdr_i))$. The algorithm for the game is given below in Algorithm 1.

The utility function is a vital factor in the power control scheme, since the nodes are punished or rewarded according to their transmit power and PDR. The utility function $U(\cdot)$ guarantees that when the SINR is significantly high or extremely low, power consumption dominates $U(\cdot)$. Note that the natural logarithm $\log(1 + pdr)$ in $U(\cdot)$ is different to the common rate utility $\log_2(1 + \gamma)$, in order to provide better PDR performance while minimising power. And since $pdr \in [0, 1]$, the value of $\log(1 + pdr)$ is confined, while high

SINR is over-rewarded in $\log_2(1+\gamma)$ that can increase power consumption.

Algorithm 1 The Proposed Game

1: When $\tau = 0$, $p_i(0) \in [P_i^{min}, P_i^{max}]$ is randomly chosen
2: From the received packet the hub could get information of the current SINR $\gamma_i(\tau)$
3: The PDR $pdr_i(\tau)$ could be estimated by using $pdr = \exp\left(a\gamma_i^b\right)$
4: The transmit power for next time slot could be obtain by $p_i(\tau+1) = argmax(U(p_i(\tau), pdr_i))$, where $p_i(\tau+1) \in [P_i^{min}, P_i^{max}]$

The action profile $\mathbf{P}^o = (p_1^o, p_2^o, p_3^o ... p_n^o)$ for $n \geq 2$ BANs is a Nash Equilibrium, if p_i^o is the best response towards $\mathbf{P^o}_{-i}$, which implies for all players $U_i(p_i^o, pdr_i^o) \geq U_i(p_i, pdr_i^o)$, for any choice of $p_i \in \mathbf{P}$, where pdr_i^o is a function of $\mathbf{P^o}_{-i}$. This leads to the following two theorems:

3.3.1 Existence:

Theorem 3.1. The game G admits at least one Nash Equilibrium

Proof. In game G, for $i \in \mathcal{N}$ the following condition can be verified. The strategy set $[P_i^{min}, P_i^{max}]$ is a non-empty, convex, bounded in finite dimension vector space. The utility function U is continuous for all $p_i \in [P_i^{min}, P_i^{max}]$. As the first derivative of the utility function is well defined as:

$$\frac{\delta U_i}{\delta p_i} = -C \cdot wp^{w-1} + v\left(1 - \frac{1}{(1+pdr_i^v)}\right) ab\frac{\gamma_i^b}{p_i} \tag{3.4}$$

where $\frac{|h_i^i(k_i)|^2}{I_{-i}} = \frac{\gamma_i}{p_i}$, therefore, as $p_i \in [P_i^{min}, P_i^{max}]$ is real and the pdr_i is non-zero, the Theorem 3.1 is proved [103]. □

3.3.2 Uniqueness:

Theorem 3.2. The Nash Equilibrium in each stage of the game G is unique, and independent of history so it is a unique sub-game perfect equilibrium.

Proof. To prove the theorem, the second derivative of $U(\cdot)$ is shown to be negative $\forall i$, so that $U(\cdot)$ is strictly concave. Since,

$$\frac{\delta^2 U_i}{\delta p_i^2} = -C \cdot w(w-1)p_i^{w-2} + \left(1 - \frac{1}{(1+pdr_i^v)}\right) v\gamma_i^b ab(b-1)/p_i^2 - \frac{v^2 pdr_i^v}{(1+pdr_i)^2} a^2 b^2 \gamma_i^{2b}/p_i^2 \quad (3.5)$$

where pdr_i is always positive and between (0,1), and the term $(b-1)$ is less than 0. In addition w is positive thus $\frac{\delta^2 U_i}{\delta p_i^2} < 0$. Therefore the utility function has a global maximum at p_i^* which occurs at the point where $\frac{\delta U}{\delta p_i} = 0$. □

3.4 Social Properties of the Game

The Nash Equilibrium solution of each individual BAN in the proposed game is the maximisation of its own utility. The social welfare reflects the fairness and efficiency of this best response, considering all individuals utility combined, and can be expressed as: $SW(\mathbf{P}) = \sum_{i=1}^{n} U(p_i, \mathbf{P}_{-i})$, where $U(p_i, \mathbf{P}_{-i}))$ represents the utility function for BAN i as a function of its transmit power and other players' transmit power.

Figure 3.1 represents an example comparison among all possible action profiles for all BANs at each stage of the proposed game by simulating under realistic channel conditions, which are specified in Section 3.5. The social wel-

fare for all possibilities are plotted as red dots, the aggregate utility achieved at the Nash Equilibrium for each BAN are indicated as blue diamonds, and the black dashed-line denotes the achievable social optimum. Apart from the initial stage, the social optimum equals to the aggregate utility operating at the Nash Equilibrium for each BAN. It is also noted that, at the first time slot, since the transmit power is randomly chosen in the range $[-30, 0]$ dBm by all BANs, the aggregate utility achieved at the unique Nash Equilibrium points is not socially optimal. The social welfare, given feasible constraints that can be maximised in the proposed non-cooperative game leads to the following definition:

Definition 3.1. Under specified constraints that $g_i(\mathbf{P}) \geq 0, \forall i \in \mathcal{N}$, (for example $pdr_i - threshold \geq 0$), the social welfare of the coexisting BANs has a maximum value specific action profiles $\mathbf{P}^* = (p_1^*, p_2^*, p_3^* ... p_n^*)$, where n is the number of BANs coexisting. The BANs' interaction in this game is thus constrained social efficient.

Thus the action profile $\mathbf{P}^*$ is the solution for social welfare maximisation as:

$$\begin{aligned} \underset{\mathbf{P}}{\text{maximise}} \quad & SW(\mathbf{P}) = \sum_i U\left(p_i, \mathbf{P}_{-i}\right) \\ \text{subject to} \quad & g_i(\mathbf{P}) < 0, \forall i \in \mathcal{N} \end{aligned} \tag{3.6}$$

However, sometimes the global social optimum solution is hard to obtain and without central coordinator, the social optimum is difficult to get for BANs without knowing each others transmit power. Although, properly setting the pricing factor may lead to social welfare maximisation [104], it is not practical to implement the algorithm for BANs. Therefore, we proposed the concept of constraint social optimum to reveal that the proposed game

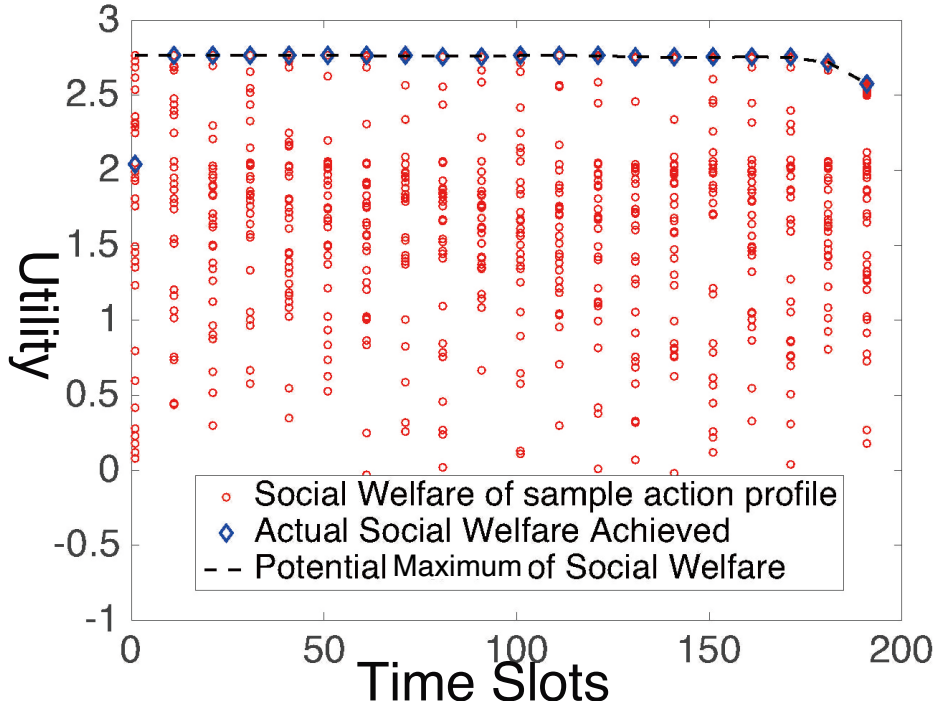

Figure 3.1: Comparison Between Social Welfare and Nash Equilibrium Points implementing the proposed game.

can lead to social welfare maximisation in feasible power levels. We consider realistic radio channel scenarios, assuming that the channel attenuation h_i^j for all i, j has relatively small variation between consecutive time slots,

For the proposed game, the constrained social efficiency, achieved from individual BAN Nash Equilibrium responses (solved based on the channel conditions in the previous time slot), will be proved in the following. The exponent w is set to be 1 for simplicity and best performance.

Theorem 3.3. At each stage of the game, when under PDR constraints where the PDR of each BAN reaches the threshold, constrained social efficiency is achieved by the action profile $\mathbf{P}^o(t) = (p_1^o(t), p_2^o(t), p_3^o(t)...p_n^o(t))$ for $n \geq 2$,

where $p_i^o(t)$ denotes the Nash Equilibrium solution for BAN i.

Proof. Theorem 3.3 can be proved by showing that the solution (social welfare) for the constrained utilities maximisation problem and the Nash Equilibrium points intersect ($\mathbf{P}^o = \mathbf{P}^*$).

As already stated, the utility function for any BAN is dependent on the transmit power of all other BANs. Hence, this competition among BANs implies that the utility functions are *coupled.* Social welfare, and hence optimality, is with respect to the coupled constraint set of feasible PDR region. We first consider the situation where the channels are static (i.e., channel attenuation does not change during the period of the game) under equality constraints. Inequality constraints will be introduced later. □

3.4.1 Static Channel Conditions

Since the channel conditions are not time varying, the PDR remains unchanged after convergence. The constraint for the social welfare maximisation problem is that $pdr_i = threshold$, for all $i \in \mathcal{N}$, where the PDR after convergence (generally larger than 0.9) is chosen to be the threshold.

The action profile at time t, $\mathbf{P}^o(t)$ that satisfies the constraints and maximises the sum of the utilities can be found from solutions of Lagrange multipliers λ_i. The Lagrange function for the social welfare function $SW(\mathbf{P}(t))$ with constraint equations $g(p_i(t), \mathbf{P}_{-i}(t)) = pdr_i(t) - threshold = 0$, $i \in \mathcal{N}$, is represented by:

$$\Lambda(\mathbf{P}(t)) = SW(\mathbf{P}(t)) + \sum_i \lambda_i(t) g(p_i(t), \mathbf{P}_{-i}(t)). \tag{3.7}$$

In order to obtain the solution of the maximisation problem (3.6), the

First Order Lagrange Condition (FOL), $\nabla\Lambda(\mathbf{P}(t)) = 0$, should be met. The solution intersects with the aggregate Nash Equilibrium solutions $\mathbf{P}^o(t) = (p_1^o(t), p_2^o(t), p_3^o(t)...p_n^o(t))$, which are evaluated based on the PDR for every BANs in time $t-1$,

$$\frac{\partial U(p_i, pdr_i(t-1))}{\partial p_i}|_{p_i=p_i^o(t)} = 0, \forall i \in \mathcal{N}. \tag{3.8}$$

When the solution intersects at $\mathbf{P}^* = \mathbf{P^o}$, the Lagrange Multiplier $\lambda_i > 0$ can be proved to exist $\forall\, i$, then Theorem 3.3 holds once the game converges.

It should be noted that positive Lagrange Multipliers $\lambda_i > 0, \forall\, i$ show that the gradient of the objective function (social welfare function) is in the opposite direction to the gradient of the constraint function. The non-negativity ensures that the constraint function and the social welfare cannot be increased at the same time. The inequality constraints $g\left(p_i(t), \mathbf{P}_{-i}\right) = pdr_i - threshold > 0$, can be handled by the Karush-Kuhn-Tucker (KKT) conditions, which extend the ideas of Lagrange multipliers:

- Gradient of the Lagrangian: $\nabla\Lambda\left(\mathbf{P}(t)\right) = 0$;
- Constraints: $g\left(p_i(t), \mathbf{P}_{-\boldsymbol{i}}(t)\right) \geq 0, i \in \mathcal{N}$;
- Complementary slackness: $\lambda_i(t) g\left(p_i(t), \mathbf{P}_{-i}(t)\right) = 0$;
- Sign condition: $\lambda_i(t) \geq 0$;

As stated above, the Lagrange Multipliers are always non-negative, therefore the KKT conditions will also be met by the action profile $\mathbf{P}^o(t) = (p_1^o(t), p_2^o(t), p_3^o(t)...p_n^o(t))$. Then Theorem 3.3 holds. However, the local optimum solution of the KKT condition happens at the boundaries where $g\left(p_i(t), \mathbf{P}_{-i}(t)\right) = 0)$. In other words, there are no action profiles that can improve the social

welfare of the players without making the PDR going below the threshold. Thus the Nash Equilibrium solution of the game is said to be constrained social efficient, and hence also Pareto efficient.

Remark. For static channel conditions when the transmit powers are the same for two consecutive time slots and the PDRs all reach the threshold, then the game has converged and a socially optimal outcome is achieved.

3.4.2 Time-varying Channel Conditions

In a realistic scenario, the channels are varying through time, thus it becomes difficult to show that the solution for the social welfare optimisation problem intersects with the Nash equilibrium solution, However, the utility function has been shown to be concave and twice differentiable. Meanwhile, in real cases, the transmit power is constrained in $[-30, 0]$ dBm due to hardware limitations [11, 37]. Furthermore, by making use of the convexity constraints, the social efficiency can be analysed through the Lagrange duality of social welfare maximisation 3.6 problem. With the help of decomposition for the coupled constraints, the upper or lower bounds of (3.6) are derived.

Theorem 3.4. Consider the social welfare maximisation problem (3.6), where the solution represents the constrained socially optimal solution for the BANs in time t, under power constraints. If the NE solutions in t are less than or equal to those in $t-1$, then social optimality can be achieved.

Proof. The social welfare maximisation problem in (3.6) can be rewritten is

term of power constraints as:

$$\begin{aligned} \underset{\mathbf{P}(t)}{\text{maximise}} \quad & SW(\mathbf{P}(t)) = \sum_i U\left(p_i(t), \mathbf{P}(t)_{-\boldsymbol{i}}\right) \\ \text{subject to} \quad & p_i(t) \geq q_i, \ \forall i \in \mathcal{N} \end{aligned} \tag{3.9}$$

The objective function (3.9) is coupled with $p_i(t)$ and $\mathbf{P}(t)_{-\boldsymbol{i}}$. By introducing *auxiliary variables* and additional equality constraints, the coupling in objective function is transferred to coupling of constraints, solved by additional *consistency pricing*. Thus (3.9) can be expressed as: □

$$\begin{aligned} \underset{\mathbf{P}(t)}{\text{maximise}} \quad & \sum_i U_i(p_i(t), \left[y_{i,j}\right] j \in L(i)) \\ \text{subject to} \quad & p_i(t) \geq q_i, \ \forall i \in \mathcal{N}. \\ & y_{i,j} = p_j(t), \ \forall i \in \mathcal{N}. j \in L(i), \end{aligned} \tag{3.10}$$

where $y_{i,j}$ are the *auxiliary variables*, and $L(i)$ denotes the set of BANs coupled with i_{th} utility. Note that $p_i(t)$, $y_{i,j}$ are local variables for the i_{th} BAN. Therefore, the Lagrangian is:

$$\begin{aligned} L(\mathbf{P}(t), \mathbf{y}, \boldsymbol{\lambda}, \mathbf{r}) = & \sum_i U_i(p_i(t), \left[y_{i,j}\right] j \in L(i)) \\ & + \sum_i \lambda_i(p_i(t) - q_i) + \sum_{i,j \in L(i)} r_{i,j}(p_j(t) - y_{i,j}), \end{aligned} \tag{3.11}$$

where $r_{i,j}$ are the *consistency pricing*. By taking the dual decomposition approach, the Lagrangian (3.11) is separated into sub-problems, maximised by

local variables. The dual function $g(\mathbf{r}, \boldsymbol{\lambda})$ can be expressed as:

$$g(\boldsymbol{r}, \boldsymbol{\lambda}) = \sum_i \underset{\mathbf{P}(t), \mathbf{y}}{\text{supremum}} \quad U_i(p_i(t), [y_{i,j}]\, j \in L(i)) \\ + \lambda_i p_i(t) + \sum_{j, i \in L(j)} r_{j,i} p_i(t) - \sum_{i, j \in L(i)} r_{i,j} y_{i,j}. \quad (3.12)$$

It can be seen from (3.12) that for positive λ_i and $r_{i,j}$, it is possible to have $p_i(t) > q_i$ that makes the Lagrangian (3.11) go to $+\infty$. Thus, to get the supremum of $L(\mathbf{P}(t), \mathbf{y}, \boldsymbol{\lambda}, \mathbf{r})$, the Lagrange multiplier λ_i and the consistency pricing $r_{j,i}$ together have to meet the condition that $\lambda_i p_i(t) = 0, \sum_{j, i \in L(j)} r_{j,i} = 0$, so that the solution of the dual function (3.12) equals the aggregate Nash equilibrium solutions. Otherwise, $-C + \lambda_i p_i(t) + \sum_{j, i \in L(j)} r_{j,i} \leq 0$. Furthermore, if the channel is slowly time-varying ($h_i^j(t) \approx h_i^j(t-1), \forall i, j$), and assuming that the noise σ^2 is relatively negligible, then PDR maximisation can be achieved over two time slots. This approximation can be applied in the dual problem:

$$\begin{aligned} &\underset{\boldsymbol{\lambda}, \boldsymbol{r}}{\text{minimise}} \quad g(\boldsymbol{r}, \boldsymbol{\lambda}) \\ &\text{subject to} \quad \boldsymbol{\lambda} \geq 0 \end{aligned} \quad (3.13)$$

with solution

$$\min \quad \Bigg[-C \sum_i p_i^o + \sum_i \log(1 + pdr_i(\boldsymbol{P}^o_{-i})) \,, \\ -C \sum_i q_i + \sum_i \log\left(1 + pdr_i(\boldsymbol{q}_{-i})\right) \Bigg], \quad (3.14)$$

where p_i^o represents the Nash equilibrium solution from $\boldsymbol{q}_{-i}$. Consider when this constraint is $q_i = p_i(t-1)$. The Slater's condition [105] are met by the

constraints (reducing the duality gap to zero), implying power allocation $\boldsymbol{P}$ giving strictly feasible constraints. Therefore the solution of (3.9) equals (3.14). Thus objective (3.9) is maximised at $SW(\mathbf{b} = \mathbf{P}(t-1)) \geq SW(\mathbf{P}(t))$, for any $\mathbf{P}(t)$. Furthermore, by changing the power constraints into $p_i(t) \leq q_i,\ i \in \mathcal{N}$, it can be similarly shown that $SW(\mathbf{P^o}) \geq SW(\mathbf{P}(t)))$, for any feasible $\mathbf{P}(t)$. Thus, if the updated power (Nash Equilibrium solution) is strictly-less-than-or equal to the previous power vector, $\mathbf{P}(t) \leq \mathbf{P}(t-1)$, which occurs when the power vectors $\mathbf{P}$ in the game are feasible, then the outcome is constrained socially optimal

3.5 Performance Evaluation

To evaluate the performance of our proposed socially optimal power control game, namely **SOG** (Socially Optimal Game), both intra-BAN and inter-BAN channels are first modeled. It is assumed that 8 BANs with the same topology are coexisting and moving randomly within a $6 \times 6\ m^2$ square area. The walking speed of the BAN wearer is modeled as 1.5 ± 0.3 m/s, which is updated every 1 ms. The channel attenuation is modeled as $h_i^j = A_t(d_o/d_i^j)^{(3/2)}A_{SE}A_{SC}$, where the path loss exponent is 3. d_i^j represents the distance between BAN i and j, and the reference distance $d_o = 5m$ corresponds to a channel attenuation of 50 dB. The shadowing effect A_{SE} is assumed to be 42 dB, and a Jakes model with Doppler spread of 1.1Hz as the $\mathcal{CN}(0,1)$ Rayleigh distribution for small scale fading A_{SC} between BANs. Gamma fading with a mean 60 dB attenuation, a shape parameter of 1.31, and a scale parameter of 0.562 is employed for the on-body channels. Each individual plays the proposed game repeated over 100 stages. The 100-stage

game is played on 50 occasions, in which the walking patterns of the players are different.

In terms of the inter-BAN TDMA scheme, when total M BANs operating within a close proximity, all with transmit power in the range $[-30, 0]$ dBm, where a shared channel is divided into N_c orthogonal time slots with a length of T_d. The probability of m BANs transmitting simultaneously could be expressed as below:

$$Pr\left(|\text{Active BANs}| = m\right) = \binom{M}{m}\left(\frac{2}{N_c}\right)^{m}\left(1-\frac{2}{N_c}\right)^{M-m}, \tag{3.15}$$

where $1 \leq m \leq M, N_c \geq 2$. The rationale for this expression is described in [102, 64]. In this paper, 4 orthogonal channels $(Nc = 4)$ are used. The pricing factor C in the utility function is set to be 2, while the exponents $w = 1$ and $v = 4$. The generic form for utility functions for different exponents versus transmit power are described in Figure 3.2[2]. It can be seen from Figure 3.2, that by setting $w = 1, v = 4$, the trade-off between PDR and transmit power can be optimised, properly punishing for power usage according to $w = 1$, while rewarding for higher throughput, according to $v = 4$. It should be noted that the turning point at the optimum when $w = 2$ and $v = 4$ is similar with $w = 1$ and $v = 4$. However, the choice of $w = 1$ and $v = 4$ allows analysis to be more computationally tractable.

Other potential power control methods such as **Sample-and-Hold** [11], **SINR Balancing** [47], **GPC** (Game theory power control)[64], **SINR Game**[63] (another power control game)and constant transmit power at 0 dBm are also evaluated in the same simulation. **GPC** employs a utility function defined as:

[2]In Figure 3.2, power on the x-axis is in dB-scale, in linear scale all curves are strictly concave, enabling a unique Nash equilibrium with respect to power.

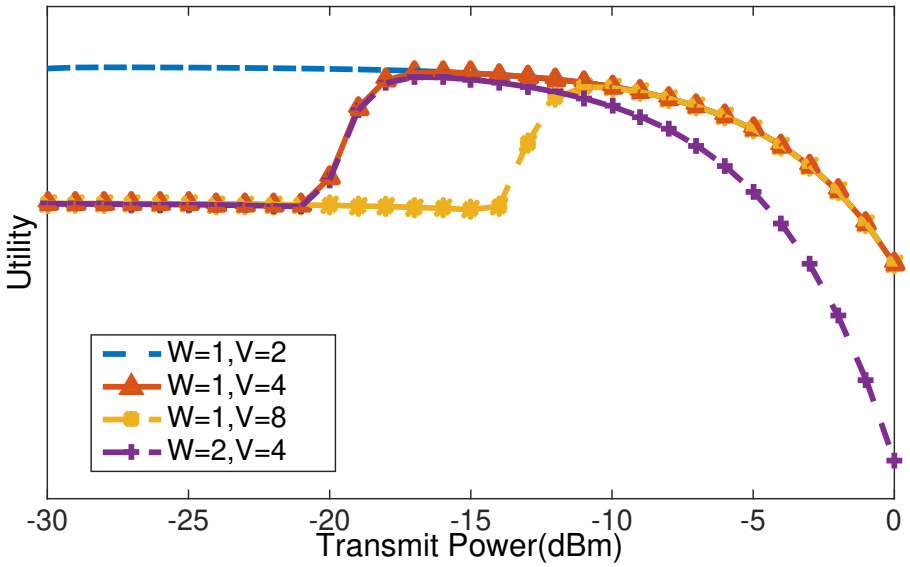

Figure 3.2: Average Utility Function for Different Exponents

$$U(p_i, pdr_i) = -p_i^w - \frac{d_i}{pdr_i^v}, \tag{3.16}$$

and **SINR Game** employs a utility function as:

$$U(p_i, SINR_i) = \frac{c}{p_i}(0.5 \cdot \exp(-\frac{SINR_i}{2})), \tag{3.17}$$

where the value of c is related to the packet size and data rate. Meanwhile, in **Sample-and-Hold** the current SINR is used as a prediction of the SINR in the next time slot, and the sensor can adjust the transmit power according to the prediction. **SINR balancing** propose a fully distributed power control scheme to mitigate inter-cell interference, which is expressed as $P_{t+1} = \max(\frac{\min(SINR, \bar{SINR})}{SINR} \cdot P_t, P_{min})$, to guide the evolve of transmit power. The comparison of the transmit power at each stage and the percentage of BANs reaching the PDR threshold (chosen as 0.9 according to IEEE 802.15.6

requirements [20]) is outlined.

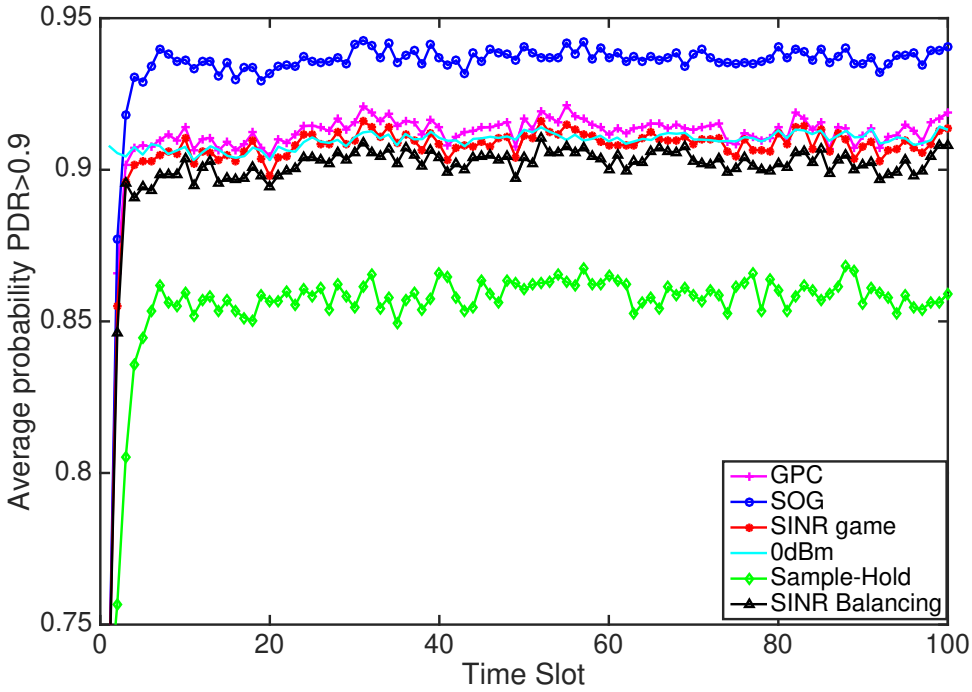

Figure 3.3: Average Probability PDR>0.9 under DPSK modulation. Socially-Optimal Game (SOG) is the method proposed here.

All power control methods are applied, with BPSK and DPSK modulation respectively and BCH(31,19) coding. It is shown in Figure 3.3, with DPSK modulation, that nearly 92.8% of the time the BANs in the proposed **SOG** achieve a PDR at 0.9 while this is only achieved 85% and 89.1% of the time for **Sample-and-Hold** and **SINR Balancing**. In Figure 3.4. a significant reduction in transmit power is shown for the proposed **SOG** with an average of -23.2 dBm compared to that for **Sample-and-Hold** and **SINR Balancing** method, averaging -15.2 dBm and -17.8 dBm respectively. For **GPC** it uses more than twice (3.5 dB) the transmit power of **SOG**, with 3% less probability than **SOG** that PDR can reach the target, from Figure 3.3. **SINR Game** uses

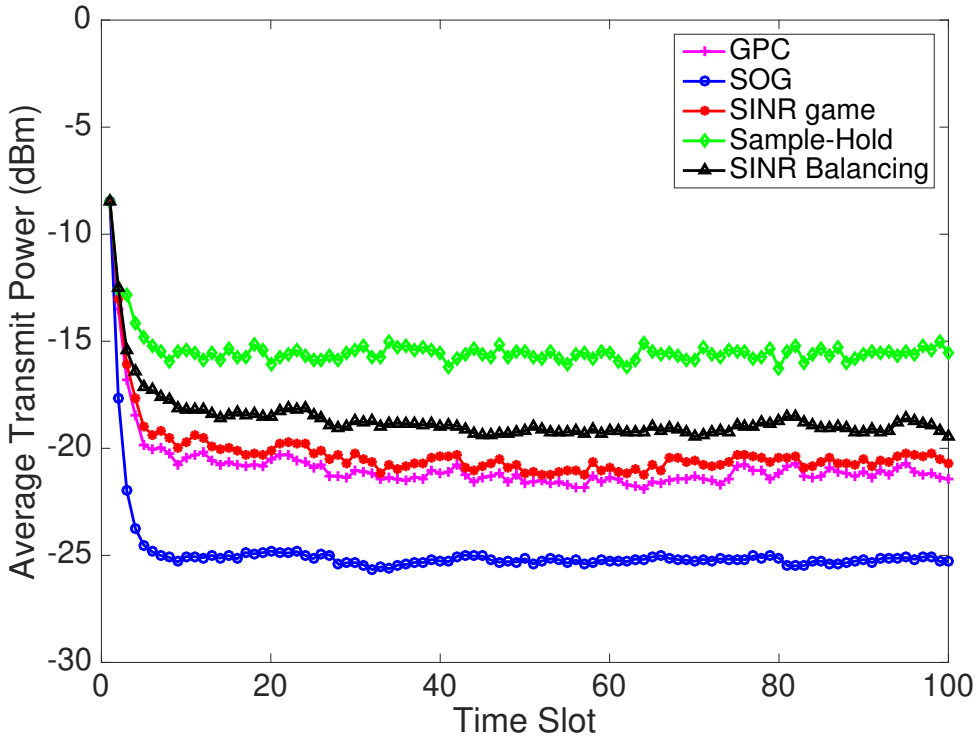

Figure 3.4: Average Transmit Power under DPSK modulation. Socially-Optimal Game (SOG) is the method proposed here.

more than 5 dB extra transmit power with average probability of 90% that PDR is greater than 0.9. Furthermore, compared with 0 dBm constant transmit power **SOG** has 3% greater probability that PDR can reach the target and 23 dB less transmit power. When BPSK modulation is employed, similar results with respect to comparing transmit power and PDR performance are obtained as summarised in Table 3.1. Using BPSK needs 0.7 dB less average transmit power than DPSK and improves the probability of PDR reaching the threshold by 1.5% for our proposed **SOG**.

The average circuit power consumption evaluated by non-linear mapping [106] is shown in Figure 3.5. The average circuit power consumption of the proposed **SOG** is around 1.96 mW for DPSK modulation. While from Fig-

Table 3.1: Performance under BPSK modulation. SOG is the proposed game.

	SOG	GPC	SINR-Game	SINR-Balancing	Sample and Hold
Transmit Power (dBm)	−23.9	−20.6	−20.1	−18.8	−15.4
Probability PDR > 0.9	94.3%	92.2%	91.5%	91.2%	86.5%

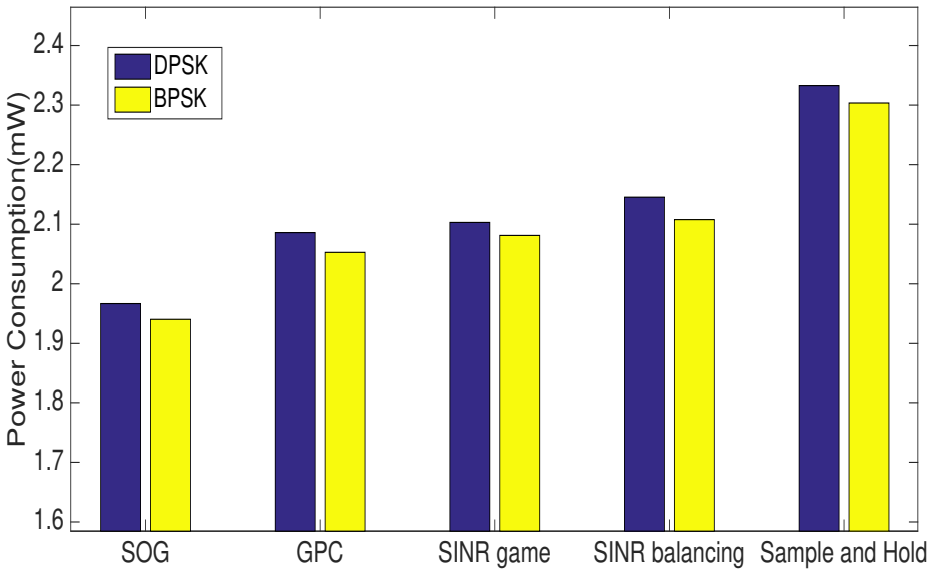

Figure 3.5: Circuit Power Consumption. SOG is the proposed game.

ure 3.5 with DSPK modulation, **SINR Balancing** uses 2.1 mW, while the **GPC** method and the **SINR Game** consumes around 2.08 mW and 2.09 mW of circuit power respectively. In Figure 3.5 the proposed **SOG** uses 17% less circuit power than **Sample-and-Hold** and 67% less than constant transmission at 0 dBm. Thus the proposed **SOG** will significantly extend BAN lifetime. Meanwhile, the power consumption for BPSK is 0.04 mW less than for DPSK modulation for all schemes as shown in Table 3.1.

3.6 Concluding Remarks

In this chapter, we have presented an non-cooperative game-theoretic transmit power control approach for closely-located BANs. The proposed method provides better interference mitigation and energy efficiency and guarantees the fairness of the system which always overlooked by other methods. It was mathematically proven that the Nash Equilibrium outcomes of each stage of the game are socially optimal for the system under practical constraints for both static and slowly time-varying channels. Meanwhile, the numerical results validate our analysis by demonstrating that the maximum of social welfare is achieved at the Nash Equilibrium for each player. This social efficiency analysis could be extended to other power control approaches.

Based on simulation results over different channel models, the proposed game can reduce circuit power consumption and prolong the lifetime of the battery's sensor node in a BAN. Moreover in a scenario with many BANs coexisting, 94% of the time the PDR of each BAN reaches a threshold PDR of 0.9 by adopting the proposed game. As we demonstrated in this chapter, game-theoretic methods enhance the performance of coexisting BANs. To further optimise scarce radio resources, in the next chapter, we will provide game-theoretic cross-layered design for interfering BANs.

Chapter 4

Game Theoretic Approaches to Time-Division MAC for Wireless Body Area Networks' Coexistence

4.1 Introduction

Toward the realisation of next-generation BAN enabled IoH, high levels of quality of service (QoS) of BANs are in great demand for the management of critical health information. Although in Chapter 3, we proposed the non-cooperative game that controls transmit power for BAN sensor that provides higher energy efficiency and PDR. The proposed method only provides a solution for resource allocation at the PHY layer. However, to improve QoS of BANs on other aspects, such as lower the latency, increase overall throughput, reduce retransmission rate and minimise packets discard probability, radio resource allocation schemes across different layers of the protocol stack are required. To address this, link adaptation mechanisms that exploit the interdependence between transmission scheduling and transmit power allocation can be used to provide cross-layer design. Further exploiting the strength of game theory, thereby, we propose a game-theoretic formulation of

a TDMA-based MAC protocol to achieve high energy efficiency, reduce inter-BAN interference, improve overall throughput and reduce latency across all co-existing BANs.

The study in this chapter has two principal features: (i) a novel MAC layer protocol and (ii) game-theoretic resource allocation schemes. The MAC layer protocol focuses on rescheduling unsuccessfully transmitted packets to reduce the probability of packet collision among other co-located BANs. Two games are proposed for better resource allocation: a Link Adaptation Game and a Contention Window Game (as an extension of the Link Adaptation Game). The Link Adaptation Game tunes the node's transmit power and data rate from the Nash equilibrium of its utility function to obtain optimised throughput (in terms of Packet Delivery Ratio, PDR) and power consumption. In the Contention Window Game, the sensor node adjusts its transmit probability by dynamically changing the contention parameters (contention window size), to improve throughput performance further and minimise transmission delay. Due to the difference in delay performance and power consumption, a trade-off of the two games can be made according to BAN application.

4.2 Proposed Time-Division MAC

Here, we propose a TDMA-based MAC protocol to achieve energy efficiency, reduce inter-BAN interference and obtain low delivery latency for co-existing BANs. Depending on the special random back-off mechanism to minimise the probability of packets collision among sensors in different BANs, the overall level of interference and power consumption can be consequently reduced.

4.2.1 System Model

We consider star-topology BANs that are closely located and coexisting. Each BAN consists of a single hub with multiple sensors as described in Figure 2.4. The hub is not energy-constrained, so the energy consumption of the sensor is mainly considered. The hub facilitates the main BAN operations such as synchronisation, re-transmission and determining transmission schedules.

As interference across all co-existing BANs is the main reason for dropped-packets and energy wastage, the following assumptions apply:

A1. All BANs are saturated, which means that they always have a packet to send (packer arrive rate is 1).

A2. Interference-dominated, where packet loss due to additive noise is negligible.

A3. All hubs are not energy constrained

A4. Time-slots across every superframe are normalised to unity

Within each BAN the sensor devices acquire data and use TDMA to transmit to the hub to avoid idle-listening and overhearing. The intra-BAN interference is collision free when each sensor is transmitting using round-robin scheduling. However, it is infeasible to implement central coordinator among co-existing BANs that are closely located. Thus, the transmission between different BANs can not be synchronised. Therefore, co-channel interference may arise due to collisions amongst concurrent transmissions made by sensors in different BANs.

4.2.2 MAC Layer Specification

4.2.2.1 Superframe Structure

As described above, the sensors in each BAN are synchronised by periodic transmission of the superframe, with constant length T_s. Each superframe consists of a beacon, ACK reception, several slots used for data transmission and an inactive (idle) period. The beacon is configured to contain control information for broadcasting to sensors. The turnaround time is negligible. After the reserved transmission slots followed by ACK reception, the remaining slots in the superframe are considered as an inactive or idle period. The basic structure of the superframe is depicted in Figure 4.1.

Each superframe starts with broadcasting a beacon packet from the hub to the sensors, which consists of information for establishing links and synchronisation. Due to Assumption A.3, the probability that beacon or ACK is not received at the sensor is negligible, as the hub can apply higher transmit power to avoid SINR outage. The beacon is immediately followed a data frame, which mainly consist of up-link data traffic from the sensors to the hub.

Figure 4.1: Superframe Structure

4.2.2.2 Back-off Mechanism

In order to avoid collisions when many BANs sharing the medium, a back-off algorithm is used in here for BAN MAC. Since, if a transmission fails due to interference, it is highly likely that a following transmission will also be blocked, which results in extreme inefficiency. Keeping the sensor in back-off states for a period of time will increase throughput and reduce collision probability. Figure 4.2 also illustrates the back-off mechanism and the operation mode of the sensor. As depicted in Figure 4.2, all the sensors may be in one of three different operation states: back-off state, channel occupancy state, and inactive state. If the transmission is not correctly received by the coordinator, then it will back-off its next beacon broadcast to reduce the collision cause by consecutive transmission. Figure 4.2 illustrates the back-off mechanism

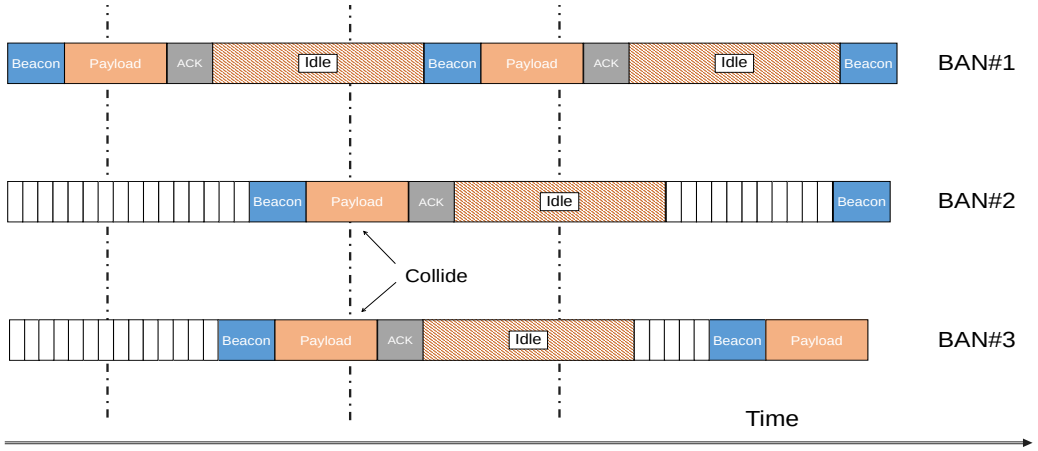

Figure 4.2: Timing Scheme and Operations

and the operation mode of the sensor. As depicted in Figure 4.1, all the sensors may be in one of three different operation states: back-off state, channel occupancy state, and inactive state.

During the random back-off procedure, the back-off counter w is set as

a uniformly distributed random integer number over the interval $[1, W]$, i.e., $w \in \mathcal{U}(1, W)$. The value W, namely the contention window size is determined by the back-off stage b and the number of maximum back-off stages m. The back-off stage b equals to the number of transmissions failed for the packet. After each successful transmission attempt, W is set as 0. After each unsuccessful transmission, W is set as the W_{min} multiplied by the persistence coefficient λ ($W = \lambda^b W_{min}$), until it reaches its maximum value $W = \lambda^m W_{min}$. In this paper $\lambda = 2$, so that the contention window size, W is doubled after each failed transmission. In order to analytically evaluate the performance of the MAC layer protocol, we develop a Markov Chain model. We demonstrate that performance metrics numerically obtained from the steady-state solution of the Markov Model matches monte-carlo simulated results. Both analytical results and simulated results show that the proposed MAC protocol reduces the packet collision and improves the throughput, when multiple BANs are co-located. The basic algorithms are listed in Algorithm 2. If the payload is not received by the sensor, the hub executes a random back-off procedure to reduce the collision probabilities among BANs and the next beacon is transmitted after the back-off counter reaches zero.

4.2.3 Markov Model

A Markov Model was initially proposed by Bianchi for IEEE 802.11 DCF [107]. The model describes the basic fundamental process of MAC layer scheme through a Markov Chain. The model has been extended in several directions.

In this section, we proposed a discrete-time Markov Chain, which models the operation of the proposed algorithm in the tagged BAN and captures the key characteristics of the MAC layer timing scheme, such as, superframe

Algorithm 2 The Proposed MAC Layer Protocol

1: Initialising MAC Parameters when, $W = CW_{min}$, $b = 0$,$w = 0$
2: Hub send the sensor a beacon to sensor i with synchronisation information
3: After receive the beacon, the sensor i transmit data using the scheduled slots.
4: **if** Hub successfully receives the packet **then**
5: Sensor keeps inactive for a period of T_{idle} until the end of the superframe.
6: **go to** 2
7: **close**;
8: **else if** The transmission fails because of the interference, the sensor will not receive the ACK **then**
9: $b \leftarrow b + 1$
10: **if** $b >$ MaxRetransmissionLimit **then**
11: Discard The Packet
12: **go to** 2
13: **close**;
14: **end if**
15: The hub calculates the back-off length
16: $W_b = \lambda^b CW_{min}$
17: $w = random\{0, W_b\}$
18: Sensor keeps inactive for a period of T_{idle}, and the hub starts back off at the end of the superframe.
19: $w \leftarrow w - 1$
20: **if** $w = 0$ **then**
21: **go to** 2
22: **close**;
23: **else**
24: **go to** 19
25: **end if**
26: **end if**

structure, and re-transmission mechanism. The Markov Chain model can help us investigate features of the proposed MAC layer timing scheme, such as throughput and delay.

Figure 4.3. shows the state transition diagram of the Markov Chain of the proposed MAC scheme. In the Markov Model, the state at time t for tagged BAN is represented by the stochastic process $(b(t), w(t))$. $b(t), w(t)$ represent

the back-off stage and the back-off counter respectively. Here, $b(t) \in [0, m]$ represents the back-off stage of the tagged BAN at time t, where m is the maximum back-off stages. $w(t)$ represents the value of the back-off counter at time t.

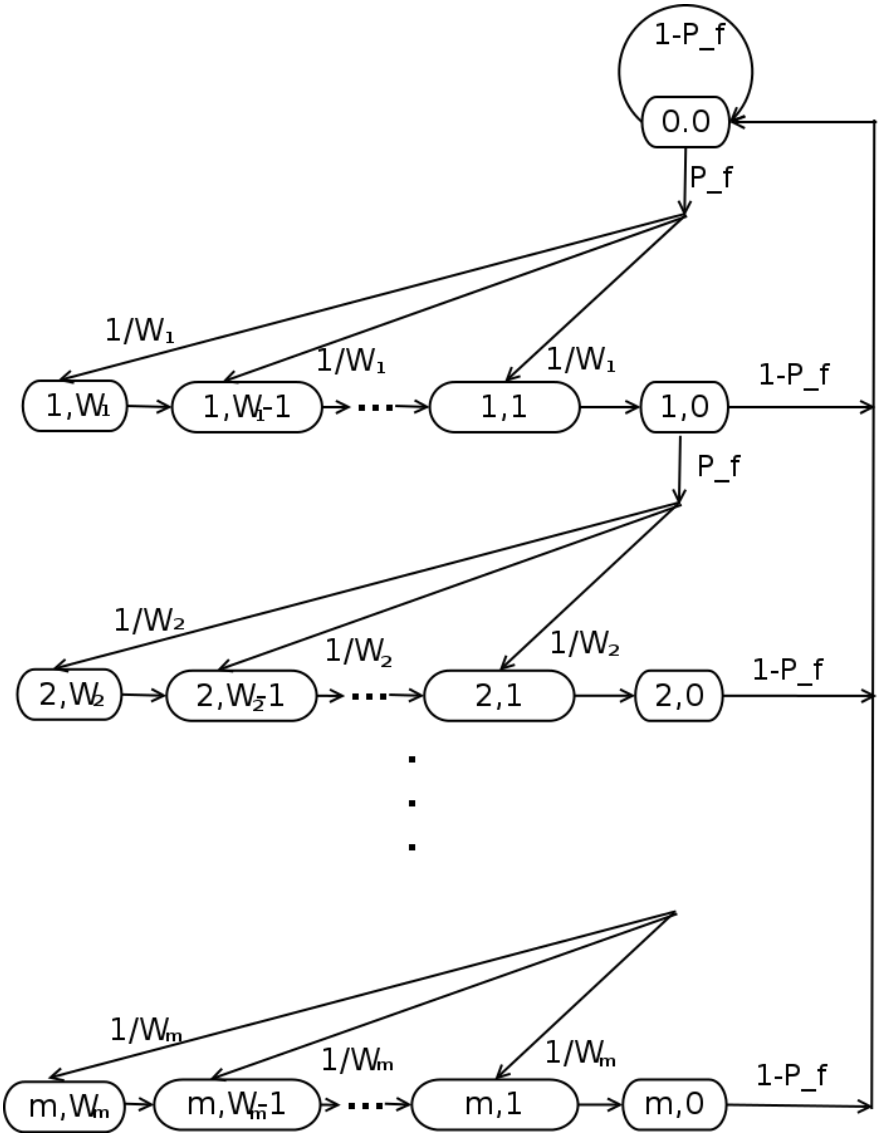

Figure 4.3: Markov Chain for Proposed MAC Scheme

Initially, the values of back-off counter and re-transmission counter are set to zero. In the back-off stage, when the value of back-off counter reaches zero,

the hub will re-transmit the packet. If the transmission attempt is successful, the state will move to $\{0,0\}$, ($b(t)$=0, $w(t)$=0), and the BAN starts to transmit in the next frame after the in-active period. Otherwise, the sensor moves from back-off stage j to $j+1$ with its re-transmission counter incremented by 1. In addition, at the state $\{m,0\}$, the data from the sensor will either be successfully transmitted or discarded by the sensor. The parameter p_f is the probability of transmission failure due to the inter-BAN interference, which is the probability of ACK reception under collision of packets. The state transition probabilities are:

$$\begin{cases} P_r((i,j-1)|(i,j)) & = 1 \\ P_r((i+1,j)|(i,0)) & = p_f \frac{1}{W_i} \\ P_r((0,0)|(i,0)) & = 1-p_f \\ P_r((0,0)|(0,0)) & = 1-p_f \end{cases}, \tag{4.1}$$

where $W_i = 2^i CW_{min}, i \geq 1$.

4.2.3.1 Steady-State Solution

Here, we derive the steady solution of the Markov Chain described in Figure 4.3. Let the stationary distribution of the Markov Chain be, $b_{i,j} = \lim_{t\to\infty} \Pr(s(t) = i, b(t) = j)$, where $i \in (0,m), j \in (0,W_i)$. Then, we can calculate the stationary distribution for all the values of $b_{i,j}$. According to the state transition probabilities (4.1), $b_{i,j}$ can be expressed as functions of the value $b_{0,0}$ and of the transmission failure probability p_f. $b_{0,0}$ is finally determined

by imposing the normalisation condition:

$$b_{0,0} + \sum_{k=1}^{m} \sum_{j=0}^{W_k} b_{k,j} = 1, \tag{4.2}$$

that simplifies to:

$$b_{0,0} = \frac{2(1-p_f)(1-2p_f)}{2CW_{min}p_f(1-(2p_f)^m)(1-p_f) + (2+p_f)(1-p_f^m)(1-2p_f)}. \tag{4.3}$$

We can now get τ, which is the probabliity of a BAN sensor attempts to carry out a superframe transmission in a randomly chosen slot time. As each transmission starts when the back-off counter reaches zero, τ can be expressed as:

$$\tau = \sum_{k=0}^{m} b_{k,0} \tag{4.4}$$

$$= \frac{2(1-2p_f)(1-p_f^{m+1})}{2CW_{min}p_f(1-(2p_f)^m)(1-p_f) + (1-2p_f)(2+p_f)(1-p_f^m)}. \tag{4.5}$$

The probability of transmission failure p_f is the intersection of the probability of collision and the packet error rate (PER):

$$p_f = p_c \cap \text{PER} = (1 - \text{PDR})(1 - (1-\eta_\tau\tau)^{N-1}), \tag{4.6}$$

where PDR is the packet deliver ratio and η_τ is a coefficient that normalises τ by the average number of time slots staying in an arbitrary state of the Markov Chain. The values of p_f, τ and $b_{0,0}$ can be solved using Eq. (4.5), Eq. (4.6) respectively.

4.2.4 MAC Layer Performance

By comparing the analytical modeling with simulation results, we can evaluate the accuracy of the Markov Model described in the previous section. We simulated N single-link star topology BANs co-existing in the saturated regime (all BANs always have a packet to transmit). A performance analysis is also conducted based on the steady-state solutions. We assumed when intra-BAN interference occurs that the packets collision will result in transmission failure $p_f = p_c$ as PER $= 1$(PDR $= 0$).

In our experiment, the data rate is set as $32\,\mathrm{kbit\,s^{-1}}$. The retransmissions limits $m = 4$, and the minimum back-off length $CW_{min} = 64$. The duration of one superframe is $T_s = 64$ms. Each superframe consist of 256 time slots. Each time slot last for $T_{\text{slot}} = 250$µs. The beacon, payload and the ACK are set to be 30, 110, 10 bytes respectively.

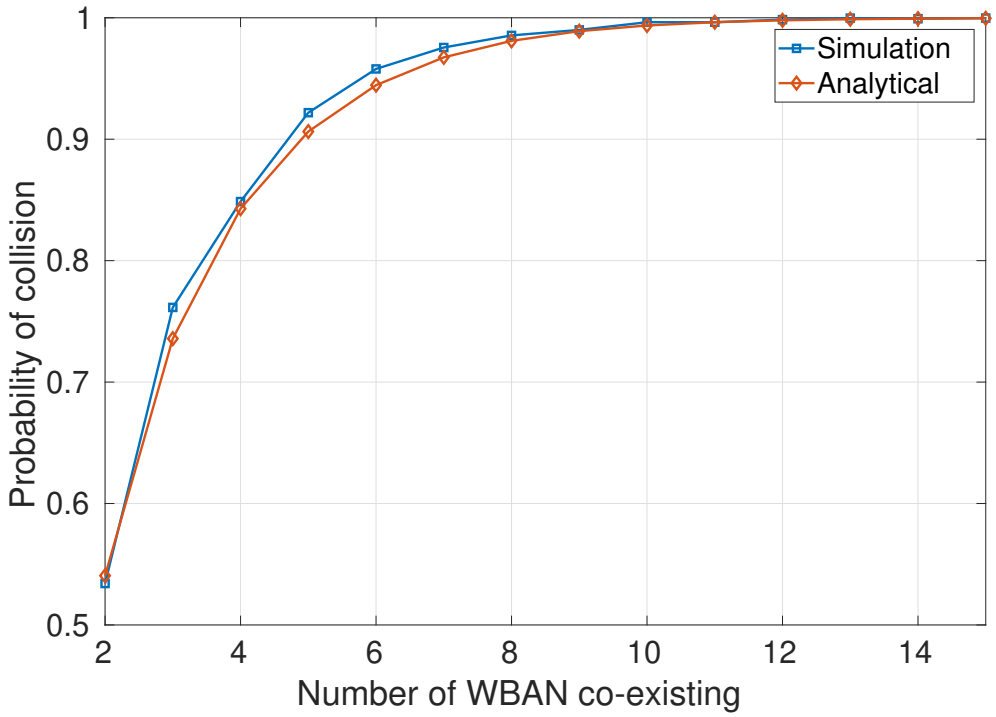

Figure 4.4: The Comparison of Probability of Collision

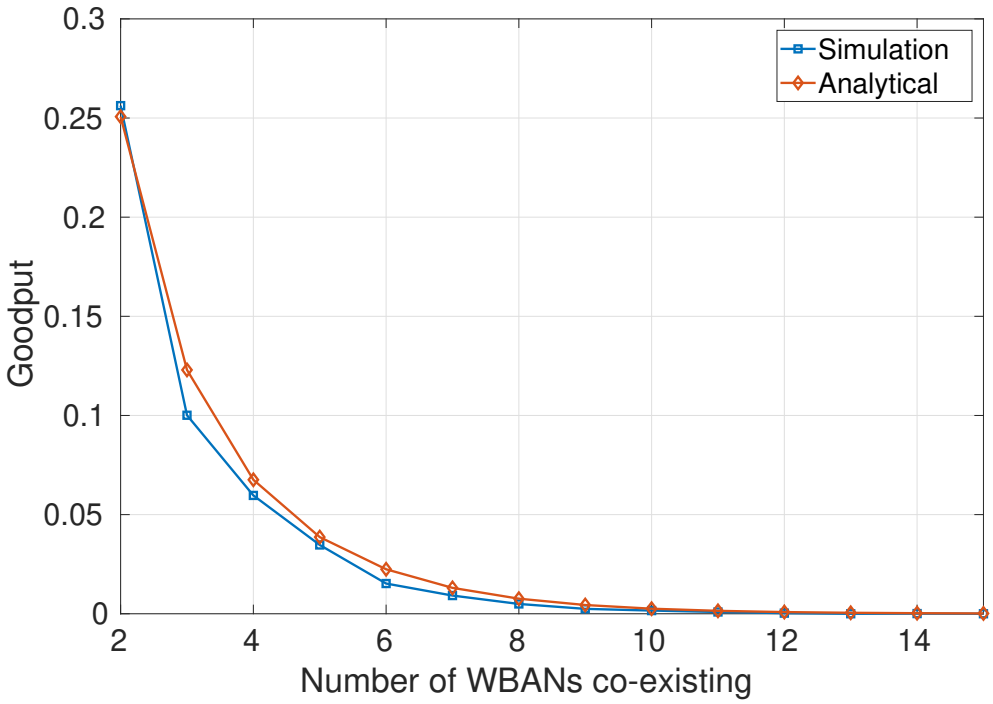

Figure 4.5: The Comparison of Goodput

Figure 4.4 and Figure 4.5 show that, in terms of Probability of Collision and Goodput (S), the analytical model matches the simulation results accurately. Goodput is defined as the ratio between time elapsed to delivery the payload and the total time. Therefore, analytically, Goodput is calculated as:

$$Goodput(S) = \frac{(1-p_f)\tau T_{payload}}{\tau T_s + (1-\tau)T_{\text{slot}}}, \tag{4.7}$$

where

$$T_s = T_{beacon} + T_{payload} + T_{ack} + T_{idle}, \tag{4.8}$$

$T_{beacon}, T_{payload}, T_{ack}, T_{idle}$ represent the duration of beacon, payload, ACK and idle respectively. However, weak matching occurs when less BANs are co-existing, as randomness of the back-off counter in the simulation is relatively large. Figure 4.5 shows that when more BANs are co-located, the system's

Goodput decreases as the collision probability increases.

4.3 Link Adaptation Game

The majority of existing game theoretic algorithms in BANs only focus on transmit power control. However, when considering saturated traffic conditions, in particular interfering networks, selfishly changing the transmit power may increases packet losses, and thus, reduce the overall throughput. From previous numerical analysis, we observed that greater system efficiency can be achieved by varying performance-impacting characteristics such as modulation and data rate. One of the objectives in this paper is to exploit the above MAC layer scheme to find a method that further increases the system's energy efficiency and reduces interference. In this section, we develop a utility-based game theory model that is a function of two variables: transmission power and data rate to address interference and packet contentions. The transmitter chooses the value of the transmit power and data rate to maximise energy efficiency whilst meeting the PDR requirements. Since the transmitter's action will be a function of the choice of data rate and transmit power, these two parameters need to be executed jointly. According to experimental results, an increase in data rate will result in the BAN's PDR degradation in the same SINR regime. However, the length of payload transmission time is also related to the BAN's data rate, so that higher data rate may also reduce the intra-BAN packet collision probability as the transmission time is reduced, which mitigates interference. Furthermore, the proposed game theoretic algorithm handles packet re-transmissions, until the retry limit is reached.

4.3.1 Game-theoretic System Model

We consider the system model of the form described in Section III where multiple BANs are co-located. All BANs are within each others interference range, and the corresponding transmitters always have packets to send. our proposed TDMA scheme with the same random back-off scheduling mechanism is applied in all BANs and the minimum back off slot length cannot be changed. There are no pre-assigned priorities among different BANs such that all links can expect identical priorities in traffic.

Each coexisting BAN is a player in the Link Adaptation Game, the player set is denoted by $\mathbf{N} = \{1, 2, 3...N\}$. Within each BAN, the sensor adapts its power and data rate by utilising the game-theoretic algorithms. Data rate of BAN i, R_i is chosen from a discrete finite set $\overline{R} = \{R_{min}, ..., R_{max}\}$, where R_{min} is the base data rate and R_{max} is the maximum data rate. In each packet transmission, applying different data rate will changes the PDR (as shown in Table 4.1). Additionally, each BAN can adjust its power P_i within $[P_{min}, P_{max}]$, therefore, the action space of player $i \in \mathbf{N}$ is defined as the pair $A_i = (P_i, R_i)$, where P_i is the transmit power of player i and R_i is the data rate of player i. The aggregation of all players action is denoted as $\mathbf{A} = (\mathbf{P}, \mathbf{R}) = \{\mathbf{A_1}, \mathbf{A_2}...\mathbf{A_n}\}$.

It is obvious that each player is always trying to maximising its own utility. However, due to the non-cooperative nature of this game, it is easy to see that in an attempt to maximize its own benefits at any cost [64, 108], each BAN is likely to consume maximum power, and the highest data rate. This will also create excessive interference, leading to performance degradation. To penalise the use of excessive transmit power, a pricing mechanism is intro-

duced, where the utility function of each player is defined as follows:

$$U(P,R) = -c \cdot P^g + \ln(1 + \mathrm{PDR}(P,R)) - q \cdot \frac{1}{R}, \tag{4.9}$$

where the coefficients in the cost function c, g, q, are positive constants that can be tuned depending on channel conditions. The linear cost function (where the exponent $g = 1$) is commonly used in the literature, however, in the proposed game g is generally greater than 1 to provide strictly concavity. c, q are constant non-negative weighting factors.

In Eq. (4.9), a sigmoid approximation of PDR is introduced. This model has been shown to be capable of approximating the PDR versus SINR of a wireless channel [109]. Here, the SINR is defined as:

$$\gamma_i = \frac{h_{ii}P_i}{\sum_{j=1,j\neq i}^{N} h_{ij}P_j + \sigma^2}, \tag{4.10}$$

where, h_{ij} represents the channel attenuation between BAN i and BAN j. h_{ii} denotes the on-body channel attenuation in BAN i. σ is the noise gain. The sigmoid PDR function of SINR is presented as follows:

$$\mathrm{PDR} = \exp\left(\alpha \cdot \gamma^{\beta}\right), \tag{4.11}$$

where α, β of the sigmoid model that best approximate the simulation curves are selected by computer-aided search and summarised in Table 4.1. Figure 4.6 shows the comparison between approximated and simulated PDR vs. SINR for different data rates ($R_1 \sim R_5$) respectively.

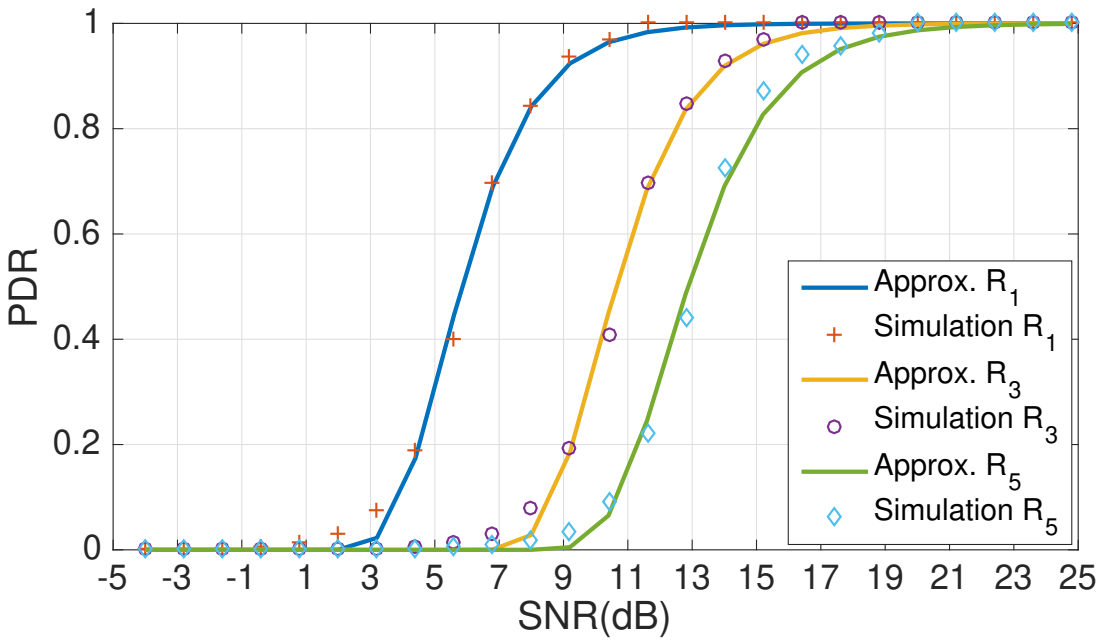

Figure 4.6: PDR vs. SINR

Table 4.1: Coefficients for PDR Estimation

Data Rate	α	β
$R_1 = 25.6kbps$	-100.02	-3.66
$R_2 = 51.2kbps$	-214.95	-2.82
$R_3 = 76.8kbps$	-663.69	-2.79
$R_4 = 102.4kbps$	-1182.7	-2.73
$R_5 = 128.0kbps$	-1433.5	-2.58

4.3.2 Nash Equilibrium

The Nash Equilibrium is a set of strategies that guarantee the best response of each player with respect to the chosen utility. In the proposed non-cooperative game, the game is played by rational players, which implies that every player adopts the strategy achieving the Nash Equilibrium. For each sensor, the main steps of the Link Adaptation Game are described in Algorithm 3.

Definition 4.1. Let $\mathbf{A}^* = (\mathbf{P}^*, \mathbf{R}^*)$ be the Nash Equilibrium in the Link Adap-

Algorithm 3 Main steps of Link Adaptation Game

Initialising MAC Parameters when, $CW = CW_{min}$, $b = 0$,$w = 0$
Hub sends a beacon to sensor i with synchronisation information
After receiving the beacon, the sensor i transmits data using the scheduled slots with $(P(t), R(t))$.
if Hub successfully receives the packet **then**
    The Hub choosing the transmit power and rate for next transmission by Eq. (4.13):$\{P_i(t+1), R_i(t+1)\} = \arg\max U\{(P_i, R_i), \mathbf{P}^*_{-\mathbf{i}}, \mathbf{R}^*_{-\mathbf{i}}\}$
    The Hub keeps inactive for a period of T_{idle} until the end of the superframe.
    go to 2
    $i \leftarrow i + 1$
    $t \leftarrow t + 1$
    close;
else if The transmission fails because of the interference, the sensor will not receive the ACK **then**
    $b \leftarrow b + 1$
    if $b >$ MaxRetransmissionLimit **then**
        Discard The Packet
        go to 2
        close;
    end if
    The Hub choosing the transmit power and rate for next transmission by Eq. (4.13):$\{P_i(t+1), R_i(t+1)\} = \arg\max U\{(P_i, R_i), \mathbf{P}^*_{-\mathbf{i}}, \mathbf{R}^*_{-\mathbf{i}}\}$
    The hub calculates the back-off length
    $W = \lambda^b CW_{min}$
    $w = random\{0, CW\}$
    The Hub keeps inactive for a period of T_{idle}, and starts back off until the end of the superframe.
    $w \leftarrow w - 1$
    if $w = 0$ **then**
        go to 2
        $t \leftarrow t + 1$
        close;
    end if
end if

tation Game, then for every $i \in N$:

$$U(P_i^*, R_i^*) \geq U\{(P_i, R_i), \mathbf{P^*}_{-i}, \mathbf{R^*}_{-i}\}, \tag{4.12}$$

where $(\mathbf{P_{-i}}, \mathbf{R_{-i}})$ represents all other player strategies except for player i. At the end of every transmission (say t), players update their next transmit power and rate jointly to maximise the outcome of adapting the utility function based on the current SINR:

$$\{P_i(t+1), R_i(t+1)\} = \arg\max U\{(P_i(t), R_i(t)), \mathbf{P^*}_{-i}, \mathbf{R^*}_{-i}\}. \tag{4.13}$$

The action profile $\mathbf{P^*} = (P_1^*, P_2^*, P_3^* ... P_n^*)$ for $n \geq 2$ is the best response towards $\mathbf{P^*}_{-i}$.

4.3.3 Existence and uniqueness of the Nash equilibrium

The existence and uniqueness of the Nash Equilibrium of the proposed game are proved as follows:

Lemma 1. The action space $\overline{A} = (\overline{P}, \overline{R})$ is not a convex set. However, under the condition that R is fixed, $\overline{A} = (\overline{P}, \overline{R})$ is a convex set.

Proof. We simply choose two points, $A_1 = (P_{max}, R_1)$, $A_2 = (P_{max}, R_2)$ that have the same power component. A line connecting these points consists of only two points A_1,A_2 themselves. The intervening points on this line do not belong to (P, R). Hence, (P, R) is not convex. However, suppose the data rate is fixed at, say R_1. We note that a convex combination $A' = \Lambda A_1' + (1 - \Lambda) A_2'$, $\Lambda \in [0, 1]$, where $A_1' = (P_1, R_1)$, $A_2' = (P_2, R_1)$ are any two arbitrarily selected actions in A, such that $P_{min} < P_1, P_2 < P_{max}$ belongs to the set $\overline{A}$. Hence the set $\overline{A}$ is convex when R is fixed. □

Theorem 4.1. (Existence) The game G admits at least one Nash Equilibrium, when assuming R is fixed.

Proof. In game G, for BAN i, $i \in \mathcal{N}$ the following condition can be verified. When the data rate of BAN i is fixed, the action set $A = (P, R)$ is a nonempty, convex, bounded in finite dimension vector space as proved in **Lemma** 1. The utility function U is continuous for all $P_i \in [P_i^{min}, P_i^{max}]$. As the first derivative of the utility function U is well defined as:

$$\frac{\delta U_i}{\delta P_i} = -c \cdot g P^{g-1} + \left(1 - \frac{1}{(1 + \text{PDR}_i)}\right) \alpha\beta \frac{\gamma_i^{\beta}}{P_i}, \tag{4.14}$$

where $\frac{|h_i^i(k_i)|^2}{I\_i} = \frac{\gamma_i}{P_i}$, therefore, as $P_i \in [P_i^{min}, P_i^{max}]$ is real and the PDR_i is non-zero, the Theorem 4.1 is proved. □

Theorem 4.2. (Uniqueness): The Nash Equilibrium in each stage of the game G is unique, and independent of history so it is a unique sub-game perfect equilibrium.

Proof. The second derivative of $U(\cdot)$ is shown to be always negative $\forall i$, so that $U(\cdot)$ is strictly concave.

$$\begin{aligned}\frac{\delta^2 U_i}{\delta P_i^2} = -c \cdot g(g-1) P_i^{g-2} + \left(1 - \frac{1}{(1 + \text{PDR}_i)}\right) \gamma_i^{\beta} \alpha\beta(\beta - 1)/P_i^2 \\ - \frac{\text{PDR}_i}{(1 + \text{PDR}_i)^2} \alpha^2 \beta^2 \gamma_i^{2\beta}/P_i^2,\end{aligned} \tag{4.15}$$

where PDR_i is always positive and between (0,1), and the term $(\beta - 1)$ is less than 0. In addition w is positive, thus $\frac{\delta^2 U_i}{\delta P_i^2} < 0$. Therefore the utility function has a global maximum at P_i^* which occurs at the point where $\frac{\delta U}{\delta P_i} = 0$. □

However, in practice, the data rate R is not always fixed. Hence, we need to make sure that the game only admits a unique Nash Equilibrium solution over the action space $\overline{A}$. As the concavity of the utility function leads to

the uniqueness of the Nash Equilibrium, we use the concept of a potential game [110], which provides useful properties concerning the justification of the Nash equilibrium.

4.3.4 Forming a Potential Game

For game G, when in a high PDR regime (where the system usually operates), we can get the following approximation using Taylor's series for the last term in Eq. (4.12):

$$\ln(1 + \text{PDR}(A_i, A_{-i})) \approx \ln(2) + \frac{\alpha \cdot \gamma^{\beta}}{2} + \frac{(\alpha \cdot \gamma^{\beta})^2}{8} ... \tag{4.16}$$

Substituting this approximation in to the utility function (only takes the first order term), we can get a new game with utility function defined as:

$$U_P(P, R) = -c \cdot P_i^g - q \cdot \frac{1}{R_i} + \ln(2) + \frac{\alpha(R_i) \cdot \gamma^{\beta(R_i)}}{2} \approx U(P, R). \tag{4.17}$$

Thus we transform the game G to a potential game denoted by $G_P = \{\mathbf{N}, \mathbf{A}, U_P\}$, where U_P is the new utility function.

We firstly provide the definition of the exact potential game, and proceed to show that the game belongs to the class of exact potential games.

Definition 4.2. A game is said to be an exact potential game if there exists a function satisfying:

$$U(S_i, S_{-i}) - U(T_i, S_{-i}) = F(S_i, S_{-i}) - F(T_i, S_{-i}), \tag{4.18}$$

where F is called the potential function that can map the action space of the game in to a real space.

The Game G_P is an exact potential game, with a potential function defined as:

$$F(A) = \sum -cP_i^g - q\frac{1}{R_i} + \frac{\alpha(R_i)\cdot\gamma^{\beta(R_i)}}{2}. \tag{4.19}$$

Notice that we discard $\ln(2)$ in the utility function when constructing the potential function as the constants can be canceled out. We can see that F satisfies the Definition 2.1 in [111]:

$$\begin{aligned} F(A_i, A_{-}i) - F(T_i, A_{-i}) &= -cP_i^g - q\frac{1}{R_i} + \frac{\alpha\cdot\gamma^{\beta}}{2} - cT_i^g \\ &- q\frac{1}{R_{T_i}} + \frac{\alpha\cdot\gamma^{\beta}}{2} = U_P(A_i, A_{-i}) - U_P(T_i, A_{-i}), \end{aligned} \tag{4.20}$$

where $T_i = (P_{T_i}, R_{T_i})$, and thus it is a potential function of the game G_P. Also, game G_P is a best response potential game, which is defined as :

Definition 4.3. The game G is a best-response game if and only if a potential function F exists such that,

$$\arg\max U(A_i, A_{-i}) = \arg\max F(A_i, A_{-i}), \tag{4.21}$$

according to [112], this leads to the following lemma:

Lemma 2. For the best-response game G defined over action space $\overline{A}$, with a potential function F, then i f $A \in \overline{A}$ maximises F, then it is a Nash Equilibrium for G.

4.3.5 Large Midpoint Property and Discrete Concavity

For an exact potential game, the change of the potential function attributes the same amount of change in a player's utility function due to its strategy

deviation. A concave potential function guarantees that every Nash equilibrium of the game also maximises a potential function. Therefore, with the help of the results in [113] on discrete concavity for potential games, we can prove the uniqueness of the Nash equilibrium in G_p: since the maximiser in the potential function F is unique, so is the Nash Equilibrium in game G. The large midpoint property (LMP)[113] is defined as:

Definition 4.4. For a function defined over discrete set satisfies LMP if for any $x, y \in X$ with $|x - y| = 2$,

$$\max_{|x-z|=|z-y|=1} f(z) = \begin{cases} > \min\{f(x), f(y)\}, \text{if} f(x) \neq f(y) \\ \geq f(x) = f(y), \text{otherwise} \end{cases} \tag{4.22}$$

We show that the potential function satisfies the LMP for the discrete strategy $\overline{R}$. As data rate $[R_{min}, R_{max}]$ is discrete, and $\overline{P}$ is continuous, we have the following theorem:

Theorem 4.3. For a certain power strategy $P \in \overline{P}$, the potential function $F(A)$, where $A = (P, R)$ satisfies LMP for $R \in \overline{R}$.

Proof. See Appendix 8.2. □

This leads to the following proposition:

Proposition 4.1. Suppose that $A = (P, R)$ satisfies LMP for $R \in \overline{R}$. Then, only if $F(A = (P, R_x), A_{-i}) \geq F(A = (P, R_y), A_{-i})$ for all y, $F(A = (P, R_x), A_{-i}) \geq F(A = (P, R_y), A_{-i})$ for all $|x - y| \leq 1$

This means that if LMP is satisfied for a discrete potential function, then the local optimality in the potential function implies global optimality. Thus, when at a certain transmit power level, only one maximiser exists over the

discrete set of data rate. The proof of the Proposition 4.1 is shown in Appendix 8.3. As **Theorem 4.2** shows that when R is fixed, the utility function admits one optimiser (maximiser). Hence, for exact potential game, the potential function also admits unique maximiser.

Theorem 4.4. The maximizer in the action space A, namely $A^o = \arg\max F(A_i, A_{-i})$ is unique and:

$$F(A^o, A_{-i}) = \max\{F(P^{*min}, R_{min}), F(P^{*1}, R_1)...F(P^{*max}, R_{max})\}, \tag{4.23}$$

where, P^{*x} is the maximiser when $R = R_x$. To show that the equilibrium of the propose potential game is unique, it is sufficient to prove that the set of maximisers of the potential function is a singleton, as the only maximiser is at R_x for one P^{*x}. Therefore, the best-response for the potential game G, $A^* = (P^*, R^*)$ is unique and equals A^o.

4.4 Contention Window Game

By implementing the proposed back-off algorithms, the collision during the frame transmission can possibly be avoided. Because, before each transmission, each BAN waits for a random time, based on the contention window size. This mechanism space out repeated retransmissions of the data packet in each BAN. Generally, each BAN is able to tune their transmission probability by modifying the back-off control parameters, such as CW_{min} value and maximum back-off stages (m value). Therefore, each BAN can dynamically choose a suitable contention window size by the contention level of current network to effectively improve system performance.

However, due to the non-cooperative nature of the system, each selfish player attempts to increase its utility by increasing its transmission probability or equivalent by decreasing its contention window size. Increasing the transmission probability by one player encourages other players to shorten their contention window sizes, which increases collisions, thus the delay and packets drop ratios are also increased. Here, we proposed the Contention Window Game G_{CW} based on the aforementioned MAC layer scheduling, which aims to balance the trade-off between packet delay and system throughput.

In the Contention Window Game, the action selected by any player is their minimum contention windows size CW_{min}, where CW_{min} is the action space. As described by the Markov Model, by changing the contention window size, players transmission probability can be adjusted accordingly. As, in a high PDR regime, we have the following approximation:

$$\tau \approx \frac{1}{p_f \cdot CW_{min} + 1}, \tag{4.24}$$

where p_f is transmission failure probability.

Empirically, in order to get the estimated number of players n_{est}, each node can measure p_f and τ through several counters independently. The number of coexisting BANs can be estimated from the following equations[114]:

$$\begin{aligned} \tau_{est} &= \frac{TransmittedFragmentCount}{SlotCount} \\ p_{est} &= \frac{AckFailureCount}{TransmittedFramentCount} \\ n_{est} &= f(p_{est}, \tau_{est}) = 1 + \frac{\ln(1 - p_{est})}{\ln(1 - \tau_{est})}, \end{aligned} \tag{4.25}$$

where p_{est} and τ_{est} denote the estimated failure probability and the estimated τ respectively.

TransmittedFragmentCounter that counts the total number of successfully transmitted data frames, ACKFailureCounter that counts the total number of unsuccessfully transmitted data frames and the SlotCounter that counts the total number of experienced time slots. (The historical data can be used to estimate the current parameters, and the length of how far we should trace back can be adjusted accordingly).

Algorithm 4 Main steps for Contention Window Game

1: After execute line 19 in Algorithm 3
2: The Hub estimated the number of coexisting BANs n_{est} by using Eq. (4.25)
3: After obtain n_{est}. The Utility Function $V(CW_{min})$ can be constructed as a function of w, where the PDR is obtained as PDR$(\mathbf{P}^*_{-\mathbf{i}}, \mathbf{R}^*_{-\mathbf{i}})$ from the Nash Equilibrium in the Link Adaptation Game.
4: Determine the minimum contention window size CW_{min} for that given sensor, which gives the Nash Equilibrium value of the Utility Function $V(CW_{min})$
5: **go to** 20 in Algorithm 3

The objective of the game is to reach a trade-off in maximising the throughput, and minimise delay. Following from the analytical model, the throughput of each BANs is positively correlated with the Goodput(S) in Eq. (4.7). The average delay for a packet to be transmitted successfully is estimated as:

$$\begin{aligned} D &= \sum_{i=1}^{m} P_{Bi} E[D_i] \\ &= \sum_{i=1}^{m-1} [p_f^i (1-p_f) \sum_{j=0}^{i} (\frac{W_j+1}{2} T_{\text{slot}} + T_s)] \\ &\quad + p_f^m \sum_{j=0}^{m} (\frac{W_j+1}{2} T_{\text{slot}} + T_s), \end{aligned} \tag{4.26}$$

where $E[D_i]$ is the average delay in state i. It is obvious that throughput, delay may have different units in different ranges, and they have to be

normalised. Therefore, the utility function is defined as the following:

$$V_i(CW_{min}) = d \cdot S - l \cdot D - P_{\text{Drop}}, \tag{4.27}$$

where $P_{\text{Drop}} = \tau {p_f}^{m+1}$ is the probability that a packet drops due to exceed maximum retry limits. The weights d, l can be adjusted based on different scenarios. The obtained results have shown that in game G_{CW}, each user improves its chance of successful transmission by increasing transmission probability, whilst this increase of transmission probability causes an increase in collision probability, as well. Such collisions will cause large delay in packets transmission and energy wastage led by PDR reduction. Thus, when at low interference level (high SINR regime), the nodes should select a smaller CW_{min} as the best strategy. In high interference environment (or low SINR regime), greater CW_{min} is more appropriate in order to reduce the collision probability. The game is implemented in a similar distributed manner to the Link Adaptation Game.

4.4.1 Existence and uniqueness of the Nash equilibrium

The existence and uniqueness of the Nash equilibrium point for the Contention Window game is guaranteed. The proof is given as follows.

Theorem 4.5. (Existence and Uniqueness): In each stage of the game G_{CW} exists a unique Nash Equilibrium.

Proof. Similar with the Link Adaptation Game G, the utility function in G_{CW} is differentiable and strictly concave over the convex set of the minimum contention window size CW_{min}. Therefore, according to [115], the game G_{CW}

admits a unique Nash Equilibrium. The details can be found in Appendix 8.1. □

4.5 Performance Evaluation

This section discusses the simulation results of our proposed resource allocation games in comparison with conventional schemes as well as gam-theoretic methods in the literature. To evaluate and validate the performance of the proposed game, we compare throughput, energy efficiency and delay with Adaptive CSMA/CA [116] and B^{2}IRS [74] with respect to varying numbers of coexisting BANs. The values of MAC layer parameters are listed above in Table 4.2, parameters that are mainly based on the IEEE 802.15.6 Standard [117]. In addition, a non-linear power estimation [106] is made to measure the actual circuit energy consumption, to provide a more realistic evaluation of the system.

Table 4.2: MAC Parameters

Parameters	Value
Superframe Length	80 *ms*
Allocated Time Slot Length	0.312 *ms*
Minimum Data Rate	25.6 kbit s^{-1}
Maximum Data Rate	1.28 Mbit s^{-1}
Payload	175 bytes
N_{Beacon}	20 bytes
N_{ACK}	10 bytes
CW_{min}	43.75 ms
MaxBackoffLimits (m)	4

4.5.1 Scenario 1

In this scenario, realistic empirical measurements [118] in an "everyday" scenario using small body-mounted "channel sounder" radios that operated at 2.36 GHz are adopted in the simulation. The measurement set contains both inter-BAN and intra-BAN channels of the coexisting BANs, which are measured in many different environments, involving human subjects doing a mix of distinct everyday activities. It should also be noted that the measurements are re-sampled by the parameters above, thus the channel attenuation remains constant in each superframe [119].

In our experiments, it has been observed that in the Link Adaptation Game more than 90% of the packets are delivered, which meets the requirement for 10% maximum packet error rates in the IEEE 802.15.6 BAN Standard [117]. It should also be noted that in B^2IRS, because the packets are rescheduled in a collision-free manner across BANs, no interference occurs. Therefore, as shown in Figure 4.9, the PDR performance of B^2IRS is almost optimal, although such a scheme brings significant penalties to delay and requires global coordination. Figure 4.7 and Figure 4.8 show the variation in throughput and delay, respectively, with different numbers of BAN coexisting. Figure 4.7 shows that the throughput reduces with more BANs actively coexisting. When compared with other methods, Link Adaptation Game provides the highest throughput, and Contention Window Game manages to maintain the lowest delay as shown in Figure 4.7 and Figure 4.8. In terms of circuit power consumption, as illustrated in Figure 4.10, the Link Adaptation Game uses the least power, which is around 0.3 $\mathrm{J\,bit^{-1}}$, while B^2IRS and Adaptive CSMA/CA use nearly 3 times and 8 times more respectively.

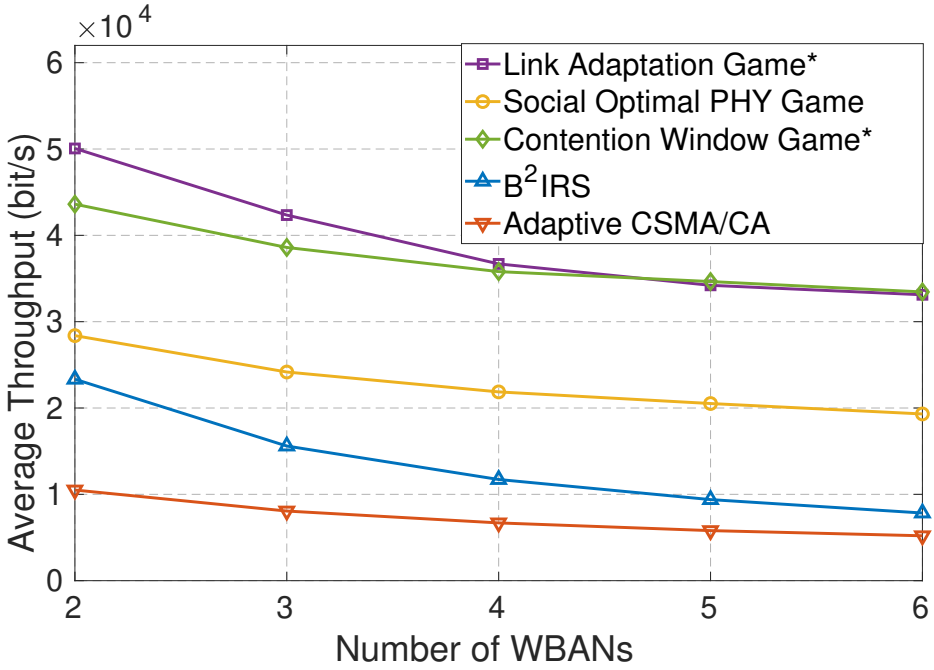

Figure 4.7: Throughput Performance of the proposed games compared to other methods under Realistic Measurement Channel Sets. Link Adaptation Game and Contention Window Game are the two proposed games. Social Optimal PHY Game is proposed in [64].

4.5.2 Scenario 2

The empirical measurements can only provide channel gains of up to 6 BANs coexisting, hence computer-simulated channels are also needed to obtain performance analysis under a crowded environment where many more BANs are co-located. In this simulation, both intra-BAN and inter-BAN channels are modeled in a similar manner to [64, 108]. It is assumed that up to 15 BANs with the same topology are coexisting and moving randomly within a 6×6 m^2 square area. The walking speed of the BAN wearer is modeled as 0.5 ± 0.1 m/s, which is updated every 1 ms. The channel attenuation is modeled as

$$h_i^j = A_t (d_o / d_i^j)^{(2.5/2)} A_{SE} A_{SC}, \tag{4.28}$$

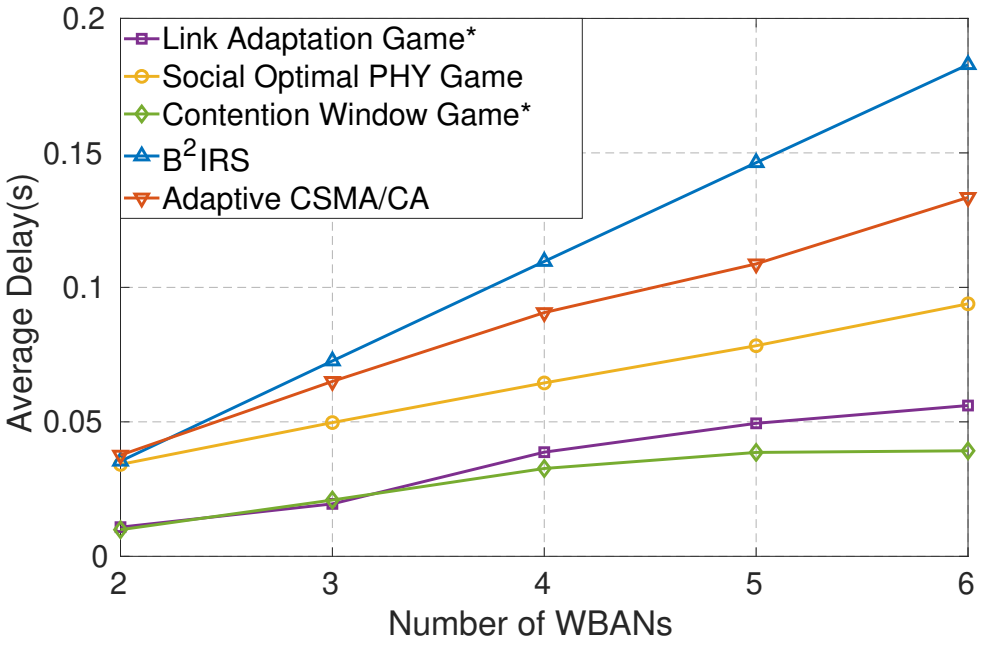

Figure 4.8: Delay Performance of the proposed games compared to other methods under Realistic Measurement Channel Sets. Link Adaptation Game and Contention Window Game are the two proposed games. Social Optimal PHY Game is proposed in [64].

where the path loss exponent is 2.5. d_i^j represents the distance between BAN i and j, and the reference distance $d_o = 5m$ corresponds to a channel attenuation of 50dB. The shadowing effect A_{SE} is assumed to be 42dB, and a Jakes model with Doppler spread of 1.1Hz as the $\mathcal{CN}(0,1)$ Rayleigh distribed small scale fading A_{SC} between BANs. Small-scale gamma with a mean 65 dB attenuation, a shape parameter of 1.31, and a scale parameter of 0.562 is employed for the on-body channels.

Basically, for the proposed methods, less than 10% of the packets are blocked. Again, PDR performances of B^2IRS and adaptive CSMA/CA are better than others, because of the low collision probabilities in these two methods.

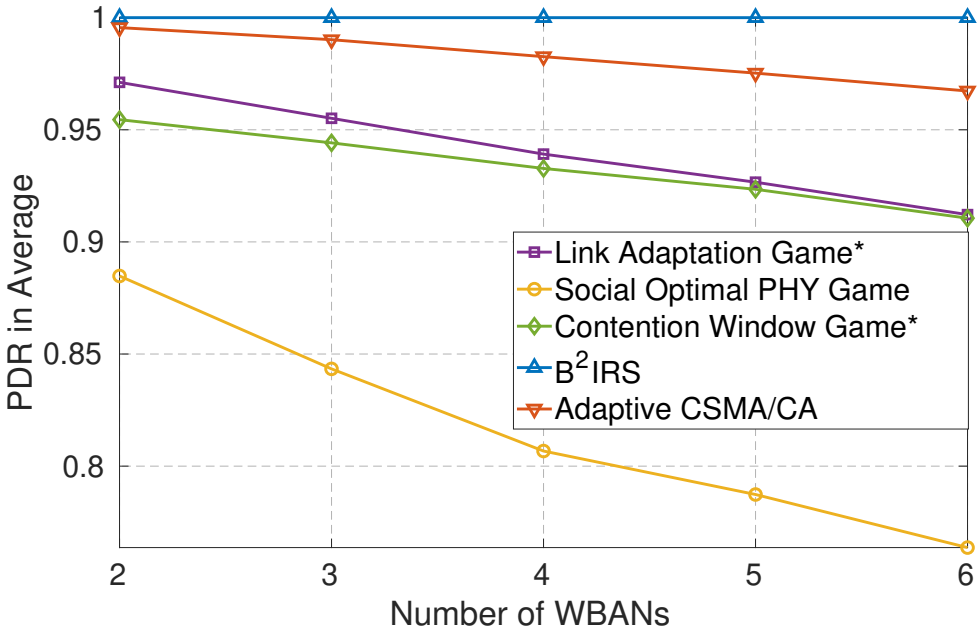

Figure 4.9: PDR performance of the proposed games compared to other methods under Realistic Measurement Channel Sets. Link Adaptation Game and Contention Window Game are the two proposed games. Social Optimal PHY Game is proposed in [64].

In Figure 4.12, there is increasing delay with increase in the number of co-located BANs. Amongst three game-theory-based methods, Social Optimal PHY Game has the highest delay due to large re-transmissions. The Contention Window Game provides smallest packet delay, and the delay time is increased a small amount at higher interference regime. At the same time, B^{2}IRS has the largest delay due to complexity of beacon re-scheduling when greater number of BANs are co-existing.

As described in Figure 4.11, when more than 4 BANs co-exiting, the Contention Window Game can provides higher throughput. Both two proposed methods have significantly larger throughput respect to other methods, as higher date rate are more preferable in the game at relative better channel

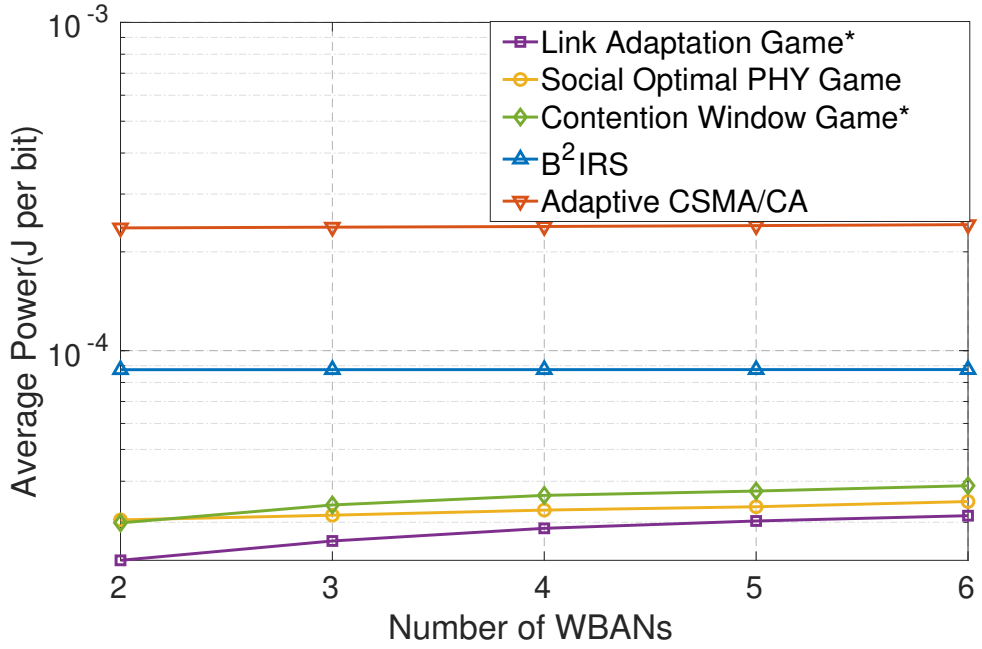

Figure 4.10: Circuit power consumption of the proposed games compared to other methods under Realistic Measurement Channel Sets. Link Adaptation Game and Contention Window Game are the two proposed games. Social Optimal PHY Game is proposed in [64].

conditions.

A non-linear circuit power mapping [106] is used to estimate the circuit power consumption of the system. ~~can be estimated.~~ As it can be seen from Figure 4.14 that Link Adaptation Game ~~method~~ provides the lowest power consumption in terms of Joules per bit (J/bit). Meanwhile, B^2IRS consumes 10 times more Joules per bit. However, the Contention Window Game uses slightly larger power than Link Adaptation Game, because in Contention Window Game, when the contention windows size is small, more packets are transmitted concurrently, hence the transmitter uses larger transmit power to achieve reasonable PDR.

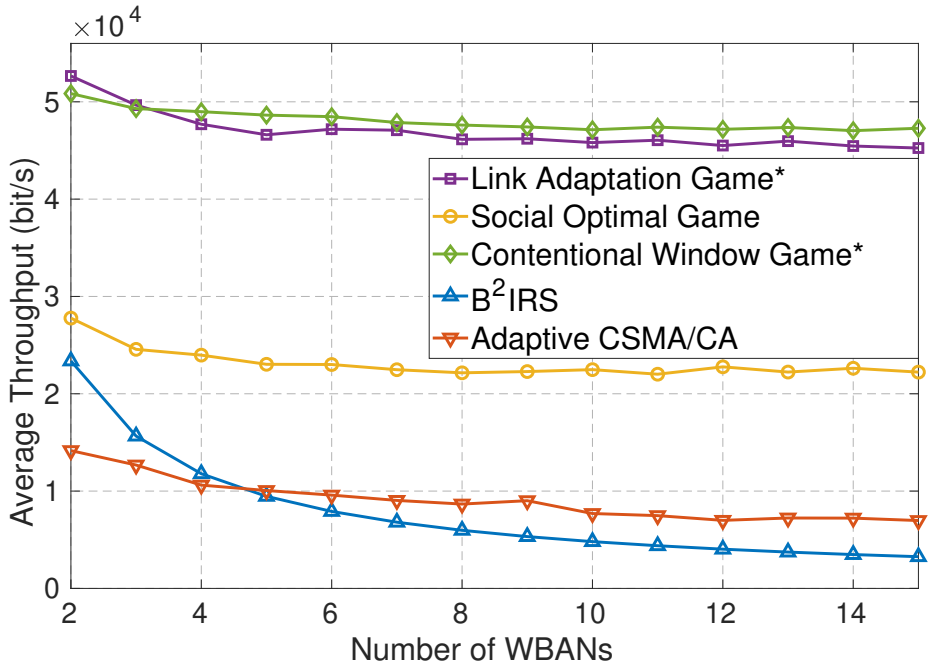

Figure 4.11: Throughput performance of the proposed games compared to other methods under Simulated Channel Sets. Link Adaptation Game and Contention Window Game are the two proposed games. Social Optimal PHY Game is proposed in [64].

4.6 Game Efficiency

The Nash Equilibrium solution of each individual BAN in the game G is the maximization of its own utility. This leads to the problem of efficiency of the network. More specifically, for a network without a central coordinator, the fairness of the system may degrade due to selfish actions of the players. Thus, it is important to investigate the equilibrium efficiency among the coexisting BANs. The social welfare reflects the fairness and efficiency of the system's best response, considering all individuals utility combined.

Definition 4.5. The social welfare is defined by the aggregation sum of each

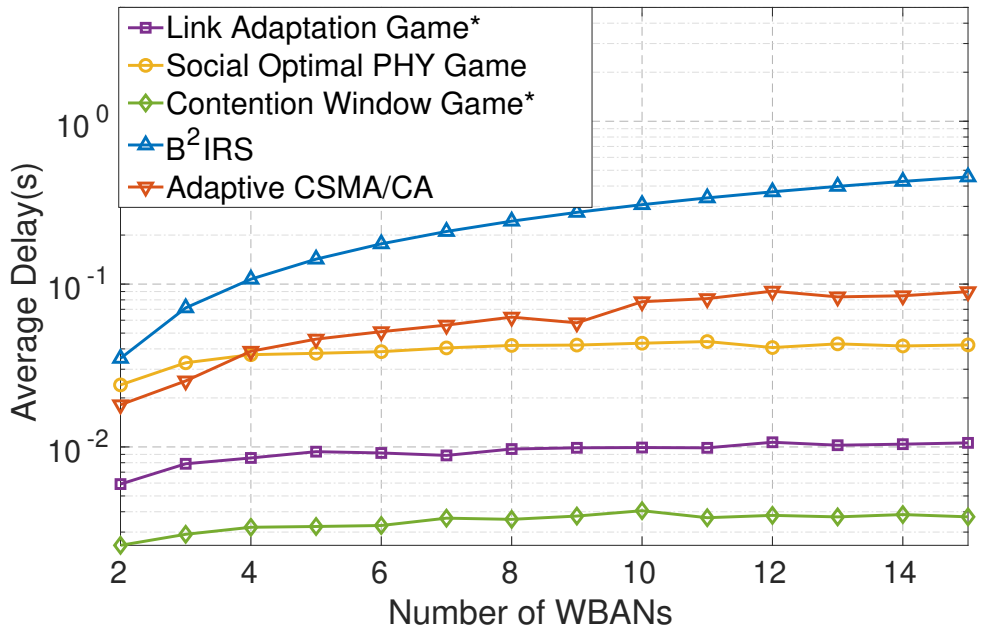

Figure 4.12: Delay performance of the proposed games compared to other methods under Simulated Channel Sets. Link Adaptation Game and Contention Window Game are the two proposed games. Social Optimal PHY Game is proposed in [64].

BAN's utility function as:

$$\Omega(\mathbf{A}) = \sum_{i=0}^{n} U_i(\mathbf{A}). \tag{4.29}$$

The maximisation of the social welfare is the social optimum, which represents the social fairness among the system. The price of anarchy (PoA) is used to measure the inefficiency of equilibriums among selfish players. With finite number of players in game G, the PoA is defined as the ration of the highest value of social welfare (social optimum) to the NE (as NE in G is unique) of the game:

$$\text{PoA} = \frac{\Omega(\mathbf{A^{opt}})}{\Omega(\mathbf{A}^*)} \geq 1, \tag{4.30}$$

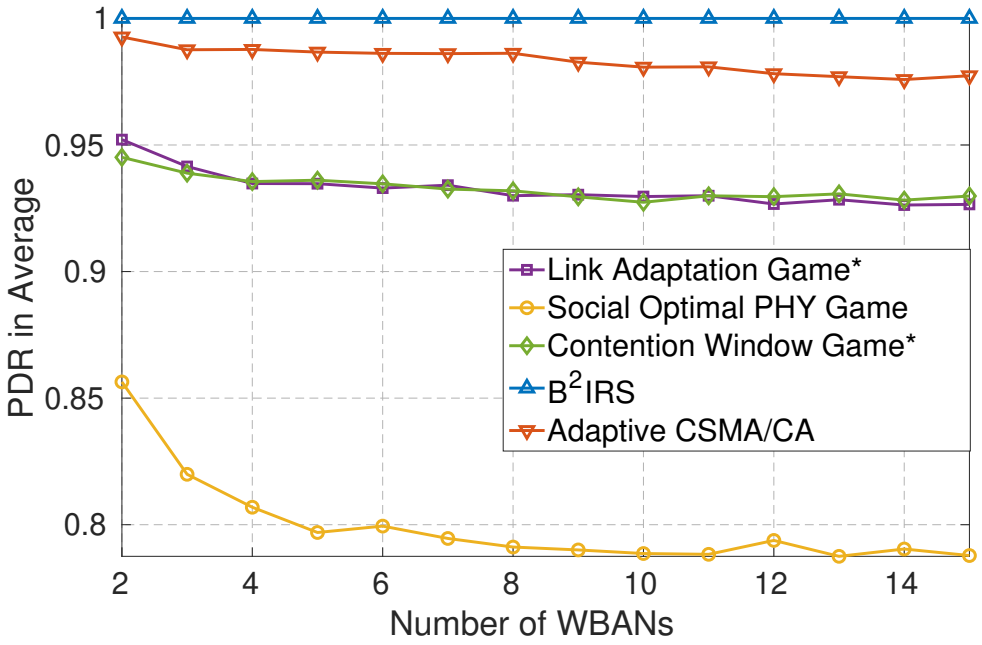

Figure 4.13: PDR performance of the proposed games compared to other methods under Simulated Channel Sets. Link Adaptation Game and Contention Window Game are the two proposed games. Social Optimal PHY Game is proposed in [64].

where $\mathbf{A^{opt}} = \arg\max \mathbf{\Omega}(\mathbf{A})$ is the global optimum solution. Similarly with the Link Adaptation Game the social welfare of the Contention Window Game G_{CW} is defined as :

$$\Omega_{CW} = \sum_{i=0}^{n} V_i. \tag{4.31}$$

With finite number of players in game G_{CW} the PoA is defined as the ration of the highest value of social welfare (global optimization) to the NE (as the Nash Equilibrium in G_{CW} is unique) of the game:

$$\text{PoA}_{\text{CW}} = \frac{\Omega_{CW}(\mathbf{B^{opt}})}{\Omega_{CW}(\mathbf{B}^*)} \geq 1, \tag{4.32}$$

where $\boldsymbol{B}^{opt} = \arg\max \Omega_{CW}(\boldsymbol{B})$ is the global optimum solution.

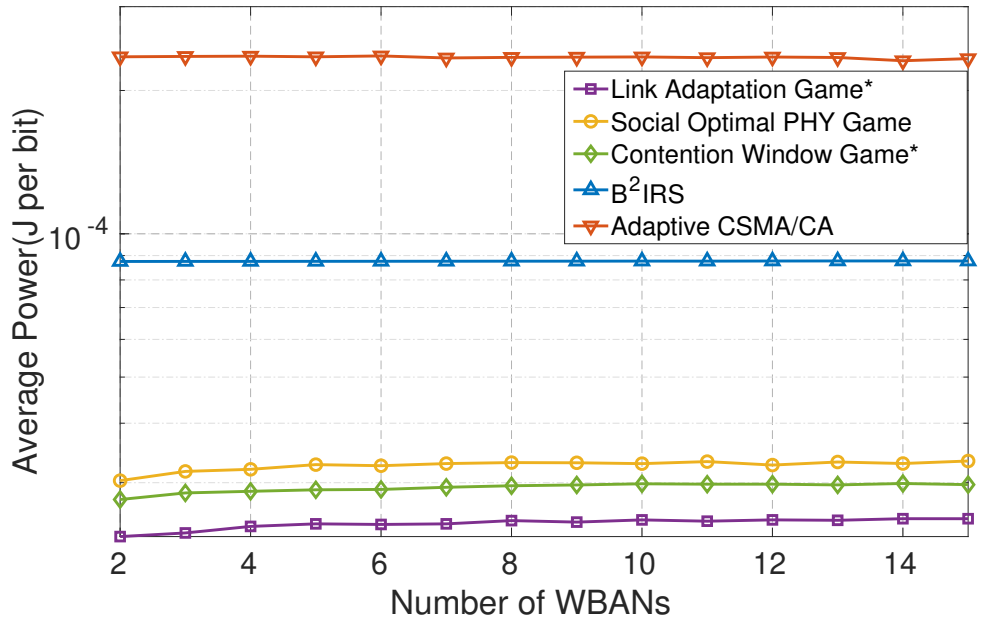

Figure 4.14: Circuit power consumption of the proposed games compared to other methods under Simulated Channel Sets. Link Adaptation Game and Contention Window Game are the two proposed games. Social Optimal PHY Game is proposed in [64].

We evaluate the Price of Anarchy (PoA) of the two prosed games by implementing a Monte Carlo simulation on time varying channels, where an interior point approach is applied to find the centralized (global) optimum of the social welfare. Figure 4.15 and Figure 4.16 above illustrate the PoA for different numbers of co-existing BANs. It can be seen that the loss due to decentralisation is relatively small as PoA $\rightarrow 1$. Also, in general , the system waste less than 10% of their welfare in terms of utility for not being coordinated from both Figure 4.15 and Figure 4.16. Meanwhile, we introduce a new metrics L,L_{CW}:

$$L = \exp(\frac{\Omega(\mathbf{A}^{\check{}})}{\Omega(\mathbf{A}^{*})}), \tag{4.33}$$

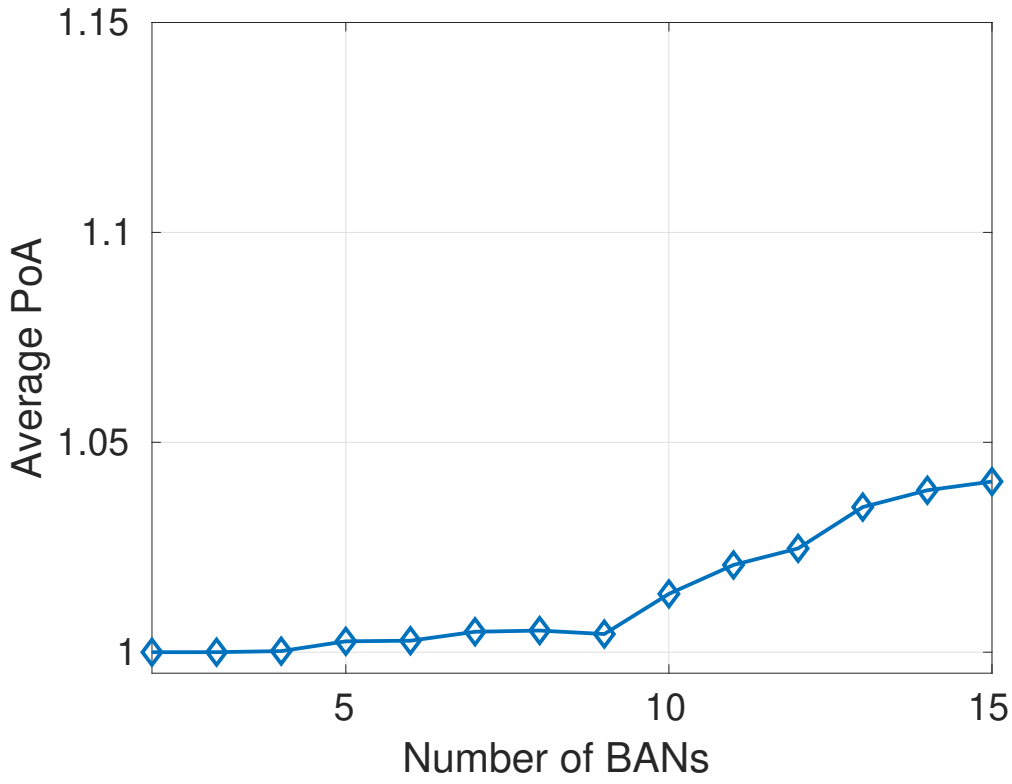

Figure 4.15: PoA in Link Adaptation Game

and,

$$L_{CW} = \exp\left(\frac{\Omega_{CW}(\check{\mathbf{B}})}{\Omega_{CW}(\mathbf{B}^*)}\right), \tag{4.34}$$

where $\boldsymbol{A}^{\kappa} \in \overline{A}, \boldsymbol{A}^{\kappa} = \arg\min \Omega(\boldsymbol{A})$, and $\boldsymbol{B}^{\kappa} \in \overline{B}$, $\boldsymbol{B}^{\kappa} = \arg\min \Omega_{CW}(\boldsymbol{B})$. L, L_{CW} correlated with the ratio of the worst value of the social welfare and the maximum value of the social welfare in game G and G_{CW} respectively (we take the exponential as sometime the value of utility function can be negative). These two metrics represent the gap between the system's best possible performance and the worst case scenario. The comparison between L,L_{CW} and $\exp(\frac{1}{\text{PoA}})$ and $\exp(\frac{1}{\text{PoA}_{CW}})$ provides some insight of how stable the Nash equilibrium is across iterations of the game. Hence, in Table 4.3, we illustrate

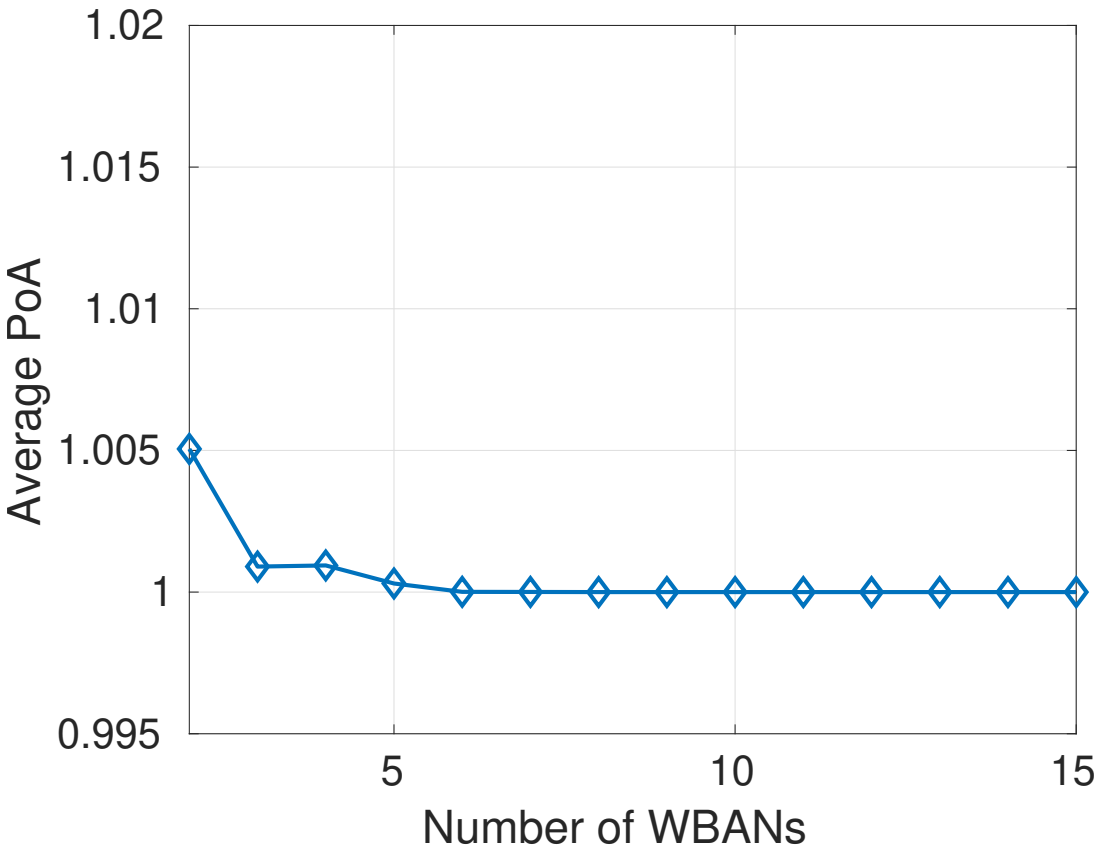

Figure 4.16: PoA in Contention Window Game

the comparison between the mean value of L and $\exp(\frac{1}{\text{PoA}})$ when different number of BANs are co-located. Meanwhile, the comparison between L_{CW} and $\exp(\frac{1}{\text{PoA}_{CW}})$ is depicted in in Table 4.4.

Comparing with $\exp(\frac{1}{\text{PoA}})$, L is much more smaller. It is because the social welfare varies a significant amount over the action space. Thus, in Link Adaptation Game, the system is socially stable as the deviation from the social optimum solution is small. On the other hand, in contention window game, the values of L_{CW} are relatively large. However, it can be seen that, the PoA_{CW} is close to 1, which represents complete stability of the game.

Table 4.3: Comparison of $\exp(\frac{1}{\text{PoA}})$ and the mean value of L

No. of BANs	L	$\exp(\frac{1}{\text{PoA}})$
2	6.832e-32	2.718
5	4.252e-32	2.704
8	2.291e-32	2.562
11	2.728e-32	2.549
14	1.141e-32	2.542

Table 4.4: Comparison of $\exp(\frac{1}{\text{PoA}_{CW}})$ and the mean value of L_{CW}

No. of BANs	L_{CW}	$\exp(\frac{1}{\text{PoA}_{CW}})$
2	2.2445	2.7056
5	2.0317	2.7175
8	1.5793	2.7183
11	1.5746	2.7183
14	1.5864	2.7183

4.7 Concluding Remarks

In this chapter, we developed two game-theoretic resource allocation schemes for co-located BANs. The proposed methods adapts to the time-varying channel and traffic by minimising the interference among all players. The model was based on a novel contention-based MAC layer protocol with special back-off mechanism, which reduces packet collision probability. The best response of each player was a utility-maximising choice of transmission parameters across superframes. We mathematically proved that the proposed schemes admit unique Nash Equilibrium solutions, which provides higher throughput and a reduction in latency and power consumption.

Evaluated by both realistic empirical measurements and simulation, the Link Adaptation Game was demonstrated to reduce radio interference by improving throughput, in conjunction with reduced power and delay when compared with the state-of-art. The Contention Window Game provided

much more lower delay (< 5ms in general), but with a slight compromise in circuit power consumption. Both of the proposed methods have PoA $\rightarrow 1$ and are very close to the social optimum, which guarantees high social efficiency at the games' Nash Equilibrium. One important finding of this study is that robust results can be obtained by perceiving channel state using historical information (ACK counts). Hence, it is interesting to explore utilising past channel samples to predict future channel states, in spite of the dynamic nature of BAN channels. Thus, in the next chapter, novel channel prediction schemes for BAN channels will be discussed in detail.

Chapter 5

Deep Learning Enabled Channel Prediction for Wireless Body Area Network Transmit Power Control

5.1 Introduction

As demonstrated in Chapter 4 and Chapter 3, our proposed methods significantly improve the overall QoS for co-located BANs using adaptive approaches. However, the characteristics of dynamic BAN channels haven't been fully exploited and utilised. To make IoH networks more intelligent, that can learn and make decisions by themselves, in this chapter, predictive optimisation schemes over BAN channels are investigated. Channel prediction techniques have recently attracted interest from researchers due to its possibility to optimise the management of scarce resources and provide high communication efficiently. Prior studies have revealed that accurate prediction of the future wireless channel status can benefit the performance of power control schemes [11], even when the prediction accuracy is low [120]. But the strong shadowing effect generated by the human body itself makes the channel prediction problem extremely challenging in BAN scenarios. Existing literature on long-term channel prediction for typical radio networks of-

ten adopts autoregressive (AR) predictive methods [88], the sum of sinusoids methods [121, 122] or weighted alternate-least-squares modelling techniques [89]. However, such methods are not robust towards realistic wireless channels. It is because of that the lack of non-stationary modelling capability prevents those traditional methods from accurately capturing the channel dynamics. Meanwhile, only very few previous studies have investigated BAN channel predictions, especially on a long-term scale. Thanks to the rapid ad-

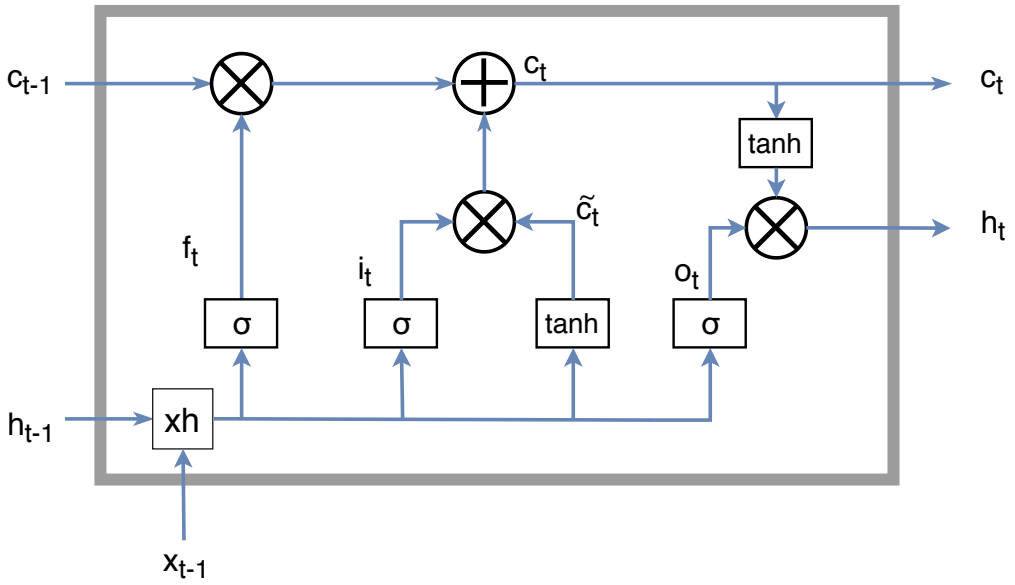

Figure 5.1: The basic operation inside a LSTM cell

vancement in recent years of deep learning (DL), in signal processing area, their applications are widely used for modelling and predicting [123], [124]. Recurrent neural network (RNN) which is a nonlinear, adaptive modelling approach has demonstrated its advanced ability in wide range of modelling and prediction tasks [125]. RNNs have shown significant improvements over state-of-the-art results in sequence modelling tasks (e.g., natural language processing, speech recognition and predictions from any form of time series

data) [97]. However, both vanishing gradient and exploding gradient problems [126] limit the capability of RNNs to model long range context dependencies to 5-10 discrete time steps between the input signals and output [97]. To address these problems, an elegant solution for RNNs, LSTM is used [96] which has some internal contextual state cells that act as long-term or short-term memory blocks, and it is used in our research as shown in Figure 5.1. Our research shows that, by training on past channel statistics with atypical variations, LSTM is potentially promising to predict future channel attenuations within BANs.

5.2 LSTM Channel Prediction

In this work, we propose an LSTM-based solution for the problem of channel prediction in wireless body area networks.

5.2.1 LSTM Network Architecture

The architecture of the proposed LSTM network is composed of one input layer, one dense layer with batch normalisation, several stacked LSTM layers, and one fully-connected layer followed by the output layer as illustrated in Figure. 5.2.

The task of the proposed network is to use the past channel samples logged in the hub to provide long term prediction of on-body channel attenuation in the future. For each channel link within the BAN system, the hub device records the RSSI from successful packet transmission. So that with such information the channel attenuation at time t can be calculated as $R_t = \text{RSSI}(t) \cdot p(t)$. To obtain the input-output pair with known data, imagine

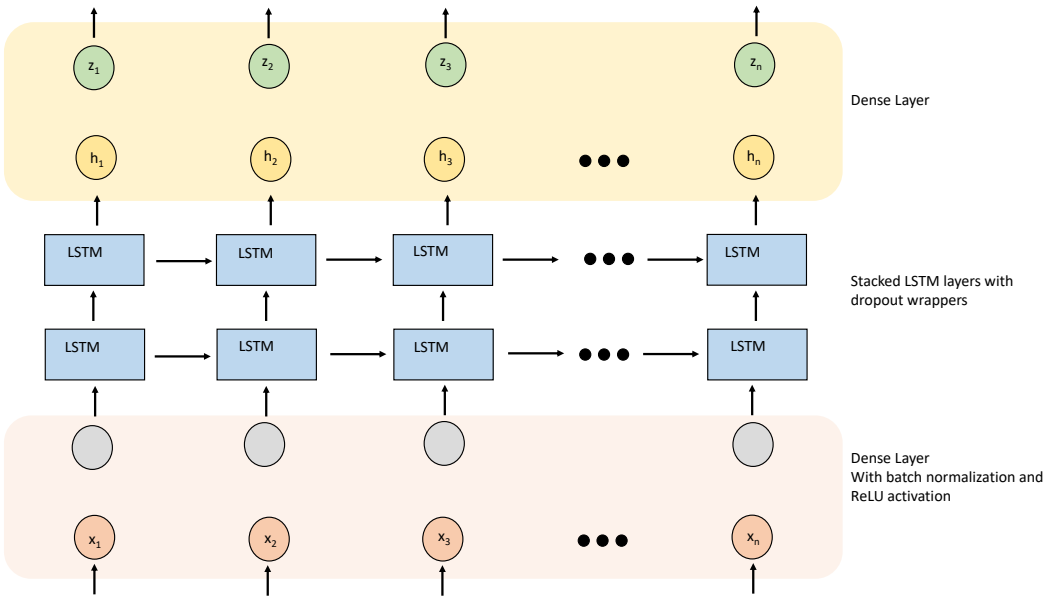

Figure 5.2: Proposed LSTM architecture.

that we have a window with fixed size w (which is equal to the input size of the LSTM network n) to collect the channel samples. The value in the window at t is denoted as $X(t)$:

$$X(t) = (R_{t-w+1}, R_{t-w+2}...R_t). \tag{5.1}$$

The channel predictor aims to predict the channel attenuation for the next N_{pred} samples (the value of N_{pred} is related with the link sample interval). Thus, for each observation $X(t) = (R_{t-w+1}, R_{t-w+2}...R_t)$, the target sequence $Y(t)$ is constructed by delaying $X(t)$ for N_{pred} steps, such that:

$$y_i = R_{i+N_{pred}}, \tag{5.2}$$

where $i \in [t-w+1; t]$, and the last N_{pred} values are the actual target. By feeding $X(t)$ into the LSTM network, the output sequence is obtained as

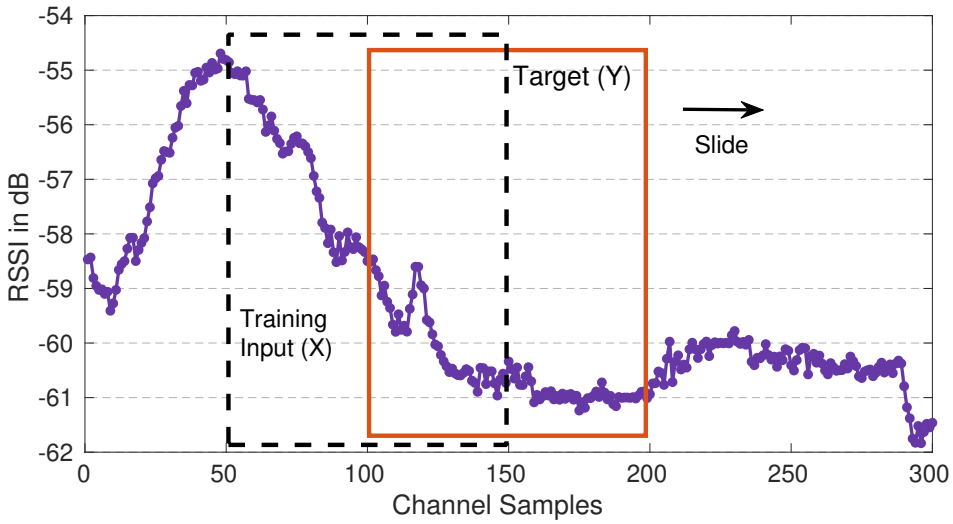

Figure 5.3: Graphical illustration of the tensor completion.

$Z(t) = (z_{t-w+1}, z_{t-w+2}...z_t)$ (generated from forward propagation). During inference phase, the last N_{pred} values of the LSTM output sequence $Z(t)$ are the actual predictions. Therefore, given an observation sequence $X(t) = (R_{t-w+1}, R_{t-w+2}...R_t)$ we train a LSTM network that predicts the next N_{pred} samples by minimising the loss function through updating the model parameters using back-propagation. Figure. 5.3 provides an example of X and Y. The loss function is defined as the mean-square error (MSE) between the predicted values and the ground truth values:

$$L(\mathbf{X}, \mathbf{Y}) = \frac{1}{N_{pred}} \sum_{i=N_{input}-N_{pred}+1}^{N_{input}} (y_i - z_i)^2. \tag{5.3}$$

The LSTM model is trained by minimising the loss function through updating the model parameters using back-propagation. However, it is generally unfeasible to pass the whole training data set to the neural network at

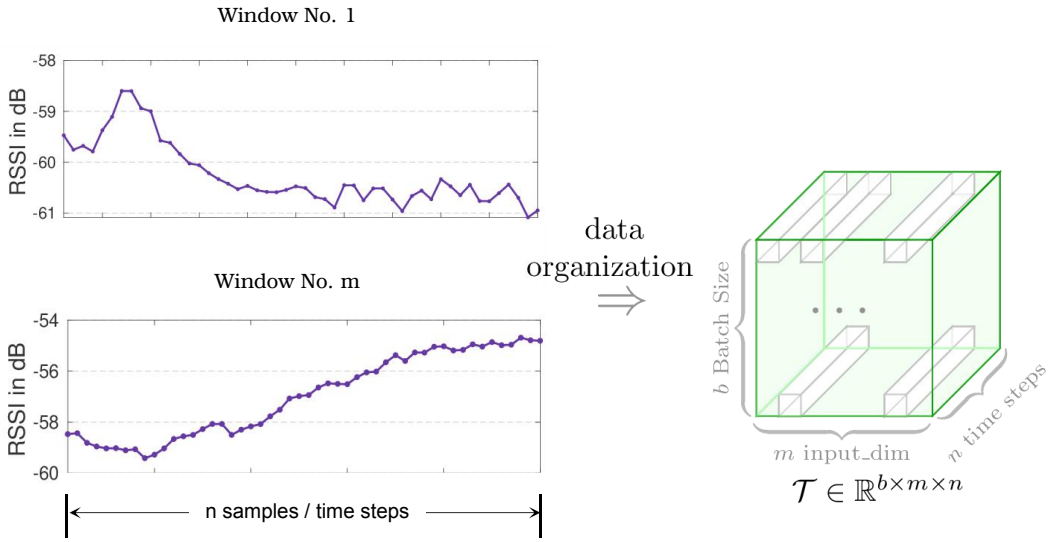

Figure 5.4: Graphical illustration of the tensor completion.

once (full batch), because a large amount of memory will be occupied and the model will easily over-fit. Thus, the data set is divided into a number of mini-batches. This is achieved by transforming several instances of **X**s and **Y**s into 3-D tensors, such a tensorization process is illustrated in Figure 5.4. Prior to feeding mini-batches for training, batch normalisation [127] is performed, which is a simple and effective way to improve the performance of a neural network. More specifically, we used a dense layer + normalisation layer + non-linear activation (ReLU) structure. Therefore, the input tensor is fed into a dense layer with a linear activation function. A ReLU activation function is added to the batch normalisation layer that has an output:

$$BN_i = (\frac{x_i - \mu}{\sqrt{\epsilon + \sigma^2}})\gamma + \beta, \tag{5.4}$$

where $x_i \in X$ is the output from the input layer, and $\mathbf{BN} = (BN_1, BN_2, ..., BN_n)$

is the normalised output. μ and σ^2 are the mini-batch mean and variance, respectively. To increase numerical stability, a constant ϵ is added to the mini-batch variance σ^2. γ and β are the parameters to learn. Avoiding over-fitting is central to the performance of the network, for this reason, LSTM cells are wrapped with dropouts mechanism, so that for a given probability, the data on the input connection to each LSTM cell will be inactivated for parameter updating.

In the training phase, given input $\mathbf{X}$, the NN continuously improves the prediction towards the correct target $\mathbf{Y}$ by adjusting its parameters (i.e., weights and states). This is performed by adjusting the model parameters (i.e., weights and biases) so as to minimise the loss function. Firstly, the nodes in all the layers of the network are initialised. In order to change those parameters in the nodes in a way to approach the minimum possible error between the input-output pairs, a gradient descent method is employed, whereby the gradient is used to alter parameters to lead it towards the minimum of the loss function. Generally, the expression of the cost function makes the gradient difficult to evaluate. However, by comparing the output of the neural network to the target $\mathbf{Y}$, we can investigate how the change in the parameters of the RNN changes the cost function. To do this for all the hidden layers of the network, back-propagation is used. This method allows us to share the cost function, i.e., error, with all the parameters in the network. The gradient descent routine is repeated until the average cost function has reached a minimum. At this point, the network is trained and ready for use.

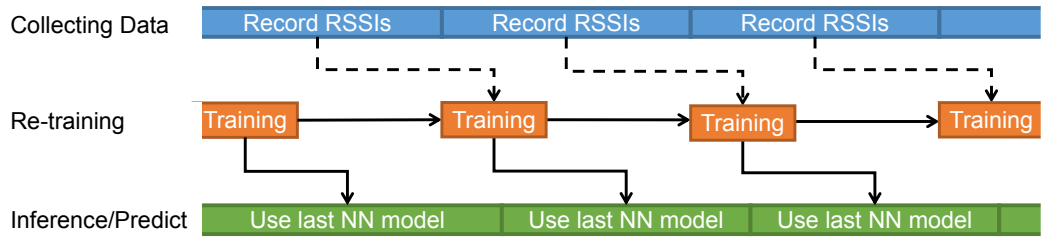

Figure 5.5: The flow chart of the incremental prediction mechanism.

5.2.2 Incremental Training Mechanism

To better cope with the dynamics of BAN channels, an incremental learning algorithm is proposed here that enables the LSTM network to continuously evolve with streaming channel samples. After finishing the initial training of the LSTM network, the hub is able to forecast the future channel situation at any time by forward-feeding recently received channel samples with the trained recurrent weights.[1] However, in traditional offline learning schemes, the acquired parameters in the network will no longer be updated after the first training process terminates. This is such that, the received channel samples will only be used for inference only. As opposed to traditional models, the proposed scheme adopts the concept of dynamic refinement, which means the existing model gradually increases knowledge over time. To do so, the hub is required to records channel gains at each time step during the inference phase. After collecting a predefined number of samples, the hub begins to fine-tune the model using new batches that are composed of acquired data. Therefore, without forgetting its existing knowledge the model can adapt to new data. When each training episode is finished, the hub will use

[1] It should be noted that in the inference phase the stored hidden state will also be replaced by the current values.

this newly trained model instance for subsequent predictions. The detailed schematic overview of the incremental learning mechanism is demonstrated in Figure. 5.5.

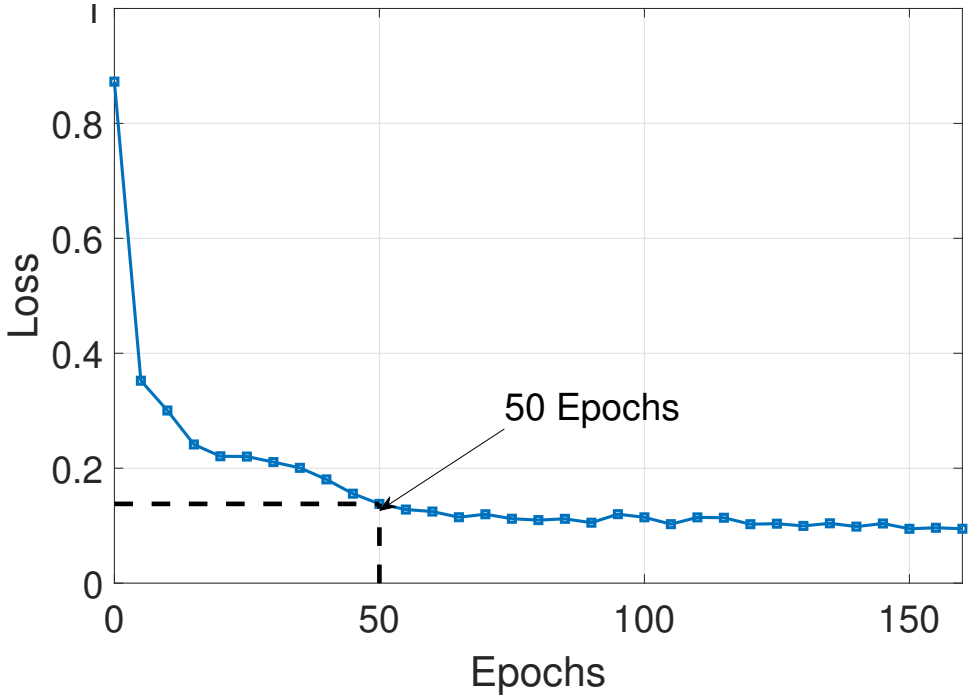

Figure 5.6: Initial Training Loss

5.3 Performance Evaluation

We use TensorFlow 1.13 to build the proposed NN model. The training and testing of the NN are conducted on a desktop with Intel i7 CPU, 8GB Memory. Recent studies [128] have suggested that using learning rate decay in Adam could result in significant performance improvement, thus the Adam optimiser [129] is used with learning rate decay. The learning rate at step/it-

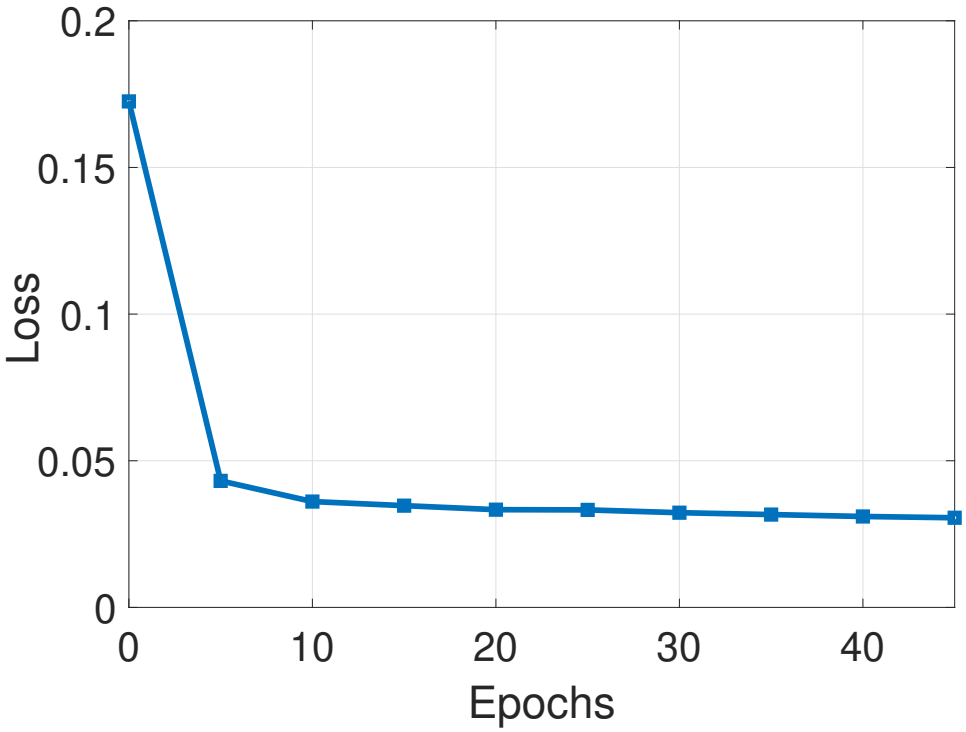

Figure 5.7: Online Training Loss

eration t is represented as:

$$lr(t) = lr_0 * r_d^{(t/g_s)}, \tag{5.5}$$

where lr_0 is the initial learning rate, r_d is the decay rate and s_d is the decay step. For better convergence, all LSTM cells are initialised by the Xavier initialiser proposed in [130]. The channel measurements are normalised and pre-processed to have zero mean and unit variance:

$$\tilde{\mathbf{X}} = \frac{\mathbf{X} - \mathbb{E}(\mathbf{X})}{\sigma(\mathbf{X})}, \tag{5.6}$$

where σ denotes the standard deviation. Via hyper-parameter searching, the size of the hidden state in each LSTM cell is set as 64, which yields optimal performance. The channel samples are batched by using a batch size of 64 and padded with zeros when required. In the proposed incremental learning scheme, the first training uses 50 batches of channel sample sequences, while 20 batches of channel sample sequences are used in each updating training phase. Therefore, when the link sampling rate is 50Hz, the proposed predictor can predict the link for approximately 30 seconds, before each model updates. The training time is set based on the realistic running time, varying from 5s to 15s depending on the size of the training set. The configuration parameters of the LSTM model are listed in Table 5.1.

Table 5.1: Detailed Configuration of the LSTM Network.

Description	Value
Number of layers in the LSTM network	2
Size of the hidden state of an LSTM cell	64
Number of sequences in each mini-batch	64
Input size of the network	100
No. of epochs for initial training	50
No. of epochs for model fine tuning	20
Training Time	10s
Learning Rate	0.0003
Dropout Probability	0.8

Figure. 5.6 and Figure. 5.7 illustrate the training loss of an initial training data set and the training loss of training data sets across epochs in a typical instance respectively. It can be seen that it takes the model less than 50 epochs to converge in initial training, and in update training the model converges before 20 epochs.

Figure. 5.8 shows a typical prediction instance of the proposed method. Here we attempted to predict 50 samples ahead of the last received sampled

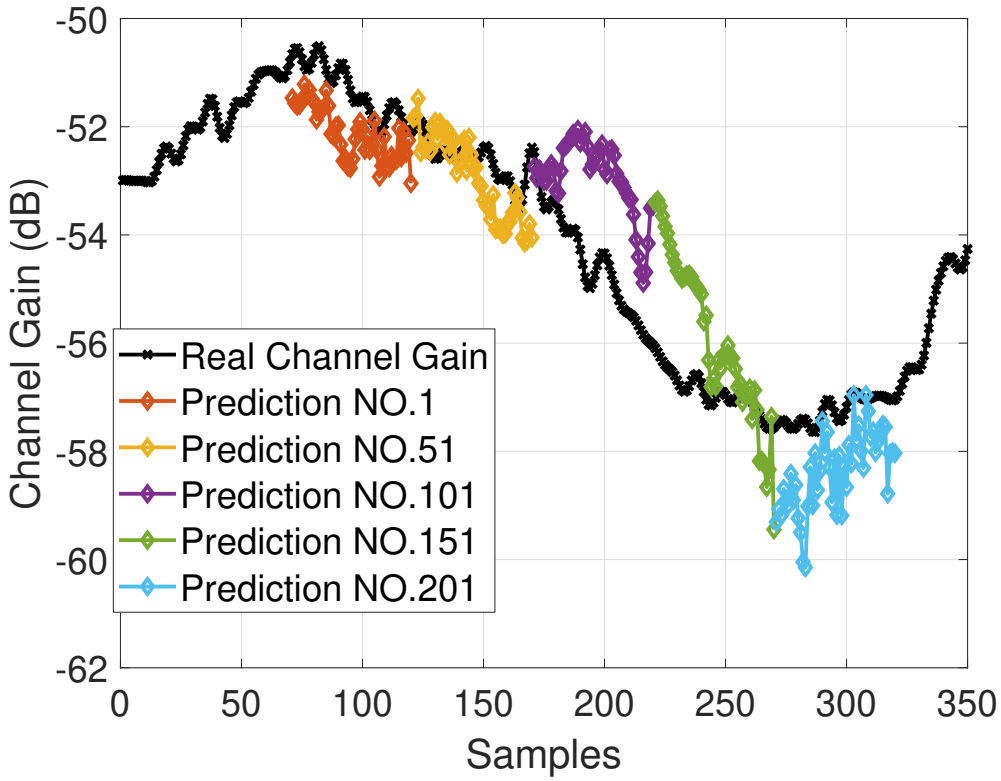

Figure 5.8: An example of LSTM network prediction with link sampling rate at 50Hz. Plot interval between predictions is 50.

by using the last 75 channel samples. The time period between link samples is $20ms$. The black line indicates the actual channel gain samples, and the coloured lines are predictions. We plotted the prediction with an interval of 50 samples to avoid overlapping.

We then evaluate the accuracy of the proposed LSTM predictor by using normalised mean square power error (NMSE) [89]. The NMSE is expressed as $\mathbb{E}[(\tilde{p}(l)/p(l) - 1)^2]$, where $\tilde{p}(l)$ is the optimal transmit power estimate mapped from each predicted samples, $p(l)$ denotes the optimal transmit power estimate mapped from the ground truth value[2] and $\mathbb{E}$ represent the

[2]The ground truth values are not practical for actual power control as no error margin is allowed

expectation. A comparison of the NMSE power error between the proposed method and two baseline methods: Moving Average method (MA) [131] and Adaptive Prediction method (AP) [132] is plotted in Figure. 5.9 with a receiver sensitivity, Rx_{sens}, of -90 dBm, and link sampling periods of 20 ms. It should be noted that the error is based on the NMSE power error of other predictors relative to the NMSE power error of the proposed method. MA forecasts the channel gain by taking an average over recently received link samples. Meanwhile, the Adaptive Prediction method combines the Least Mean Squares (LMS) adaptive tracking method and the channel inversion algorithm to provide long-term predictions for fading channels. As can be seen, comparing with the Adaptive Prediction method, the proposed method offers obvious prediction error reduction, an up-to 13 times reduction. When the prediction interval is far more than the BAN channel coherence time (normally 500ms [133]), the proposed method can provide nearly 2 times smaller NMSE compares to MA.

Obviously, the predictor's accuracy is increased with the size of the training set. However, under our proposed incremental learning scheme, when the size of the training set increases, the time interval between each model updates also increase, such that the errors in each prediction may accumulate. It is also a difficult task to guarantee the accuracy of the predictor when using a relatively small size data set. At the same time, using small training set requires frequent parameter updates, which also increase the computational cost. Hence, it is important to trade-off the size of training data. Figure.5.10 shows the NMSE power error of the proposed predictor for different sizes of the training set from 300 samples to 1800 samples when $RX_{sens} = -90$dBm. The minimum of the NMSE power error occurs at around 1000 samples. The

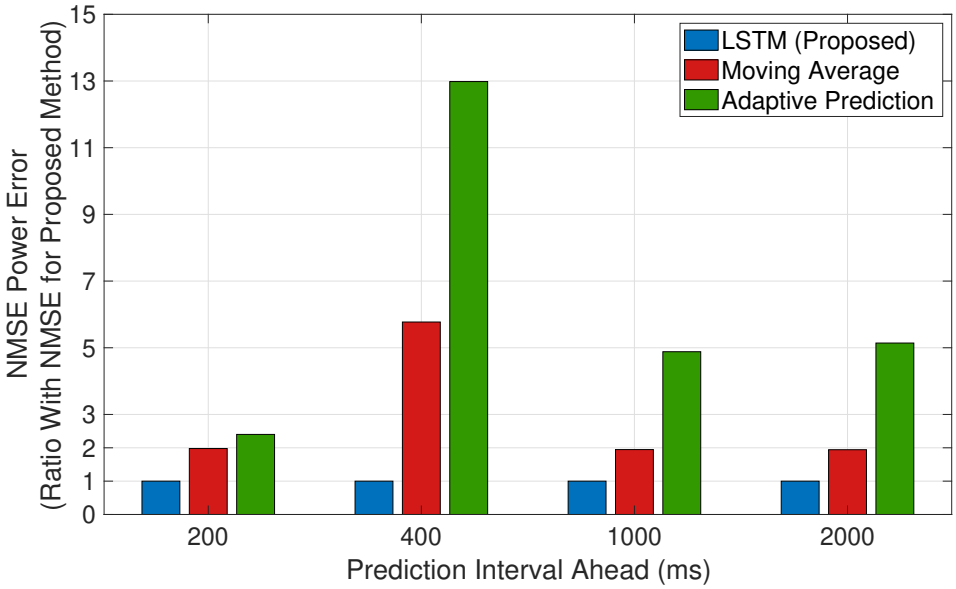

Figure 5.9: Comparison of prediction accuracy in different methods, for 200ms, 400ms, 1000ms and 2000ms prediction ahead.

NMSE power error of the LSTM predictor decreases at first and then increases when increases the size of the training set.

To produce the best possible performance from the proposed predictor, we developed a Tx power control scheme amended from the Tx power control used in [11]. The details of the Tx power control scheme is described in Algorithm 5. For power allocation, 0.5 dB is set as the step size in level scanning, to reduce outage and transmit power consumption at the same time. We use the short term mean value and the inter-quartile range (IQR) of the last w channel samples to optimise the scaling factor. IQR is a widely used metric in statistics that measures statistical dispersion, being equal to the difference between 75th and 25th percentile. $TH_H = 0.3, TH_L = 0.15$ are the high and low threshold for IQR value and $TH_C = 0$ is the threshold for the mean channel samples. Accurate prediction offered by the proposed method allows BANs to use less transmit power while avoiding outages.

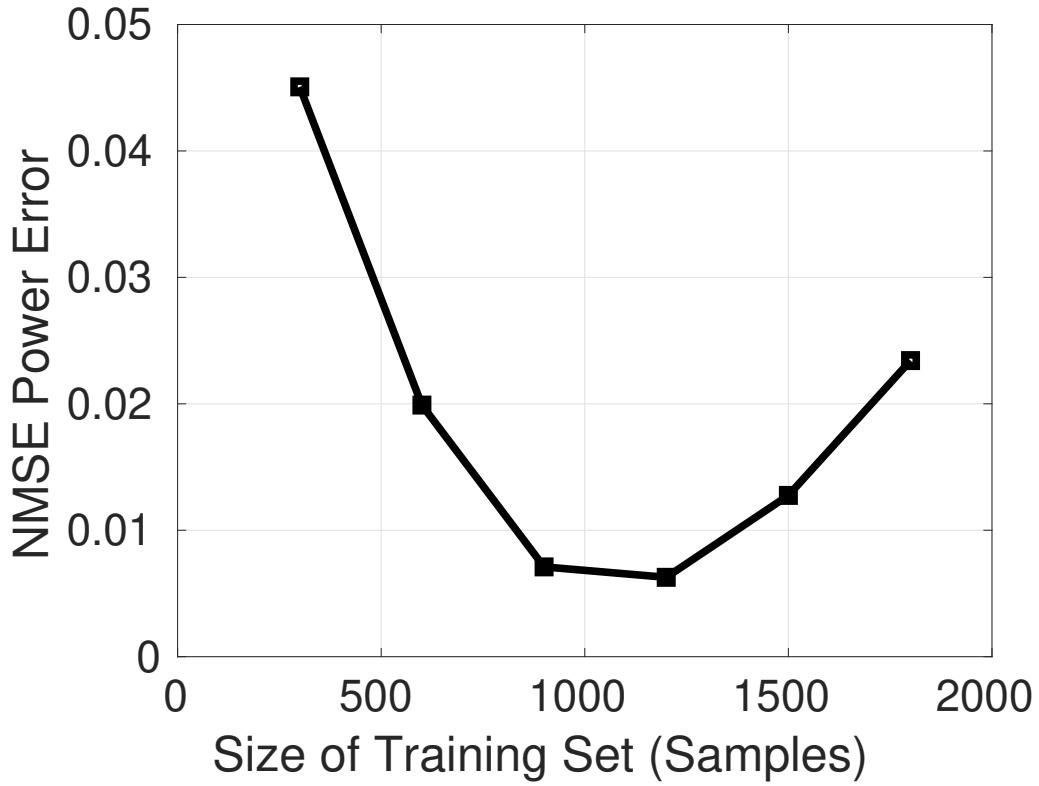

Figure 5.10: The prediction accuracy of the proposed method for different training set sizes.

Figure. 5.11 presents the outage probability and transmit power for the proposed power control when predicting 1000 ms ahead under four different Rx_{sens}, using a one-star topology with link sampling rate at 50 Hz. The performance of AP and MA are also evaluated for comparison here. Larger outage probability is expected when the Rx_{sens} is high. We observe the proposed method consumes approximately 1 dB to 3.5 dB less transmit power and has approximately 1% smaller outage probability. In Figure. 5.12, we evaluate the performance metrics when employing multi-star topology channel measurements. As expected, transmit power consumption and outage probability are slightly larger under a multi-star topology. With Rx_{sens} of -95,-93 and -90 dBm, the transmit power consumption of the proposed method is between

11% − 26% less than the MA, and provides around 2% outage reduction. However, with Rx_{sens} of −86 dBm, only marginal improvement is offered by the proposed method, under both topologies.

Algorithm 5 Transmit power control at 4 Rx_{sens} for T_{pred} samples into the future

Get Predicted channel gain S_{pred} (length of T_{pred})
Rx_{sens} = [−95, −93, −90, −86] dBm, k = 1,2,3,4
$levels_k$ = [$Rx_{sens}(k)$, Rx_{sens} + 0.5,...,Rx_{sens} + 40] dBm
Scaling Factor a = [5.5, 5, 4, 4] dB, b = [0, 0, 1, 1] dB
for t in T_{pred} **do**
    if $IQR(t) > TH_H$ and $\mathbb{E}[\tilde{\mathbf{X}}] < TH_C$ **then**
        $a = a + 2.5, b = b + 1.5$
    else if $IQR(t) > TH_H$ and $\mathbb{E}[\tilde{\mathbf{X}}] \geq TH_C$ **then**
        $a = a + 2, b = b + 1$
    else if $TH_L < IQR(t) \leq TH_H$ and $\mathbb{E}[\tilde{\mathbf{X}}] < TH_C$ **then**
        $a = a + 1.5, b = b + 1$
    else if $TH_L < IQR(t) \leq TH_H$ and $\mathbb{E}[\tilde{\mathbf{X}}] \geq \mathbf{TH_C}$ **then**
        $a = a + 1, b = b + 0.5$
    else if $IQR(t) \leq TH_L$ **then**
        $a = a + 0.5$
    end if
    Find index i, $levels_k(i-1) < S_{pred}(t) < levels_k(i)$
    $C = Rx_{sens}(k) + a(k)$
    if $levels_k(i) < C$ **then**
        $Tx_{out}(t) = 0$ dBm
    else if $C + 2.5 \leq levels_k(i) \leq C + 30$ **then**
        $Tx_{out}(t) = C + b(k) - levels_k(i)$ dBm
    else
        $Tx_{out}(t) = -30 + b(k)$ dBm
    end if
end for

Figure. 5.13 shows the circuit power consumption and outage probability comparison among the proposed method, MA and AP. The results are obtained by averaging from 5 subjects over 18 different on-body links with Rx_{sens} at −90 dBm. Among the 18 different links, 12 links are of a one-star topology. In total, over 1.5 hours of measurements data are used in this exper-

iment. In practice, the actual power consumption of the sensor circuit doesn't linearly match with the transmit power. Thus we used a non-linear mapping proposed in [106] to evaluate the circuit power consumption from the transmit power. The proposed method consumes less than around 2.9 mW circuit power on average, with approximately 2.1% outage, which is around 45% smaller than 4% of MA. In addition, MA uses nearly 13% circuit power than the proposed method. Meanwhile, AP provides a similar result to MA, with a small outage reduction.

Figure. 5.15 shows the performance over different Tx positions under a one-star topology. Over 2 hours of measurements of different subjects are used. Although the performance varies from different Tx positions, the proposed method achieves 1.2% outage reduction on average with respect to MA. At the same time, the proposed method provides up to 25% circuit power saving with respect to AP.

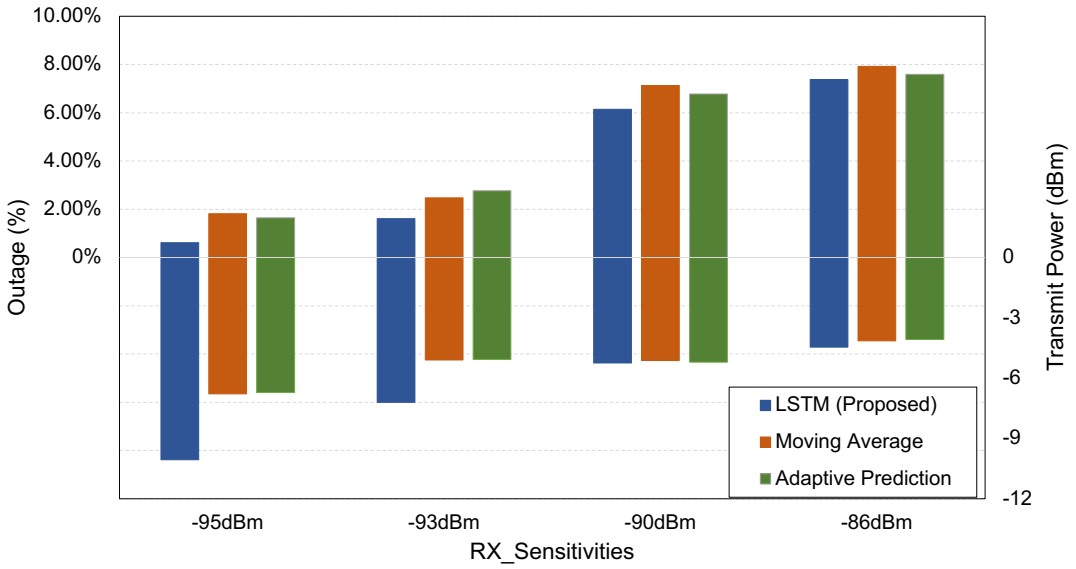

Figure 5.11: Outage Probability and Power Consumption for 4 Rx_{sens}, one-star topology. LSTM is proposed method.

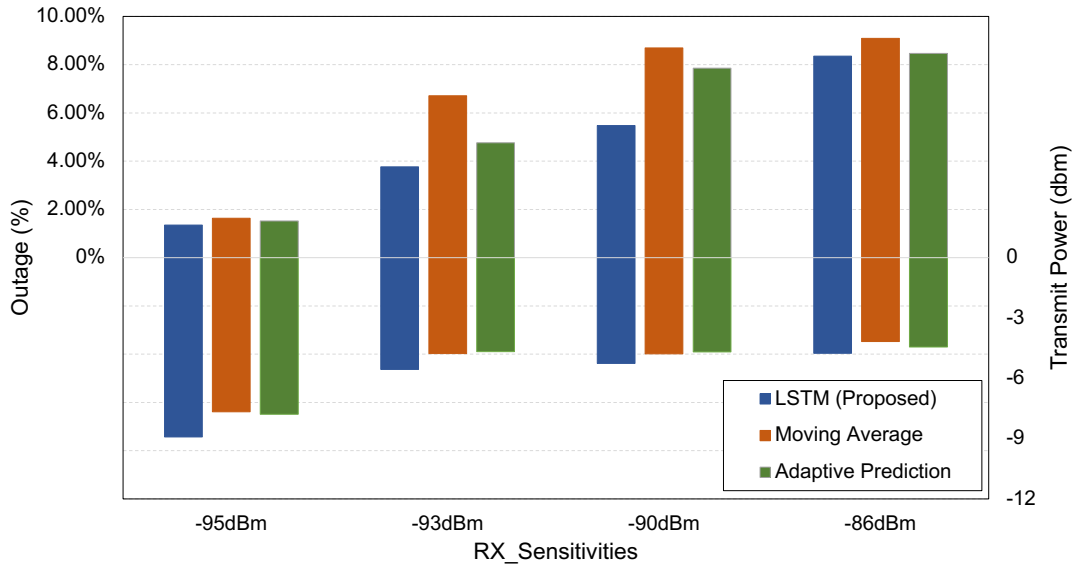

Figure 5.12: Outage Probability and Power Consumption for 4 Rx_{sens}, multi-star topology. LSTM is proposed method.

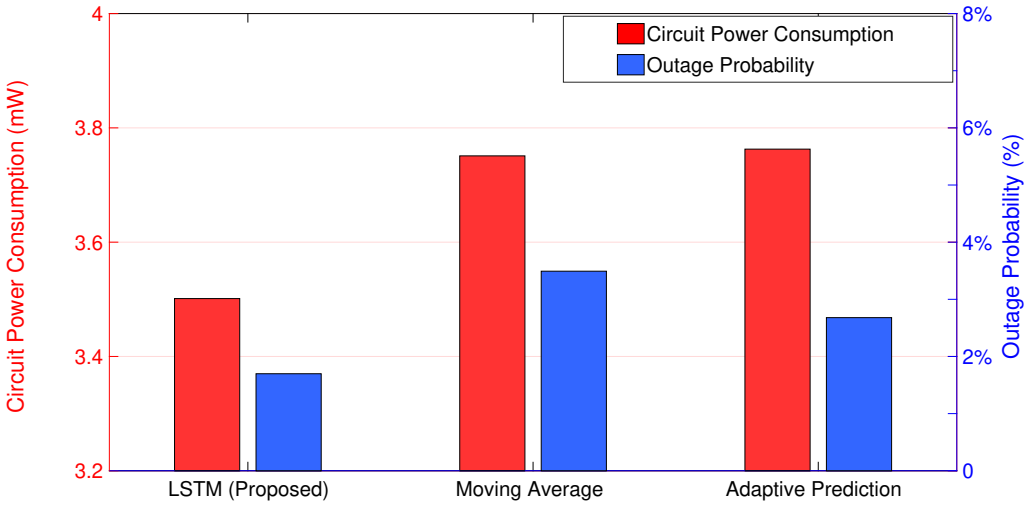

Figure 5.13: Comparison of different methods in terms of outage probability and circuit power consumption. The result is averaged over 18 separate links.

5.4 'LiteLSTM'

In typical BAN operation scenarios, smartphones are usually used as hub devices, which coordinate transmissions among all sensors. Therefore, here,

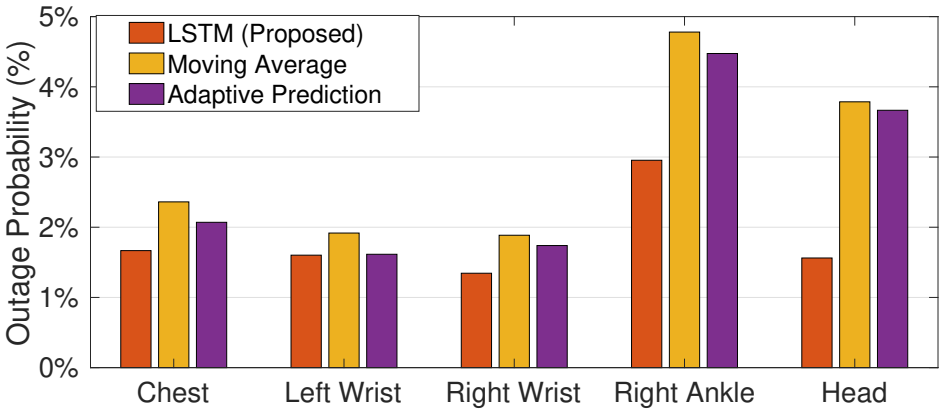

Figure 5.14: Outage Probability at $Rx_{sense} = -90$ dBm at different positions, one-star topology. Rx located at left hip pocket.

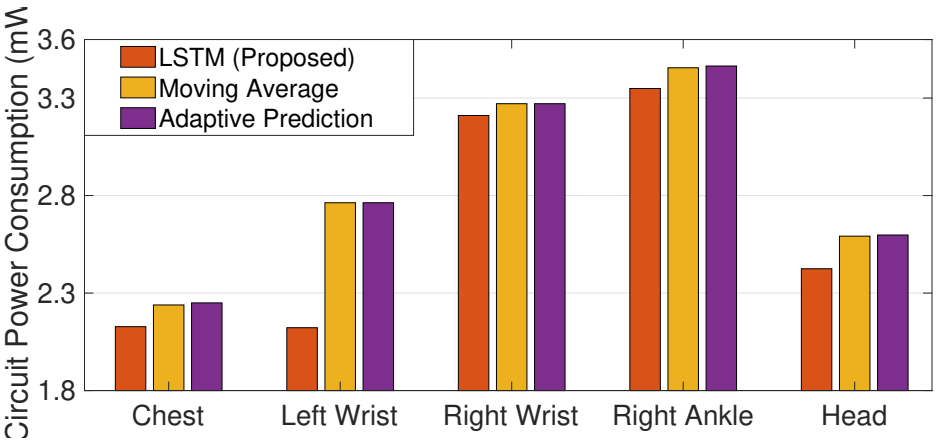

Figure 5.15: Circuit Power Consumption at different positions, one-star topology. Rx located at left hip pocket.

we investigate the feasibility of a practical deployment of the proposed neural networks based predictor. However, when employing NN-based applications on mobile devices, the performance and energy consumption restrictions make the execution of such computationally intensive algorithms burdensome, especially in training phases. Hence, in order to extend the benefit of the NN predictor to embedded devices, it is very important to reduce the complexity as well as memory footprint of the network structure due to limi-

tations in computational power and memory.

In order to suit the needs of mobile implementation, we introduce a compact LSTM channel predictor, namely 'LiteLSTM'. 'LiteLSTM' has a relative low complexity, and the computational cost of the network is therefore reduced. Although deeper neural networks often perform better, a single LSTM layer is used in 'LiteLSTM' and the size of the hidden state of an LSTM cell is reduced to 16. This is viable, because in our experiments, such removal of redundancy only shows marginal performance degradation. Meanwhile, to further reduce the number of trainable parameters, the fully connected layers are replaced by 1-D temporal convolution layers [134], since they are able to capture spatial features and converge much faster. In addition, the batch normalisation layer is also removed as the performance improvement of the BN layer in "shallow" networks is limited. At the same time, in each incremental training episode, the number of epochs should also be reduced. We also explore the use of an attention mechanism on top of the LSTM outputs in the 'LiteLSTM' network. The attention can generally be interpreted as a vector of importance weights, which allows the LSTM attend to the parts of an input that are correlated to the prediction. However, in our experiments we found that using self-attention after the LSTM/RNN layers will degrade the prediction accuracy in terms of NMSE. At the same time, attention only provide marginal outage reduction. This is because, for regression tasks, typical RNN-based attention schemes are less effective in capturing local dependencies [135, 136].

5.4.1 Time Complexity Analysis

One of the practical barriers of implementing NN-based methods on portable devices is constrained computation budgets. We here investigate the computation complexity of our proposed method. In 'LiteLSTM', the total time complexity of 1-D convolutional layers is $\mathcal{O}(k \cdot T \cdot n_l \cdot s_l)$ [137, 138], k denotes the kernel size, T is the number of time steps. n_l, s_l are the size of output and the number of channels at layer l. For the proposed 'LiteLSTM', $s = 1$, T is the number of input channel samples, $n = 1$ for the input convolutional layer and $n = h$ for the output convolution layer, where h is the number of hidden state in the LSTM cell. For an LSTM layer, the complexity of per time step is $\mathcal{O}(h^2)$ [97]. Therefore, the time complexity of the LSTM layer is $\mathcal{O}(h^2 \cdot T)$. Since 'LiteLSTM' is sequential, the overall complexity will be $\mathcal{O}([h^2 + k \cdot \sum_{l=1}^{2} n_l] \cdot T)$. Therefore, the total complexity of 'LiteLSTM' can be written as $\mathcal{O}(c \cdot T)$, where $c = h^2 + k \cdot (1 + h) \approx h^2$ is a constant determined by the structure of the network.

Hence, with respect to the number of time steps T, 'LiteLSTM' is considered to be linear in time. At the same time, most traditional methods, e.g. adaptive predictions, also require time complexity of $O(T)$. So that, theoretically, compared with traditional methods, the overhead of 'LiteLSTM' is not significantly increased.

5.4.2 Experiments and Results

5.4.2.1 Performance of Different Variants

In the following experiment, we benchmark the performance of different RNN variants. The LSTM cells in the original model are replaced by GRU

[139] and Vanilla RNN cells. Also, in 'LiteRNN' and 'LiteGRU', Vanilla RNN cells and GRU cells replace the LSTM cells in 'LiteLSTM'. The performance of the original LSTM model is used as the baseline. For different model variants, prediction accuracy (in terms of NMSE), computation efficiency and transmit power control outcomes are compared. In order to obtain comparable results, the same training sets and prediction set are employed by different model variants. Thus, the batch size of each iteration is set as 64. Again, the Adam optimiser with an initial learning rate of 0.003 is used.

The results of the comparison are shown in Table 5.2, where it can be observed that the original LSTM model can provide most robust results in terms of prediction accuracy when compared with other variants. However, this model has computational storage and complexity requirements, typically infeasible for real-time deployment and processing on a mobile device. When the original architecture is used, LSTM can provide the lowest NMSE, while other variants have nearly more than 45%. In terms of power consumption, despite having a large number of parameters, LSTM consumes nearly 12% less transmit power than other variants. When a light-weight architecture is applied, performance degradation can be seen in all variants. Among those lightweight variants, 'LiteLSTM' outperforms others by providing up to 15% outage probability reduction and 11% less transmit power. It should be noted that, although Vanilla RNN has less trainable parameters, the level crossing rate (LCR) [3] of vanilla RNN is the highest among all variants, which is around 63% higher than 'LiteLSTM'. The average outage duration (AoD) is also lowest for 'LiteLSTM' as opposed to other lightweight variants, with a small degradation from heavier variants. Thus, from Table 5.2, 'LiteLSTM' pro-

[3] The rate at which Rx power crosses below Rx_{sens} to when it next crosses below Rx_{sens}

vides small accuracy loss and greater computation/storage reduction compared with the original model. It should also be noted that the circuit power consumption of 'LiteLSTM' is 20% less than using -5dBm constant transmit power [11]. In addition, the proposed method uses even less circuit power than cooperative power control [38], which requires more complicated radio receiver design.

.

Table 5.2: Prediction performance comparison of different structures. NMSE is Normalised mean-square-error (with ratio to LSTM, higher ratio implies less accuracy). Tx_Pow is transmit power in dBm, "Circuit" is circuit power consumption in mW. LCR is level crossing rate in Hz, AoD is average outage duration in ms

Methods	Accuracy	Efficiency	Performance				
	NMSE	# of Para.	Outage	Tx_Pow	Circuit	LCR	AoD
LSTM	– –	75529	1.70%	-8.80	3.09	3.04	11.62
RNN	145.70%	19081	1.80%	-8.33	3.17	3.75	11.80
GRU	147.94%	56713	1.79%	-8.29	3.18	3.07	11.62
LiteLSTM	**119.18%**	**1171**	**1.83%**	**-8.50**	**3.13**	**3.87**	**12.28**
LiteRNN	149.26%	309	2.13%	-8.07	3.22	6.31	12.57
LiteGRU	184.76%	885	2.16%	-8.26	3.19	4.91	13.56

5.4.2.2 Sampling Rates

In order to better interpret our method in the context of IEEE 802.15.6 that supports varying superframe lengths, Table 5.3 compares the performance of different methods at sampling rates 50Hz, 20Hz, and 10Hz respectively. Apart from predictive methods, a non-predictive channel deviation-based power control [140] is also evaluated. All methods are required to provide power control for the next 1s using 2s of previous channel samples at the corresponding sampling rate. As both Adaptive Power Control and Channel Deviation-based Power Control require recursive calculation at every time

step, they use their result as the input for the next operation. In contrast, 'LiteLSTM' has the capability to perform power control to the sensor once after a longer interval of time using only previous channel samples. Following from [11], normalised power bias, which is defined as $\mathbb{E}[\tilde{p}(l)/p(l) - 1]$, is used to measure the prediction accuracy.

Table 5.3 shows that for all methods, with the increase of sampling period, the outage probability of each method reduces ~~with the sampling rate~~, whereas the transmit power of each method increases. This is because large sampling period will bring fluctuations to the sampled sequences, and Algorithm 5 will respond to those fluctuations by using more transmit power. With the sampling periods range from 100ms to 20ms, similar results can also be found in [89], which uses the same data-set as this study. As expected, with the increase of the sampling period, the performance gains of 'LiteLSTM' remain in most aspects. Compared to traditional methods, the outage probability of 'LiteLSTM' is around 40% less. Nevertheless, 'LiteLSTM' consumes similar transmit power to the Moving Average. This is because the light-weight structure slight reduces its prediction accuracy. It also can be seen that Adaptive Power Control is more sensitive to the reduced sampling rate. AoD is a dynamic representation of the system outage performance. For a system with high AoD, when re-transmission of a packet is required, it is most likely that the consecutive transmissions will fail again [7, 141]. For all the methods, AoD increases when the sampling rate sampling rate is reduced. This is because when an outage occurs it takes a longer time to recover. The AoD of Adaptive Power Control is the largest among all the methods and when lowering the sampling rate, it increases from 32.65ms to 40.42ms. Meanwhile, 'LiteLSTM' is resilient to longer sampling periods, as

the AoD of 'LiteLSTM' is the smallest and remains almost constant at around 24ms.

Table 5.3: Prediction performance comparison of different sampling rates. Higher bias implies less accuracy. Tx_Pow is transmit power in dBm. "Circuit" is circuit power consumption in mW. AoD is average outage duration in ms. STD PC, MA, AP represent Standard Deviation Power Control [140], Moving Average [131] and Adaptive Power Control [132] respectively.[5]

Rate	Method	Acc.	Performance			
		Bias	Out. Prob	Tx_Pow	Circuit	AoD
50Hz	**LiteLSTM**	2.53	5.08%	-7.90	3.24	22.18
	STD PC	– –	7.29%	-7.49	3.32	24.73
	MA	2.92	6.91%	-7.86	3.26	26.78
	AP	4.57	9.00%	-8.43	3.16	32.65
20Hz	**LiteLSTM**	1.42	3.93%	-7.58	3.29	25.10
	STD PC	– –	6.98%	-7.66	3.28	32.67
	MA	1.94	5.11%	-7.64	3.28	29.01
	AP	3.17	7.05%	-8.51	3.14	37.75
10Hz	**LiteLSTM**	1.04	3.52%	-6.61	3.47	24.00
	STD PC	– –	7.01%	-6.46	3.51	38.35
	MA	1.48	4.48%	-6.48	3.50	27.89
	AP	2.43	6.99%	-7.35	3.35	40.42

5.4.2.3 On-device Runtime Performance

Although, the linear time complexity of 'LiteLSTM' is theoretically guaranteed, the actual running time can be highly sensitive to the implementation and hardware. Meanwhile, the running time of the training process has a huge impact on the functionality of our proposed incremental learning mechanism. We, therefore, evaluate the runtime performance of the 'LiteLSTM' by using commercial mobile devices. Two devices: Raspberry Pi 3 and Pixel 3 are used to implement our proposed method. Because of the different CPU

[5]LCR is not evaluated as it is related with sampling rate.

Figure 5.16: Mobile Implementation

Table 5.4: The ratio of NMSE between the 'LiteLSTM' & the original version of the LSTM predictor

Name of the Subject	Pixel	Raspberry Pi 3
20090430_Female2	116%	113%
20090421_Male1	123%	125%
20090421_Male5	120%	121%
20090417_Male4	115%	112%
20090423_Female4	125%	122%

architectures on these two devices, different deep learning frameworks are used. On Pixel 3, we implement 'LiteLSTM' using a Keras. On Raspberry Pi 3, Tensorflow that is built from a source is used. In Table 5.4, we compare the prediction accuracy on both devices using different channel measurements in terms of NMSE against the original version of the LSTM predictor. Fig. 5.16 demonstrates our implementation running on a Pixel 3.

It can be observed that the mobile implementation of 'LiteLSTM' gives similar results compared to previous experiments. However, since 'LiteL-

STM' is deployed by different frameworks on mobile devices (using ARM CPU), the precision of the prediction is slightly degraded. The prediction accuracy of the Pixel 3 and Raspberry Pi are very similar. Most importantly, the network is compressed at an enormous scale in terms of the number of trainable parameters, which guarantees the normal operation of the mechanism. In our experiments, the on-device training time of the proposed neural network will increase due to limited computational power. Thus, if the training takes longer than the period of one segment of the incremental training, the timing scheme then overflows. As the training process continues, such overflow accumulates and will prevent the neural network from updating parameters. To make sure the incremental training mechanism operates properly, the maximum training time allowed for one epoch is defined as:

$$Tt_{max}(N_{samples}) = \frac{N_{samples}}{N_{epoch} \times f_s}, \tag{5.7}$$

where f_s is the sampling frequency. Besides, the training time is also related to the number of batches. To maintain a fully functional Incremental training scheme, the training time should be kept less than Tt_{max}. To explore the relationship between the training time and the training parameters, we evaluate the training time of the proposed predictor on a Pixel 3 with different training set sizes and batch sizes by using the same channel measurement set. Table 5.5 demonstrates such a relationship in detail. As can be seen the relationship between the actual training time and the size of the training set is not linear. Feasible settings that meet the requirements of incremental learning are highlighted. When running on Raspberry Pi, the runtime of 'LiteLSTM' is not able to meet (5.7), due to low computation capability. For Pixel implementations, when the numbers of samples for training is less than 2000,

Table 5.5: Incremental Training Time for Different Batch Sizes

Batch Size	Device	Number of Samples		
		500	1000	2000
64	Pixel	2.0s	3.6s	6.6s
	Raspberry Pi	6.9s	11.3s	14.2s
32	Pixel	3.1s	5.9s	10.4s
	Raspberry Pi	10.2s	16.4s	22.5s
16	Pixel	4.0s	8.4s	16.2s
	Raspberry Pi	15.4s	25.6s	30.1s

it is difficult to keep the incremental training mechanism fully functional by using small batches.

5.5 Concluding Remarks

In this chapter, firstly an LSTM based BAN long-term channel prediction scheme was presented. The proposed method provided noticeable improvements in reliability and power consumption in comparison to other predictive power control methods when mapped to a suitable power control algorithm. To make sure that the DL method is resilient to the dynamic changes in wireless channels, an incremental training scheme was also developed. Due to the computational limitation of hub devices in BANs, it is important to exploit the hardware applicability of the proposed DL-based method so that it can be realistically applied. Therfore, to successfully training the NN on-device, we developed 'LiteLSTM', which is much more efficient in terms of computational cost. 'LiteLSTM' occupies around 45 times less trainable parameters than the original LSTM model.

Experimental results showed that the LSTM model can provide up to 2s channel prediction ahead with 50% NMSE reduction compared to the bench-

mark Moving Average predictor. When mapped to a suitable power control algorithm, there were noticeable improvements in reliability and power consumption in comparison to other predictive power control methods. Comparable results can be obtained from 'LiteLSTM' at different sampling rates. By evaluating its runtime performance, despite being implemented on tiny devices, 'LiteLSTM' is still able to retain robust and comparable performance to LSTM. This has demonstrated that it is feasible to implement advanced DL channel prediction. Although the high computational complexity of DL methods often prevent them from realistic implementations on hand-held devices, our proposed light-weight structure can be used to provide more efficient adaptive scheduling approaches to further improve the overall system performance and enable deployment on hand-held devices. However, it is a challenging issue to demonstrate how neural networks interact with input data, especially when using dynamic BAN channel samples as inputs. Hence, in the next chapter, we using parametric modelling to reveal the relationship between BAN channel predictive characteristics and the performance of the 'LiteLSTM' described here in this chapter.

Chapter 6

Interpretation of Deep Learning Channel Prediction Model From a Wide-Sense-Stationary Perspective

6.1 Introduction

As concluded in the last chapter, recent years have seen growing interest in predictive resource allocation schemes in BANs. Among such schemes, DL techniques have achieved extremely high predictive accuracy, in many cases, outperforming traditional methods. In practice, it is also important to understand how do the DL methods provide sustainable performance gains from proper exploitation of the wireless channel features. It is known that simple models provide higher interpretability than complex ones. However, with more than thousands of parameters that can be tuned inside the neural network, DL methods could be interpreted as nonparametric, thus, it is very difficult to characterise the DL models through direct parametric modelling.

The parametric modelling of the performance of DL predictive methods with respect to the wireless channel's probability of stationarity can be used for predictive analysis towards futuristic autonomous IoH applications. As

it is very important towards understanding the nature of the neural network that allows optimization of parameters for overall performance gain. This chapter investigates the following question: *What's the relationship between the performance of DL method and the predictability of the BAN wireless channel in terms of the probability of satisfying WSS for different duration times?* By answering the above question, we provide some interpretability to the DL methods, which helps to unveil the so-called "black-boxed" mechanism behind DL-based approaches.

Previous research shows that wide-sense stationarity (WSS) is an important characteristic to estimate the predictability of a channel, and therefore plays a significant role in the design of BAN systems. The definition of the WSS or second-order stationarity is as follows:

Definition 6.1. WSS If the first and second moments (mean and auto-covariance) of a process $X(t)$ are independent of time, such that:

$$\begin{aligned} \mathbb{E}\left[X(t)\right] &= \mu_x(t_1) = \mu_x(t_1+\omega), \text{ for all } \omega \in t \\ Cov[X(t_1), X(t_2)] &= Cov[x(t_1, t_2)]] = Cov[x(t_1+\omega, t_2+\omega)], \text{for all } \omega \in t, \end{aligned} \tag{6.1}$$

where $\mu_x(t)$ denotes the mean of $X(t)$. $Cov[X(t_1), X(t_2)] = \mathbb{E}[\{X(t_1) - \mu_x(t)\}\{X(t_2) - \mu_x(t)\}]$ depends on the difference of $t_2 - t_1$.

However, in practice, BAN channels are extremely difficult to model because of the human-body dynamics and shadowing effects brought by postural movements. Previous studies suggest that real-world radio channels often demonstrate 'quasi-stationary' characteristics. In order to identify the suitable time region of wide-sense stationary, it is important to provide sys-

tematic modelling of channel behaviour. As have already been discussed[1] that WSS has not been broadly studied for BANs. In [142] provide a practical approach to examine the WSS of BAN on-body channels using null hypothesis significance testing [143]. In [142] interval over which the channel is WSS determines the interval for which the statistical models are meaningful. Where the channel is not semi-stationary, we shall refer to it as non-stationary. It is shown [11, 144] that, for BAN on-body channels the probabilities of stationarity at large intervals (> 500 ms) are relatively low, typically under 50%. Hence, it is very important to verify that how do the low probabilities of stationarity affect the performance of DL channel prediction schemes.

Therefore the main contributions of the study are:

- The parametric modelling of the performance of DL predictive methods with respect to the wireless channel's probability of stationarity.

- We show that outage probability is a Reciprocal Logarithm function of the average probability of stationarity and MSE has a sigmoidal relationship with the average probability of stationarity.

In the following sections, we describe how to measure the BAN channel stationarity via null hypothesis significance testing (NHST) in detail, and discuss the experimental outcomes of different window lengths from benchmarking the previously proposed 'LiteLSTM' over real-life experimental channel measurements. Finally, conclusions and remarks are summarized.

[1]Some related work has been reviewed in Chapter 2

	Tx	Rx				
One-Star	Lh	Lc	Lw	Rw	Ra	H

Table 6.1: Sounders placement map: One-Star Topology[2]

	Tx		Rx							
Multi-Star	Lh	Rc	Lw	Rw	Ra	H	Rk	Lk	La	Le

Table 6.2: Sounders placement map: Multi-Star Topology[2]

6.2 Experiment Scenarios

In this chapter, we analyse the WSS characteristics of BAN on-body channels and benchmark DL-based predictive power control method with an extensive amount of channel measurements from [118]. Detailed descriptions of these measurements can be found in Chapter 4.

Both one-star and multi-star topologies were measured. The full map of Tx/Rx locations is illustrated in Table 6.1 and Table 6.2.

Channel gains were derived using the received signal strength indicators (RSSIs). Digital logs were made upon successful packet detection by the sounders. It is noteworthy that each Tx transmits in a roundrobin fashion, at 2.36 GHz, which in compliance with IEEE 802.15.6.

6.3 Null Hypothesis Significance Testing

We apply stationarity null hypothesis significance testing based on the definitions given in [145, 142]. WSS is tested over mean and variance via ANOVA that will be discussed later. As defined in Definition 6.1, the WSS implies mean and variance stationarity of the channel.

[2]Sounders placement map: R, L-Right, Left. w-Wrist, a-Ankle, k-Knee, e-Elbow, h-hip, H-head, c-Chest.

In this paper, WSS is tested over a wide range of window lengths L, hence, the whole channel is divided into m consecutive non-overlapping intervals of length l. This means that there will be $m-1$ pairwise independent null hypothesis test, for each window length L where $L = 2 \times l$. The Fig 6.1 illustrate the pairwise comparison across two intervals.

Thus, the average probability of stationarity of L under the null hypothesis for test statistic T_L at a significance level α can be formalized as:

$$\begin{aligned} &H_0 : L \text{ retains WSS (null hypothesis)} \\ &H_1 : L \text{ does not retain WSS (alternative hypothesis)} \end{aligned} \tag{6.2}$$

Then,

$$p_L = P\{T_l > T_{L_obs} | H_0\}. \tag{6.3}$$

When given that the null hypothesis is true, the p-value p_l that represents the probability of observing a more extreme test statistic T_l is a measure of evidence against H_0. Therefore, when at the significance level/threshold α that measures the significance of the test outcome. The p-value p_l can be interpreted as the probability of incorrectly rejecting a true null hypothesis:

$$\begin{aligned} &\text{if } \alpha > p_l, \quad \text{then } H_0 \text{ is rejected in favor of } H_1. \\ &\text{if } \alpha \leq p_l, \quad \text{then } H_0 \text{ is not rejected.} \end{aligned}$$

The average probability of stationary for window length L at threshold α is the summing over each of the $m-1$ null hypothesis significance testing :

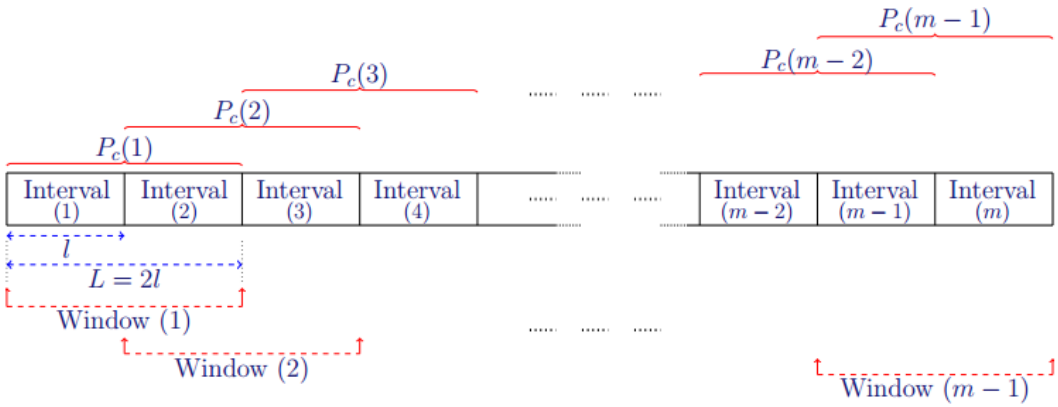

Figure 6.1: $m-1$ pairwise comparison across consecutive intervals

$\{p_L^1, P_L^2, P_L^3, ..., P_L^{m-1}\}$, which can be expressed as:

$$\gamma_L = \frac{\sum_{i=1}^{m-1}\{p_l^1 > \alpha\}}{m-1}, \tag{6.4}$$

γ_L therefore represents the percentage of pairwise comparisons that satisfy the null hypothesis significance testing over all windows.

6.3.1 One-way ANOVA Test

To evaluate the mean and variance consistency of the BAN on-body channels, a one-way ANOVA test is used in this study. The ANOVA test is the ratio of the mean square variance within each interval and the mean square variance between the intervals, which analyzes the variation or difference between the means of two or more sets of observations:

$$T_{anova} = \frac{\tilde{S}_{between}}{\tilde{S}_{within}}, \tag{6.5}$$

where,

$$\tilde{S}_{between} = \frac{\sum_{i=1}^{k} n_i(\bar{X}_i - \bar{X})^2}{k-1}, \tag{6.6}$$

and,

$$\bar{S}_{within} = \frac{\sum_{i=1}^{k}}{N-k}, \tag{6.7}$$

where N is the total number of the observations, $\bar{X}_i$ is the sample mean in the ith group, and $\bar{X}$ is the overall mean. In general, ANOVA testing requires that the variances of the underlying distribution are homogeneous and have a normal distribution. However, BAN channels are not always normally distributed. Despite this, with a large number of observations, ANOVA can be considered as robust [145]. In addition, when the sets/intervals are the same size and have a similar distribution, the sensitivity of ANOVA against the homoscedasticity assumption is relatively low [146].

6.4 Performance Evaluation

6.4.1 ANOVA Test Results

Table 6.3 shows the average probability of stationarity for the ANOVA hypothesis tests of BAN on-body channels (See Section 6.3 for details) when $\alpha = 0.95$. It should be noted that the results are averaged over all channel measurements with multiple subjects.

Overall, the average probability of stationarity is relative low (less than 40%) [3]. This suggests that in our experiments, on-body channel gains still exhibit non-stationarity in general. In addition, the stationarity reduces with the increase of window length.

[3]This finding is in agreement with [145]

Window length (No. of samples)	Duration	Avg. Prob. of stationarity p-value in average
150	3000ms	0.387
200	4000ms	0.387
250	5000ms	0.336
500	10000ms	0.275
750	15000ms	0.223
1000	20000ms	0.205

Table 6.3: ANOVA hypothesis tests for the average probability of stationarity over all channel measurements

Remark. The results of the ANOVA test demonstrate that the probability of stationarity reduces significantly with the increase in window length. Hence, this brings up the discussion of how will the reducing probability of stationarity impact the performance of DL predictive power control.

To analyse the effect of training duration in DL channel prediction models. In the next section, we evaluate the performance of 'LiteLSTM' using different input sizes that correspond to different window lengths in the null hypothesis significance testing .

6.4.2 Performance of 'LiteLSTM'

As described in Chapter 5 Section 5.4, 'LiteLSTM' is a DL channel predictor and it is much more efficient in terms of computational cost. 'LiteLSTM' uses 1-D convolution layer as input layer, and the output of the input layer is connected with a single LSTM layer, with another 1-D convolution layer as output layer. The 1-D convolution layer provide better generalization ability [147], and as shown previously in Chapter 5 the performance of 'LiteLSTM' maintains good performance under different sampling rates.

Here we demonstrate the performance outcomes of the DL method using

different input sizes N_{in}. It should be noted that for sampling frequency f_S, the corresponding duration of each instance is $T_s = \frac{1}{f_s} \times N_{in}$. The dataset we used to conduct our experiments was described in Chapter 5. And the parameter settings are listed in Table 6.4.

Table 6.4: Parameter Settings of 'LiteLSTM'

Description	Value
Number of layers in the LSTM network	1
Size of the hidden state of an LSTM cell	16
Number of sequences in each mini-batch	32
Input size of the network	N_{in}
No. of epochs for initial training	50
No. of epochs for model fine tuning	20
Learning Rate	0.003
Dropout Probability	0.8

In addition, to produce the best possible performance from the proposed predictor, we used the previously developed Tx power control algorithm. The details of the Tx power control scheme is described in Algorithm 5. It should also be noted that, error bars are also plotted to represent one sigma of uncertainty (+/- 1 σ).

Here we use *Mean Square Error* to measure the 'absolute' numerical prediction error of the 'LiteLSTM'. As shown in Figure 6.2, the MSE firstly reduces and then increases with the increase of window length. This trend is similar to Figure 5.10 in Chapter 5 where NMSE is plotted against the input size of the NN.

Figure 6.3 illustrates the Tx power consumption against different window lengths. It can be seen that Algorithm 1 provides sustainable transmit power reduction. Hence, average Tx power consumption approximately remains constant over different input sizes.

As shown in Figure 6.4, outage probability increases with an increase in

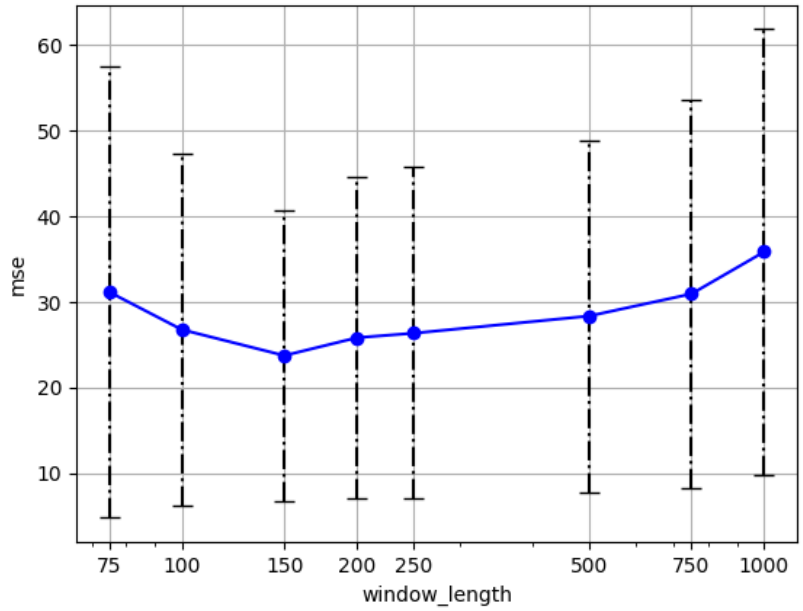

Figure 6.2: MSE at different window length

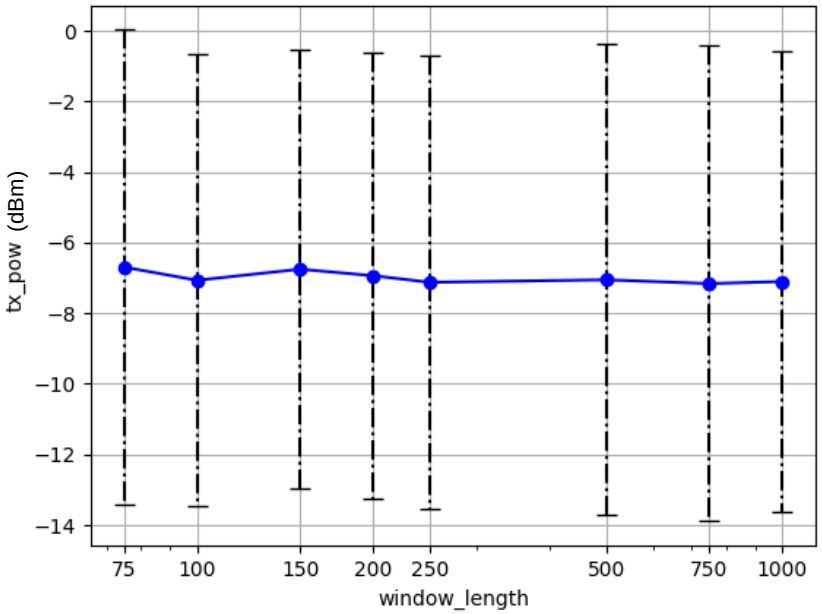

Figure 6.3: Tx power consumption at different window length

window length. Also, the standard deviation of outage probability increases, which means that large window length (less probability of stationarity) reduces the robustness of the 'LiteLSTM'. Meanwhile, Figure 6.5 demonstrates that for Average Outage Duration (AoD), a similar pattern can be identified. This is because AoD is correlated with outage probability, as higher probability of outage also increases the probability of consecutive outage that eventually increases the duration of the outage.

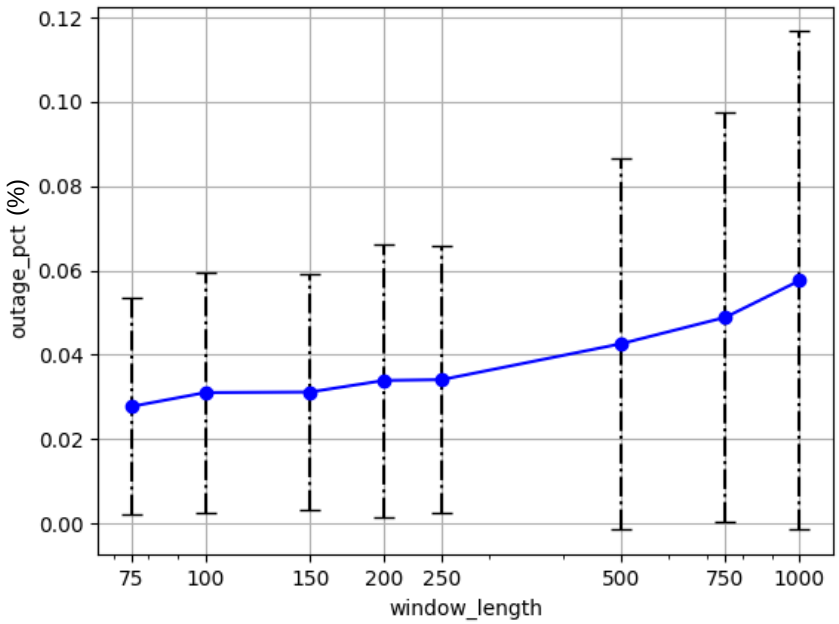

Figure 6.4: Outage probability at different window length

6.4.3 Performance Modelling

To parametrically model the performance of 'LiteLSTM' and the probability of stationarity at different window length, we use the Levenberg-Marquardt method [148], which is a fast, reliable technique for nonlinear optimization to model the non-linear relationship between them.

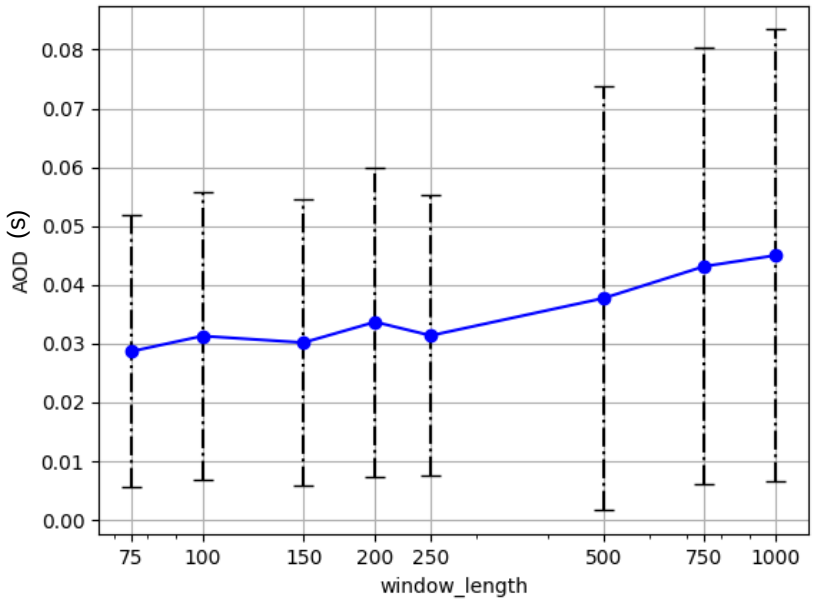

Figure 6.5: AoD at different window length

Figure 6.6 shows that relationship between MSE of 'LiteLSTM' and the probability can be characterised by a *Logistic Model*:

$$MSE = \frac{\alpha}{1 + \beta \cdot \exp^{(} -\theta \cdot p)}, \tag{6.8}$$

where the values of constants α, β and θ are listed in Table 6.5.

Constant	α	β	θ
Values	26.468	-20.833	21.494

Table 6.5: Constants' Values of the Logistic Model

In Figure 6.7 an a *Reciprocal Logarithm* model is shown to present the relationship between outage probability and the probability of stationarity. It means that the outage probability of 'LiteLSTM' can be represented as a Reciprocal Logarithm function of the probability of stationary:

$$\text{Outage} = \frac{1}{\alpha + \beta \cdot \ln p} \quad , \tag{6.9}$$

the values of parameters: α and β are listed in Table 6.6:

Constant	α	β
Values	51.018	20.934

Table 6.6: Constants' Values of the Reciprocal Logarithm Model

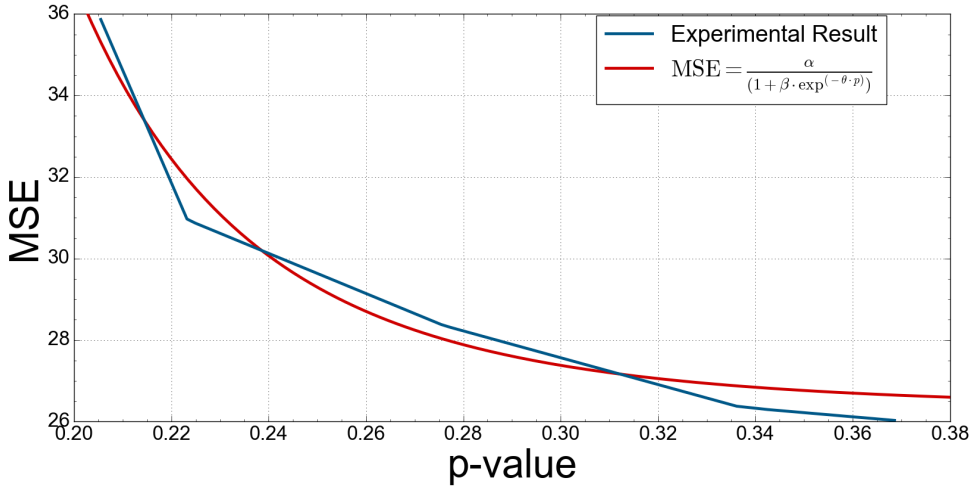

Figure 6.6: Logistic Model of MSE towards probability of stationarity (p-value)

6.4.3.1 Goodness-of-Fit

To access the goodness of fit (GOF) of the parametric modelling, two metrics are used, which are the standard error and the coefficient of determination R^2 respectively. The standard error can be expressed as $\sigma_{\bar{x}} = \frac{\sigma}{\sqrt{n}}$, where σ is the standard deviation. The Correlation Coefficient R is:

$$R = \frac{\mathbb{E}[XY] - \mathbb{E}[X]\mathbb{E}[Y]}{\sqrt{\mathbb{E}[X^2] - (\mathbb{E}[X])^2}\sqrt{\mathbb{E}[Y^2] - (\mathbb{E}[Y])^2}} \tag{6.10}$$

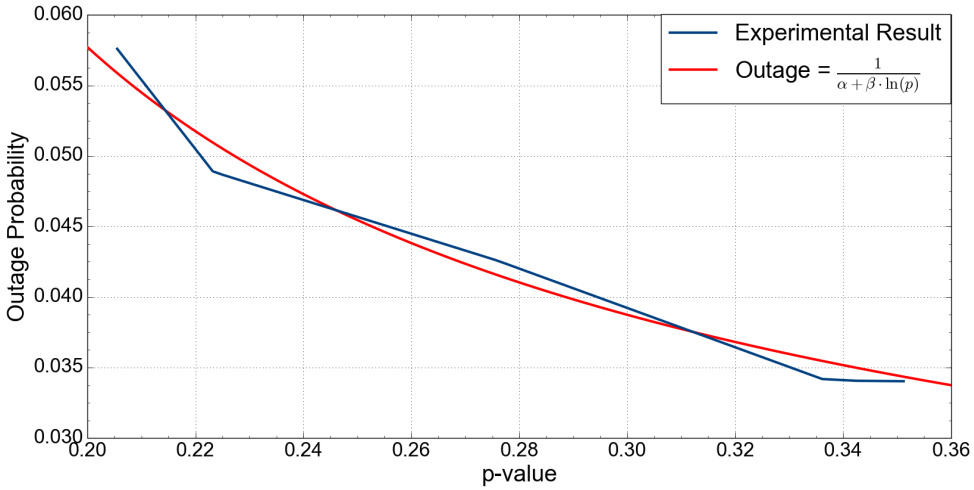

Figure 6.7: Reciprocal Logarithm of Outage Probability towards probability of stationarity (p-value)

and for sampled data, it could be represented as:

$$R = \frac{\sum_{i=1}^{n}(x_i - \bar{x})(y_i - \bar{y})}{\sqrt{\sum_{i=1}^{n}(x_i - \bar{x})^2}\sqrt{\sum_{i=1}^{n}(y_i - \bar{y})^2}} \tag{6.11}$$

coefficient determination R^2 is basically a square of a correlation coefficient, which provides one measure of goodness of fit. The closer this value is to 1 or to -1, the better the fit. Table 6.7 provides the standard error and the coefficient determination R^2 for the Reciprocal Logarithm Model of Outage Probability and the Logistic Model of the MSE respectively.

Model	Reciprocal Logarithm	Logistic Model
Standard Error	0.009	0.040
Coefficient Determination	0.991	0.989

Table 6.7: Goodness-of-fit of the Logistic Model and the Reciprocal Logarithm Model

It is clear that the standard error is relatively small, which implies that the models are effective. Also, the correlation coefficients are close to 1, so that

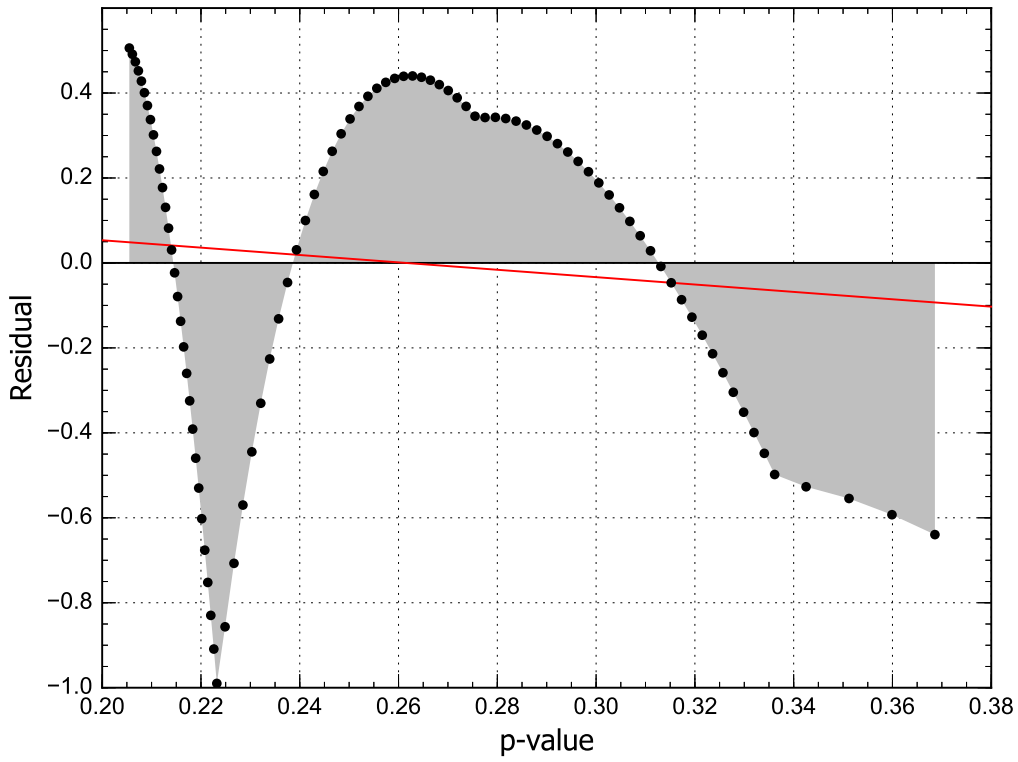

Figure 6.8: The residual plot of the logistic model

goodness-of-fit is guaranteed.

Additionally, the residual plots of these two models are illustrated in Figure 6.9 and Figure 6.8. Although, such residuals are normally used to assess the fitness of linear regressions, the randomness in both plots also corroborates that the parametric models provide a decent fit.

6.5 Concluding Remarks

In the last chapter it was shown that DL methods can achieve better performance in BAN channel prediction tasks, leading to more efficient resource allocation. In this chapter, we explored the relationship between the dynamic

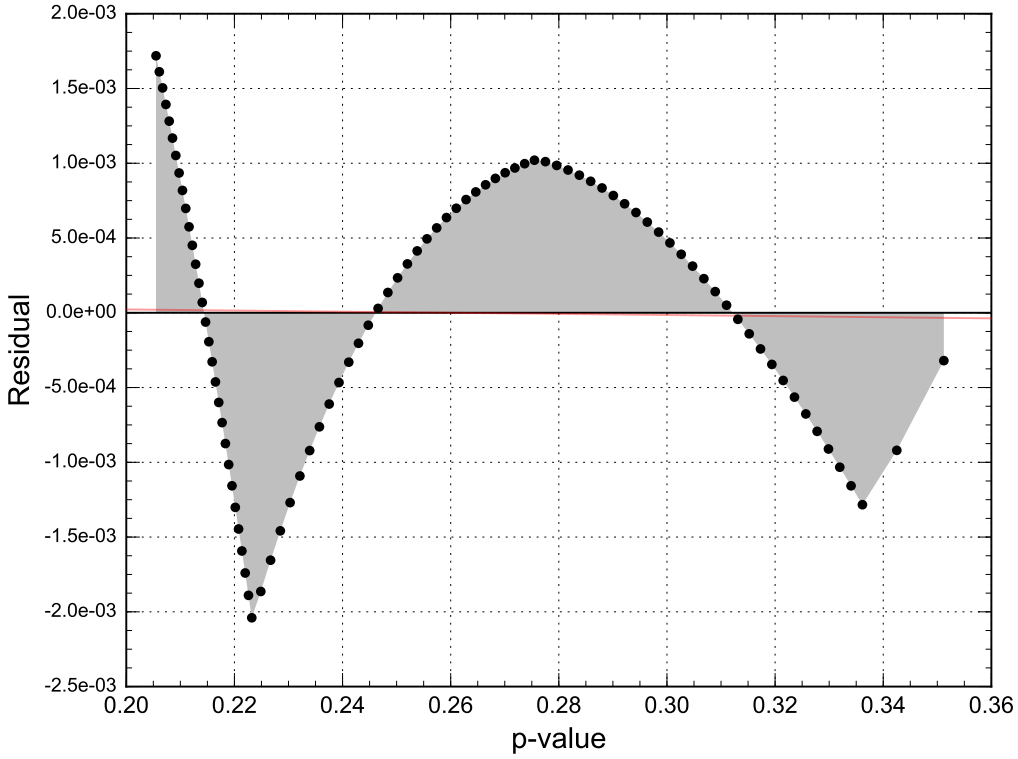

Figure 6.9: The residual plot of the Reciprocal Logarithm model

features of BAN channels and the performance of the neural network. Using the null hypothesis significance testing (NHTS), the predictability attributes of the BAN channels were characterised in terms of the probability of stationarity. More specially, here, a one-way ANOVA test was used to measure the probability of stationary with different window lengths. The results of the one-way ANOVA test demonstrated that BAN on-body channels exhibits non-stationarity in general and the probability of stationarity reduces significantly with the increase of the window length. When trained by using input sequences with different sizes (window length), the first order and second order performance statistics of 'LiteLSTM' demonstrates different non-linear relationships with input lengths.

To this end, we used parametric modelling with guaranteed goodness-of-fit to measure the relationships between the level of stationarity of the channel and the actual performance metric of 'LiteLSTM' to provide parametric observation of how exactly the dynamic features of the BAN channels impact our proposed neural network. The results showed that outage probability is reciprocal logarithm function of the average probability of stationarity and MSE has a sigmoidal relationship with the average probability of stationarity.

Chapter 7

Conclusion and Future Work

In this chapter, the key contributions made in this thesis are remarked upon, and future research directions are also illustrated and discussed.

7.1 Conclusion

The overall goal of this thesis has been to achieve high-reliability and improve energy efficiency for BAN enabled IoH systems, via adaptively and intelligently distributing limited radio resources and accurately predicting dynamic wireless channels.

There is no denying that because of its promising advantages, BANs are becoming a reality in meeting current and future requirements of the IoH systems. Recently proposed BAN communication standards and current research challenges associated with the realisation of BAN enabled IoH were described in detail. BAN sensor nodes are often constrained in sizes that lead to limited transmit power to meet the requirements of next-generation IoH. Moreover, the lack of central network coordinators results in heavy inter-BAN interference, which makes it challenging to maintain high QoS when radio resources are limited. Therefore, due to these challenges and the unique features of BANs, we argued that the existing literature is not well suited for real-world BAN enabled IoH systems. To this end, our line of works explored

the use of effective radio resource schemes with game-theoretic mechanisms and accurate wireless channel prediction technology to improve overall communication QoS, maintain high reliability and increase energy efficiency of BANs. It should be noted that we used extensive BAN channel measurements that were collected from subjects performing different "everyday" activities in practical scenarios, which captures dynamic factors of the BAN channels in realistic settings, which we used extensively to evaluate our proposed solutions.

Below, we provide conclusions of each technical chapter (from Chapter 3 to Chapter 6) and short answers to the research questions raised in the thesis statement (Chapter 1).

In Chapter 3, a non-cooperative game transmit power control was used, which adaptively allocated limited transmit power for each BAN sensor. When compared with traditional methods, the proposed game provided a remarkable reduction in energy consumption and guaranteed good communication reliability. Most importantly, the postulate of social optimality of the game was mathematically proven across all players/BANs when giving feasible constraints. This chapter provided answers to the questions raised in: Q1, Q2.

In Chapter 4, we further strippped down the strength of game-theoretic methods by developing two cross-layer radio allocation schemes (Link Adaptation Game and Contention Window Game)employed with a time-division multiple access (TDMA) MAC that has a novel back-off mechanism, to jointly adjust the different transmission parameters of BAN nodes. It was demonstrated that the proposed methods provide robust transmission under strong inter-BAN interference. This chapter provided answers to the questions raised

in: Q2, Q3.

In Chapter 5, we explored deep learning frameworks for long-term channel predictive power control, which demonstrated great improvement in energy efficiency when compared with traditional predictive power control methods. To utilise a DL method in realistic BAN applications, a light-weight network with low computational cost and comparable performance that can be implemented on hand-set devices was proposed. This chapter provided answers to the questions raised in: Q4, Q5, Q6.

In Chapter 6, we characterised the interpretability of our proposed DL methods in Chapter 5 in terms of predictive behaviour of the BAN on-body channels. Null Hypothesis Tests (NHPT) were applied over a varies number of channel measurements to analyse the wide-sense-stationarity of the wireless channels. Parametric modelling was also conducted, which showed relationships between channel characteristics and the performance metrics of DL methods, and such relationships numerically explained the proposed neural networks. This chapter provided answers to the questions raised in: Q4, Q7.

7.2 Future Work

In this thesis, we have shown that non-cooperative game theory power control schemes can significantly save energy consumption of BAN sensors and prolong the system lifespan, and provide significant interference mitigation for co-existing networks.

7.2.1 Recommended Future Research Work for Chapter 3

In the future, the scalability and computational cost of game-theoretic methods using hardware implementations could be investigated. For next-generation IoH applications that consist of sensors with a varying number of types, BANs need to be able to adapt to various transmission priorities, especially for on-demand emergency packet transmissions. Hence, the development of resource allocation schemes cross MAC/PHY layers that support different communication priorities will be paramount in the future.

7.2.2 Recommended Future Research Work for Chapter 4

Although game theory provides a promising solution towards multi-BAN coexistence, practical implementation of such algorithm on a hardware level still requires further research. Meanwhile, it would also be promising to apply a software-defined network (SDN) that allows the network to be managed from a logically central point and could simplify the control and management operations of BAN systems. This would be in order to support comprehensive BAN solutions that have different PHY layer standards: narrowband, ultra-wideband (UWB), and human body communication (HBC) at the same time. Considering that the interference between BAN communications and other wireless systems such as Bluetooth, WLAN, ZigBee, etc.., will become inevitable, it will be essential to address the inference management challenge in heterogeneous IoH network environments in the future.

7.2.3 Recommended Future Research Work for Chapter 5

Attention mechanisms have been widely used in different tasks in text classification, video segmentation and time series prediction, which are able to

relate different positions of a sequence in order to compute a better representation. It would be worth investigating how to combine attention with our proposed LSTM channel predict to further improve prediction accuracy. Apart from that, it would also be interesting to use a Seq2seq model [125] with a novel architecture – transformers (also based on attention), as the sequential nature of the RNN-based Seq2seq architecture prevents parallelization in the end-to-end model (as used in this thesis). Going forward, we would like to borrow ideas like graph convolution networks (GCN) [149] and random geometry graph frames in order create better topology management for optimal resource allocation in a BAN's link layer.

7.2.4 Recommended Future Research Work for Chapter 6

In order to empirically estimate the influence of the dynamic features of BAN channels on the prediction made by a DL model, a Null Hypothesis Test was used to provide interpretability. However, in order to explore the relationship between wireless channel dynamics and different neural network structures in depth, it would be interesting to numerically analyse the latent space which represents the hidden 'compressed state' of the neural network. In addition, one could also provide interpretability not only by statistic or parametric models, but by addressing the dimensions of decomposability and algorithmic transparency of the IoH.

Chapter 8

Appendix

8.1 Proof of Theorem 4.5

Firstly, the utility function (4.27) denoted as:

$$V = d \cdot S - c \cdot D - P_{\text{Drop}} \tag{8.1}$$

It can be seen that the first derivative of the utility function is continuous:

$$\begin{aligned} d \cdot \frac{\partial S}{\partial CW} &= \frac{\partial S}{\partial \tau}\frac{\partial \tau}{\partial CW} \\ &= \frac{\partial \tau}{\partial CW} \cdot \frac{(1-P)T_{\text{payload}}[T_{\text{slot}} + \tau(T_{\text{s}} - T_{\text{slot}})] - (T_{\text{s}} - T_{\text{slot}})\tau(1-P)T_{\text{payload}})}{[T_{\text{slot}} + \tau(T_{\text{s}} - T_{\text{slot}})]^2} \\ &= -(aCW+1)^{-2}\frac{d(1-P)T_{\text{payload}}T_{\text{slot}}}{[T_{\text{slot}} + \tau(T_{\text{s}} - T_{\text{slot}})]^2} \end{aligned} \tag{8.2}$$

Hence, according to [103], in this contention window game, the Nash equilibrium exists.

$$\begin{aligned} d \cdot \frac{\partial^2 S}{\partial CW^2} =& \frac{2d(1-P)T_{\text{payload}}T_{\text{slot}}([T_{\text{slot}} + \tau(T_{\text{s}} - T_{\text{slot}})]^2)\tau^2(T_{\text{s}} - T_{\text{slot}})}{[T_{\text{slot}} + \tau(T_{\text{s}} - T_{\text{slot}})]^4} \\ &+ 2\tau^3\frac{d(1-P)T_{\text{payload}}T_{\text{slot}}}{[T_{\text{slot}} + \tau(T_{\text{s}} - T_{\text{slot}})]^2} \end{aligned} \tag{8.3}$$

Meanwhile, delay is a linear function of the contention window size, thus $\frac{\partial^2 D}{\partial CW^2} = 0$.

$$\frac{\partial^2 P_{\text{Drop}}}{\partial CW^2} = 2\tau^3 P^{m+1}, \tag{8.4}$$

which should always be positive. Therefore, the second order derivative of the utility function can be obtained as follows:

$$\begin{aligned}\frac{\partial^2 v}{\partial CW^2} =& -2\tau^3 P^{m+1} + 2\tau^3 \frac{d(1-P)T_{\text{payload}}T_{\text{slot}}}{[T_{\text{slot}} + \tau(T_{\text{s}} - T_{\text{slot}})]^2} \\ &+ \frac{2d(1-P)T_{\text{payload}}T_{\text{slot}}([T_{\text{slot}} + \tau(T_{\text{s}} - T_{\text{slot}})]^2)\tau^2(T_{\text{s}} - T_{\text{slot}})}{[T_{\text{slot}} + \tau(T_{\text{s}} - T_{\text{slot}})]^4}\end{aligned} \tag{8.5}$$

When d is set in a reasonable range, $\frac{\partial^2 v}{\partial CW^2}$ will always be less than zero. Hence, the utility function is concave.

8.2 Proof of Theorem 4.3

In BAN i, for any $x, y, z \in X$, $\|x - y\| = 2$, $\|x - z\| = \|z - y\| = 1$, we have

$$\begin{aligned}F(A_i = (P, R_x), A_{-i}) &= -cP_x^g - q\frac{1}{R_x} + \frac{\alpha(R_x)\cdot\gamma^{\beta(R_x)}}{2} + \sum_{j\neq i} -cP_j^w - q\frac{1}{R_j} + \frac{\alpha(R_j)\cdot\gamma^{\beta(R_j)}}{2} \\ &= C(P_x) + G(R_x) + H(A_i) + Q(A_{-i}),\end{aligned} \tag{8.6}$$

where $H(A_i) = H((P, R_x)) = \frac{\alpha(R_x)\cdot\gamma^{\beta(R_x)}}{2}$, $Q(A_{-i}) = \sum_{j\neq i} -cP_j^g - q\frac{1}{R_j} + \frac{\alpha(R_j)\cdot\gamma^{\beta(R_j)}}{2}$. Meanwhile, $F(A_z, A_{-i})$ and $F(A_y, A_{-i})$ are expressed in a similar way.

Obviously, $G(R)$ is strictly concave, and increase with R. Hence, $2G(R_z) >$

$G(R_x) + G(R_y)$. Also, as shown in table 4.1, $0 > 2\alpha(R_z) > \alpha(R_x) + \alpha(R_y)$. When at high PDR regime, where $\gamma > 0dB$, as $\beta(R_x)$ increases with R and $\gamma^{\beta}(R_x) > 0$ is convex:

$$\begin{aligned} (\gamma^{\beta}(R_y) - \gamma^{\beta}(R_z)) - (\gamma^{\beta}(R_z) - \gamma^{\beta}(R_x)) > 0 \\ \alpha(R_x) \cdot \{(\gamma^{\beta}(R_y) - \gamma^{\beta}(R_z)) - (\gamma^{\beta}(R_z) - \gamma^{\beta}(R_x))\} < 0 \end{aligned} \tag{8.7}$$

Also,

$$\gamma^{b}(R_X) \cdot \{(\alpha(R_x) - \alpha(R_z)) - (\alpha(R_z) - \alpha(R_y))\} < 0 \tag{8.8}$$

Combining equation 8.8 and equation 8.7:

$$\begin{aligned} \alpha(R_x) \cdot \{(\gamma^{\beta}(R_y) - \gamma^{\beta}(R_z)) - (\gamma^{\beta}(R_z) - \gamma^{\beta}(R_x))\} \\ + \gamma^{\beta}(R_X) \cdot \{(\alpha(R_x) - \alpha(R_z)) - (\alpha(R_z) - \alpha(R_y))\} < 0, \end{aligned} \tag{8.9}$$

and

$$\begin{aligned} \alpha(R_x) \cdot \{(\gamma^{b}(R_y) - \gamma^{b}(R_z)) - (\gamma^{b}(R_z) - \gamma^{b}(R_x))\} \\ + \gamma^{b}(R_X) \cdot \{(\alpha(R_x) - \alpha(R_z)) - (\alpha(R_z) - \alpha(R_y))\} \\ - (\alpha(R_x) - \alpha(R_z))(\gamma^{b}(R_y) - \gamma^{b}(R_z)) \\ - (\alpha(R_z) - \alpha(R_y))(\gamma^{b}(R_z) - \gamma^{b}(R_x)) < 0 \end{aligned} \tag{8.10}$$

Thus:

$$\alpha(R_y)\gamma^{\beta}(R_y) - 2\alpha(R_z)\gamma^{\beta}(R_z) + \alpha(R_x)\gamma^{\beta}(R_x) < 0, \tag{8.11}$$

which means $2H(A_i = (P, R_z)) \geq H(A_i = (P, R_y)) + H(A_i = (P, R_x))$,

such that:

$$2F(A_i = (P, R_z), A_{-i}) > F((P, R_x), A_{-i}) + F((P, R_y), A_{-i}) \tag{8.12}$$

Therefore, the potential function F satisfies Lemma1.

8.3 Proof of Proposition 4.1

Let x satisfy $F((P, R_x), A_{-i}) \geq F((P, R_y), A_{-i})$ for all y with $|x - y| \leq 1$. For y with $d = |x - y| \geq 2$, we can make a sequence $x_{k=0}^{d}$ such that $x^0 = x$ and $x^d = y$ with the following steps:

$$x^{k+1} \in \underset{|x-z|=1, |y-z|=d-k-1}{\arg\max} F((P, R_z), A_{-i}) \tag{8.13}$$

Suppose $|x^k - z| = |x^{k+2} - z| = 1$, then we have $d - k = |x^k - y| = |x^k - z + z - y| \leq |z - y| + 1$. Meanwhile, $|z - y| = |z - x^{k+2} + x^{k+2} - y| \leq |z - x^{k+2}| + |x^{k+2} - y| = d - k - 1$. Therefore, $d - k - 1 = |z - y|$, which gives the following equation:

$$F((P, R_{x^{k+1}}), A_{-i}) = \max_{\substack{|x^k - z|=1, \\ |z-y|=d-k-1}} F((P, R_{x^z}), A_{-i}) \geq \max_{\substack{|x^k - z| = x^{k+2} - z|, \\ |x^{k+2} - z|=1}} F((P, R_{x^z}), A_{-i}) \tag{8.14}$$

Since F satisfies LMP as proved above, for $0 \leq k \leq d-2$:

$$\max_{|x-z|=|z-y|=1} F((P, R_{x^{k+1}}), A_{-i}) = \begin{cases} \geq F((P, R_{x^k}), A_{-i}) = F((P, R_{x^{k+2}}), A_{-i}) \\ \qquad \text{, if } F((P, R_{x^k}), A_{-i}) = F((P, R_{x^{k+2}}) \\ > \min\{F((P, R_{x^k}), A_{-i}), F((P, R_{x^{k+2}}), A_{-i})\} \\ \qquad \text{, otherwise} \end{cases} \tag{8.15}$$

Since $|x^0 - x^1| = 1, F((P, R_{x^0}), A_{-i}) \geq F((P, R_{x^1}), A_{-i})$, Also, by using the above properties, for all k we have: $F((P, R_{x^k}), A_{-i}) \geq F((P, R_{x^{k+1}}), A_{-i})$. Thus, by induction we can have:

$$\begin{aligned} F((P, R_x), A_{-i}) = F((P, R_{x^0}), A_{-i}) \geq F((P, R_{x^1}), A_{-i}) \ldots \\ F((P, R_{x^{d-1}}), A_{-i}) \geq F((P, R_{x^d}), A_{-i}) = F((P, R_y), A_{-i}) \end{aligned} \tag{8.16}$$

References

1. C. T. Kulik, S. Ryan, S. Harper, and G. George, "Aging populations and management," 2014. (cited on page 1)

2. F. Xing, G. Peng, T. Liang, and J. Jiang, "Challenges for deploying iot wearable medical devices among the ageing population," in *International Conference on Distributed, Ambient, and Pervasive Interactions*. Springer, 2018, pp. 286–295. (cited on page 1)

3. "internet of things (iot) in healthcare market: growth, trends, and forecast (2020-2025)," 2019. [Online]. Available: https://www.mordorintelligence.com/industry-reports/internet-of-things-in-healthcare-market (cited on page 1)

4. "Internet of things in healthcare market size report, 2019 - 2025," 2018. [Online]. Available: https://www.grandviewresearch.com/industry-analysis/internet-of-things-iot-healthcare-market (cited on pages 1 and 18)

5. PricewaterhouseCoopers, "Top health industry issues of 2020: Will digital start to show an roi?" 2020. [Online]. Available: https://www.pwc.com/us/en/industries/health-industries/top-health-industry-issues.html (cited on page 1)

6. E. Borelli, G. Paolini, F. Antoniazzi, M. Barbiroli, F. Benassi, F. Chesani, L. Chiari, M. Fantini, F. Fuschini, A. Galassi *et al.*, "Habitat: An iot solu-

tion for independent elderly," *Sensors*, vol. 19, no. 5, p. 1258, 2019. (cited on page 1)

7. S. Movassaghi, M. Abolhasan, J. Lipman, D. Smith, and A. Jamalipour, "Wireless body area networks: A survey," *IEEE Communications surveys & tutorials*, vol. 16, no. 3, pp. 1658–1686, 2014. (cited on pages 2, 28, and 116)

8. T.-Y. Wu and C.-H. Lin, "Low-sar path discovery by particle swarm optimization algorithm in wireless body area networks," *IEEE Sensors Journal*, vol. 15, no. 2, pp. 928–936, 2014. (cited on page 2)

9. S. L. Cotton, R. D'Errico, and C. Oestges, "A review of radio channel models for body centric communications," *Radio Science*, vol. 49, no. 6, pp. 371–388, 2014. (cited on page 3)

10. Y. I. Nechayev, P. S. Hall, C. C. Constantinou, Y. Hao, A. Alomainy, R. Dubrovka, and C. G. Parini, "On-body path gain variations with changing body posture and antenna position," in *2005 IEEE Antennas and Propagation Society International Symposium*, vol. 1B, 2005, pp. 731–734 vol. 1B. (cited on page 3)

11. D. Smith, T. Lamahewa, L. Hanlen, and D. Miniutti, "Simple prediction-based power control for the on-body area communications channel," in *2011 IEEE International Conference on Communications (ICC)*. IEEE, 2011, pp. 1–5. (cited on pages 3, 27, 30, 43, 47, 93, 106, 115, 116, and 125)

12. G. E. Box, G. M. Jenkins, G. C. Reinsel, and G. M. Ljung, *Time series analysis: forecasting and control*. John Wiley & Sons, 2015. (cited on pages 3 and 30)

13. A. Tealab, "Time series forecasting using artificial neural networks methodologies: A systematic review," *Future Computing and Informatics Journal*, vol. 3, no. 2, pp. 334–340, 2018. (cited on page 3)

14. Z. Lv, J. Xu, K. Zheng, H. Yin, P. Zhao, and X. Zhou, "Lc-rnn: A deep learning model for traffic speed prediction." in *IJCAI*, 2018, pp. 3470–3476. (cited on page 3)

15. M. Cleary, "Anticipating the Impact of an Aging World." [Online]. Available: https://www.ispor.org/publications/journals/value-outcomes-spotlight/abstract/september-october-2019/anticipating-the-impact-of-an-aging-world (cited on page 11)

16. A. I. of Health and Welfare, "Older Australia at a glance, Demographics of older Australians," 2018. [Online]. Available: https://www.aihw.gov.au/reports/older-people/older-australia-at-a-glance/contents/demographics-of-older-australians (cited on page 11)

17. G. De Micheli, "E-health: From sensors to systems," in *2015 Transducers-2015 18th International Conference on Solid-State Sensors, Actuators and Microsystems (TRANSDUCERS)*. IEEE, 2015, pp. 3–6. (cited on page 11)

18. IEEE Standards Association and others, "802.15.1-2005 - ieee standard for information technology– local and metropolitan area networks– specific requirements– part 15.1a: Wireless medium access control (mac) and physical layer (phy) specifications for wireless personal area networks (wpan)," 2005. (cited on page 12)

19. ——, "802.15.4-2015 - ieee standard for low-rate wireless networks," 2015. [Online]. Available: https://standards.ieee.org/content/

ieee-standards/en/standard/802_15_4-2015.html (cited on page 12)

20. ——, "802.15.6-2012 - ieee standard for local and metropolitan area networks - part 15.6: Wireless body area networks," Feb 2012. [Online]. Available: https://standards.ieee.org/standard/802_15_6-2012.html (cited on pages 12, 18, 35, and 49)

21. T. ETSI, "Smartban," smart body area networks (smartban)," 2015. [Online]. Available: https://www.etsi.org/technologies/smart-body-area-networks (cited on page 14)

22. M. Hämäläinen, T. Paso, L. Mucchi, M. Girod-Genet, J. Farserotu, H. Tanaka, W. H. Chin, and L. N. Ismail, "Etsi tc smartban: Overview of the wireless body area network standard," in *2015 9th international symposium on medical information and communication technology (ISMICT)*. IEEE, 2015, pp. 1–5. (cited on page 15)

23. Y. I. Nechayev, P. S. Hall, C. C. Constantinou, Y. Hao, A. Alomainy, R. Dubrovka, and C. G. Parini, "On-body path gain variations with changing body posture and antenna position," in *2005 IEEE antennas and propagation society international symposium*, vol. 1. IEEE, 2005, pp. 731–734. (cited on page 17)

24. M. D. Pereira, G. A. Alvarez-Botero, and F. R. de Sousa, "Characterization and modeling of the capacitive hbc channel," *IEEE Transactions on Instrumentation and Measurement*, vol. 64, no. 10, pp. 2626–2635, 2015. (cited on page 17)

25. M. R. Yuce, "Implementation of wireless body area networks for healthcare systems," *Sensors and Actuators A: Physical*, vol. 162, no. 1, pp. 116–

129, 2010. (cited on page 17)

26. P. Lamkin, "Smart wearables market to double by 2022: $27 billion industry forecast," *Forbes Magazine*, Oct 2018. (cited on page 18)

27. M. Chen, S. Gonzalez, A. Vasilakos, H. Cao, and V. C. Leung, "Body area networks: A survey," *Mobile networks and applications*, vol. 16, no. 2, pp. 171–193, 2011. (cited on pages 19 and 28)

28. R. Fantacci, "Proposal of an interference cancellation receiver with low complexity for ds/cdma mobile communication systems," *IEEE Transactions on Vehicular Technology*, vol. 48, no. 4, pp. 1039–1046, Jul 1999. (cited on page 20)

29. H. Zhang and H. Dai, *Design fundamentals and interference mitigation for cellular networks*. Nova Science Publishers, 2008. (cited on page 20)

30. X. Wang and L. Cai, "Interference analysis of co-existing wireless body area networks," in *Global Telecommunications Conference (GLOBECOM 2011), 2011 IEEE*. IEEE, 2011, pp. 1–5. (cited on page 20)

31. R. Kazemi, R. Vesilo, E. Dutkiewicz, and G. Fang, "Inter-network interference mitigation in wireless body area networks using power control games," in *2010 10th International Symposium on Communications and Information Technologies*. IEEE, 2010, pp. 81–86. (cited on pages 20, 22, 26, and 34)

32. W.-B. Yang and K. Sayrafian-Pour, "Interference mitigation for body area networks," in *2011 IEEE 22nd International Symposium on Personal, Indoor and Mobile Radio Communications*. IEEE, 2011, pp. 2193–2197. (cited on page 20)

33. S. Movassaghi, M. Abolhasan, and D. Smith, "Smart spectrum allocation for interference mitigation in wireless body area networks," in *2014 IEEE International Conference on Communications (ICC)*. IEEE, jun 2014. [Online]. Available: https://doi.org/10.1109%2Ficc.2014.6884228 (cited on pages 20 and 28)

34. S. Movassaghi, M. Abolhasan, D. Smith, and A. Jamalipour, "Aim: adaptive internetwork interference mitigation amongst co-existing wireless body area networks," in *2014 IEEE Global Communications Conference*. IEEE, 2014, pp. 2460–2465. (cited on page 20)

35. K.-J. Wu, Y.-W. P. Hong, and J.-P. Sheu, "Coloring-based channel allocation for multiple coexisting wireless body area networks: A game-theoretic approach," *IEEE Transactions on Mobile Computing*, 2020. (cited on page 20)

36. J. Dong and D. Smith, "Opportunistic relaying in wireless body area networks: Coexistence performance," in *2013 IEEE International Conference on Communications (ICC)*. IEEE, 2013, pp. 5613–5618. (cited on page 21)

37. ——, "Cooperative body-area-communications: Enhancing coexistence without coordination between networks," in *Personal Indoor and Mobile Radio Communications (PIMRC), 2012 IEEE 23rd International Symposium on*. IEEE, 2012, pp. 2269–2274. (cited on pages 21 and 43)

38. ——, "Joint relay selection and transmit power control for wireless body area networks coexistence," in *2014 IEEE International Conference on Communications (ICC)*. IEEE, 2014, pp. 5676–5681. (cited on pages 21 and 115)

39. L. Wang, C. Goursaud, N. Nikaein, L. Cottatellucci, and J.-M. Gorce, "Cooperative scheduling for coexisting body area networks," *IEEE Transactions on Wireless Communications*, vol. 12, no. 1, pp. 123–133, 2013. (cited on page 21)

40. J. Cui, Y. Sun, J. Wang, and Y. Ji, "Node-position-based joint relay selection and adaptive power control scheme in wireless body area networks," *Wireless Personal Communications*, vol. 96, no. 1, pp. 1519–1535, 2017. (cited on page 21)

41. T. Watteyne, M. Palattella, and L. Grieco, "Using ieee 802.15.4e time-slotted channel hopping (tsch) in the internet of things (iot): Problem statement," *RFC*, vol. 7554, pp. 1–23, 2015. (cited on page 21)

42. C. Boucetta, B. Nour, H. Moungla, and L. Lahlou, "An iot scheduling and interference mitigation scheme in tsch using latin rectangles," in *2019 IEEE Global Communications Conference (GLOBECOM)*. IEEE, 2019, pp. 1–6. (cited on page 21)

43. E. M. George and L. Jacob, "Interference mitigation for coexisting wireless body area networks: Distributed learning solutions," *IEEE Access*, vol. 8, pp. 24 209–24 218, 2020. (cited on page 21)

44. G. Fang, E. Dutkiewicz, K. Yu, R. Vesilo, and Y. Yu, "Distributed internetwork interference coordination for wireless body area networks," in *2010 IEEE Global Telecommunications Conference GLOBECOM 2010*. IEEE, 2010, pp. 1–5. (cited on page 22)

45. J. Zander, "Distributed cochannel interference control in cellular radio systems," *IEEE Transactions on Vehicular Technology*, vol. 41, no. 3, pp.

305–311, 1992. (cited on page 22)

46. ——, "Distributed cochannel interference control in cellular radio systems," *IEEE transactions on vehicular Technology*, vol. 41, no. 3, pp. 305–311, 1992. (cited on page 22)

47. T.-H. Lee and J.-C. Lin, "A fully distributed power control algorithm for cellular mobile systems," *IEEE Journal on Selected Areas in Communications*, vol. 14, no. 4, pp. 692–697, may 1996. (cited on pages 22 and 47)

48. F. Di Franco, C. Tachtatzis, R. C. Atkinson, I. Tinnirello, and I. A. Glover, "Channel estimation and transmit power control in wireless body area networks," *IET Wireless Sensor Systems*, vol. 5, no. 1, pp. 11–19, 2014. (cited on page 22)

49. T. H. Cormen, Ed., *Introduction to algorithms*, 3rd ed. Cambridge, Mass: MIT Press, 2009, oCLC: ocn311310321. (cited on page 24)

50. D. E. Knuth, *The Art of Computer Programming, Volume 4, Fascicle 4: Generating All Trees–History of Combinatorial Generation (Art of Computer Programming)*. Addison-Wesley Professional, 2006. (cited on page 24)

51. M. Quwaider, J. Rao, and S. Biswas, "Body-posture-based dynamic link power control in wearable sensor networks," *IEEE Communications Magazine*, vol. 48, no. 7, pp. 134–142, 2010. (cited on pages 24 and 26)

52. W. Lee, B.-D. Lee, and N. Kim, "Hybrid transmission power control for wireless body sensor systems," *International Journal of Distributed Sensor Networks*, vol. 10, no. 10, p. 259181, 2014. (cited on pages 24 and 25)

53. R. Kazemi, R. Vesilo, E. Dutkiewicz, and R. Liu, "Dynamic power control in wireless body area networks using reinforcement learning with approximation," in *2011 IEEE 22nd International Symposium on Personal, Indoor and Mobile Radio Communications*. IEEE, 2011, pp. 2203–2208. (cited on page 25)

54. D. Smith, D. Miniutti, L. Hanlen, D. Rodda, and B. Gilbert, "Dynamic narrowband body area communications: Link-margin based performance analysis and second-order temporal statistics," in *2010 IEEE Wireless Communication and Networking Conference*. IEEE, 2010, pp. 1–6. (cited on page 25)

55. M. Quwaider, A. Muhammad, J. Choi, and S. Biswas, "Posture-predictive power control in body sensor networks using linear-quadratic gaussian control," in *2009 First International Conference on Networks & Communications*. IEEE, 2009, pp. 52–59. (cited on page 26)

56. W. Zang, S. Zhang, and Y. Li, "An accelerometer-assisted transmission power control solution for energy-efficient communications in wban," *IEEE Journal on Selected Areas in Communications*, vol. 34, no. 12, pp. 3427–3437, 2016. (cited on page 26)

57. M. Vallejo, J. R. Piorno, and J. L. A. Rodrigo, "A link quality estimator for power-efficient communication over on-body channels," in *2014 12th IEEE International Conference on Embedded and Ubiquitous Computing*. IEEE, 2014, pp. 250–257. (cited on page 26)

58. M. Vallejo, J. Recas, P. G. Del Valle, and J. L. Ayala, "Accurate human tissue characterization for energy-efficient wireless on-body communi-

cations," *Sensors*, vol. 13, no. 6, pp. 7546–7569, 2013. (cited on page 26)

59. C. U. Saraydar, N. B. Mandayam, and D. J. Goodman, "Efficient power control via pricing in wireless data networks," *IEEE transactions on Communications*, vol. 50, no. 2, pp. 291–303, 2002. (cited on page 26)

60. T. Alpcan, T. Başar, R. Srikant, and E. Altman, "Cdma uplink power control as a noncooperative game," *Wireless Networks*, vol. 8, no. 6, pp. 659–670, 2002. (cited on page 26)

61. Z. Zhang, H. Wang, C. Wang, and H. Fang, "Interference mitigation for cyber-physical wireless body area network system using social networks," *IEEE transactions on emerging topics in computing*, vol. 1, no. 1, pp. 121–132, 2013. (cited on page 26)

62. L. Zou, B. Liu, C. Chen, and C. W. Chen, "Bayesian game based power control scheme for inter-WBAN interference mitigation," in *2014 IEEE Global Communications Conference*. IEEE, dec 2014. [Online]. Available: https://doi.org/10.1109%2Fglocom.2014.7036814 (cited on page 26)

63. S. K. Suman, D. Kumar, and L. Bhagyalakshmi, "Sinr pricing in non cooperative power control game for wireless ad hoc networks." *TIIS*, vol. 8, no. 7, pp. 2281–2301, 2014. (cited on pages 26 and 47)

64. J. Dong, D. B. Smith, and L. W. Hanlen, "Socially optimal coexistence of wireless body area networks enabled by a non-cooperative game," *ACM Trans. Sen. Netw.*, vol. 12, no. 4, pp. 26:1–26:18, Sep. 2016. [Online]. Available: http://doi.acm.org/10.1145/2932191 (cited on pages xviii, xix, 26, 34, 35, 47, 66, 81, 82, 83, 84, 85, 86, 87, and 88)

65. M. Chiang and J. Bell, "Balancing supply and demand of bandwidth in wireless cellular networks: utility maximization over powers and rates," in *INFOCOM 2004. Twenty-third AnnualJoint Conference of the IEEE Computer and Communications Societies*, vol. 4. IEEE, 2004, pp. 2800–2811. (cited on page 27)

66. G. Tichogiorgos, K. K. Leung, A. Misra, and T. LaPorta, "Distributed network utility optimization in wireless sensor networks using power control," in *2008 IEEE 19th International Symposium on Personal, Indoor and Mobile Radio Communications*. IEEE, 2008, pp. 1–6. (cited on page 27)

67. A. H. Sodhro, Y. Li, and M. A. Shah, "Energy-efficient adaptive transmission power control for wireless body area networks," *IET Communications*, vol. 10, no. 1, pp. 81–90, 2016. (cited on page 27)

68. S. Kim and D.-S. Eom, "Link-state-estimation-based transmission power control in wireless body area networks," *IEEE journal of Biomedical and Health Informatics*, vol. 18, no. 4, pp. 1294–1302, 2013. (cited on page 27)

69. S. Kim, S. Kim, and D.-S. Eom, "Rssi/lqi-based transmission power control for body area networks in healthcare environment," *IEEE journal of biomedical and health informatics*, vol. 17, no. 3, pp. 561–571, 2013. (cited on page 27)

70. N. Bradai, L. C. Fourati, and L. Kamoun, "Investigation and performance analysis of mac protocols for wban networks," *Journal of Network and Computer Applications*, vol. 46, pp. 362–373, 2014. (cited on page 28)

71. S. H. Cheng and C. Y. Huang, "Coloring-based inter-WBAN scheduling

for mobile wireless body area networks," *IEEE Transactions on Parallel and Distributed Systems*, vol. 24, no. 2, pp. 250–259, feb 2013. [Online]. Available: https://doi.org/10.1109%2Ftpds.2012.133 (cited on page 28)

72. S. Movassaghi, M. Abolhasan, and D. Smith, "Cooperative scheduling with graph coloring for interference mitigation in wireless body area networks," in *2014 IEEE Wireless Communications and Networking Conference (WCNC)*. IEEE, apr 2014. [Online]. Available: https://doi.org/10.1109%2Fwcnc.2014.6952484 (cited on pages 28 and 34)

73. S. Cheng, C. Huang, and C. C. Tu, "Racoon: A multiuser qos design for mobile wireless body area networks," *Journal of Medical Systems*, vol. 35, no. 5, pp. 1277–1287, Oct 2011. [Online]. Available: https://doi.org/10.1007/s10916-011-9676-3 (cited on page 28)

74. P. R. Grassi, V. Rana, I. Beretta, and D. Sciuto, "B^2irs: A technique to reduce ban-ban interferences in wireless sensor networks," in *2012 Ninth International Conference on Wearable and Implantable Body Sensor Networks*. IEEE, may 2012. [Online]. Available: https://doi.org/10.1109%2Fbsn.2012.30 (cited on pages 28 and 79)

75. W. Huang and T. Q. S. Quek, "Adaptive csma/ca mac protocol to reduce inter-wban interference for wireless body area networks," in *2015 IEEE 12th International Conference on Wearable and Implantable Body Sensor Networks (BSN)*, June 2015, pp. 1–6. (cited on page 28)

76. A. Jamthe, A. Mishra, and D. P. Agrawal, "Scheduling schemes for interference suppression in healthcare sensor networks," in *2014 IEEE International Conference on Communications (ICC)*, June 2014, pp. 391–396.

(cited on page 28)

77. ——, "Scheduling schemes for interference suppression in healthcare sensor networks," in *2014 IEEE International Conference on Communications (ICC)*. IEEE, jun 2014. [Online]. Available: https://doi.org/10.1109%2Ficc.2014.6883350 (cited on page 28)

78. J. Polastre, J. Hill, and D. Culler, "Versatile low power media access for wireless sensor networks," in *Proceedings of the 2nd international conference on Embedded networked sensor systems*. ACM Press, 2004. [Online]. Available: https://doi.org/10.1145%2F1031495.1031508 (cited on page 28)

79. S. J. Marinkovic, E. M. Popovici, C. Spagnol, S. Faul, and W. P. Marnane, "Energy-efficient low duty cycle mac protocol for wireless body area networks," *IEEE Transactions on Information Technology in Biomedicine*, vol. 13, no. 6, pp. 915–925, 2009. (cited on page 28)

80. I. Anjum, N. Alam, M. A. Razzaque, M. Mehedi Hassan, and A. Alamri, "Traffic priority and load adaptive mac protocol for qos provisioning in body sensor networks," *International Journal of Distributed Sensor Networks*, vol. 9, no. 3, p. 205192, 2013. (cited on page 28)

81. B. J. van der Zwaag, N. Meratnia, P. J. Havinga *et al.*, "Evaluation of mac protocols with wake-up radio for implantable body sensor networks," *Procedia computer science*, vol. 40, pp. 173–180, 2014. (cited on page 29)

82. D. A. Hammood, H. A. Rahim, R. B. Ahmad, A. Alkhayyat, M. E. M. Salleh, M. Abdulmalek, M. Jusoh, and Q. H. Abbasi, "Enhancement of

the duty cycle cooperative medium access control for wireless body area networks," *IEEE Access*, vol. 7, pp. 3348–3359, 2018. (cited on page 29)

83. M. Musku, A. Chronopoulos, D. Popescu, and A. Stefanescu, "A game-theoretic approach to joint rate and power control for uplink CDMA communications," *IEEE Transactions on Communications*, vol. 58, no. 3, pp. 923–932, mar 2010. [Online]. Available: https://doi.org/10.1109%2Ftcomm.2010.03.070205 (cited on page 29)

84. M. Hayajneh and C. Abdallah, "Distributed joint rate and power control game-theoretic algorithms for wireless data," *IEEE Communications Letters*, vol. 8, no. 8, pp. 511–513, aug 2004. [Online]. Available: https://doi.org/10.1109%2Flcomm.2004.833817 (cited on page 29)

85. S. Ginde, A. MacKenzie, R. Buehrer, and R. Komali, "A game-theoretic analysis of link adaptation in cellular radio networks," *IEEE Transactions on Vehicular Technology*, vol. 57, no. 5, pp. 3108–3120, sep 2008. [Online]. Available: https://doi.org/10.1109%2Ftvt.2008.917225 (cited on page 29)

86. Y. Han, Q. Chen, and Y. Li, "A game-theoretic approach to power control in ad hoc network," in *2012 International Conference on Computer Distributed Control and Intelligent Environmental Monitoring*, March 2012, pp. 21–24. (cited on page 29)

87. A. Babaei and B. Jabbari, "Transmission probability control game for coexisting random ALOHA wireless networks in unlicensed bands," in *2010 IEEE 71st Vehicular Technology Conference*. IEEE, 2010. [Online]. Available: https://doi.org/10.1109%2Fvetecs.2010.5493687 (cited on

page 29)

88. S. Hu, H. Hallen, and A. Duel-Hallen, "Physical channel modeling, adaptive prediction and transmitter diversity for flat fading mobile channel," in *Signal Processing Advances in Wireless Communications, 1999. SPAWC'99. 1999 2nd IEEE Workshop on*. IEEE, 1999, pp. 387–390. (cited on pages 30 and 94)

89. D. Smith, L. Hanlen, and D. Miniutti, "Transmit power control for wireless body area networks using novel channel prediction," in *Wireless Communications and Networking Conference (WCNC), 2012 IEEE*. IEEE, 2012, pp. 684–688. (cited on pages 30, 94, 104, and 116)

90. V. Chaganti, L. Hanlen, and D. Smith, "Are narrowband wireless on-body networks wide-sense stationary?" *IEEE Transactions on Wireless Communications*, vol. 13, no. 5, pp. 2432–2442, 2014. (cited on page 30)

91. I. Gheyas and L. Smith, "A novel neural network ensemble architecture for time series forecasting," *Neurocomputing*, vol. 74, no. 18, pp. 3855–3864, 2011. (cited on page 30)

92. Y.-h. Chen and F.-J. Chang, "Evolutionary artificial neural networks for hydrological systems forecasting," *Journal of Hydrology*, vol. 367, no. 1-2, pp. 125–137, 2009. (cited on page 30)

93. M. Paliwal and U. A. Kumar, "Neural networks and statistical techniques: A review of applications," *Expert systems with applications*, vol. 36, no. 1, pp. 2–17, 2009. (cited on page 30)

94. H. S. Hippert, C. E. Pedreira, and R. C. Souza, "Neural networks for

short-term load forecasting: A review and evaluation," *IEEE Transactions on power systems*, vol. 16, no. 1, pp. 44–55, 2001. (cited on page 30)

95. X. Sun, G. Gui, Y. Li, R. P. Liu, and Y. An, "Resinnet: A novel deep neural network with feature reuse for internet of things," *IEEE Internet of Things Journal*, vol. 6, no. 1, pp. 679–691, 2019. (cited on page 30)

96. S. Hochreiter and J. Schmidhuber, "Long short-term memory," *Neural computation*, vol. 9, no. 8, pp. 1735–1780, 1997. (cited on pages 30 and 95)

97. H. Sak, A. Senior, and F. Beaufays, "Long short-term memory recurrent neural network architectures for large scale acoustic modeling," in *Fifteenth annual conference of the international speech communication association*, 2014. (cited on pages 30, 95, and 113)

98. A. Graves, A.-r. Mohamed, and G. Hinton, "Speech recognition with deep recurrent neural networks," in *2013 IEEE international conference on acoustics, speech and signal processing*. IEEE, 2013, pp. 6645–6649. (cited on page 30)

99. D. Amodei, S. Ananthanarayanan, R. Anubhai, J. Bai, E. Battenberg, C. Case, J. Casper, B. Catanzaro, Q. Cheng, G. Chen *et al.*, "Deep speech 2: End-to-end speech recognition in english and mandarin," in *International conference on machine learning*, 2016, pp. 173–182. (cited on page 30)

100. H. Palangi, L. Deng, Y. Shen, J. Gao, X. He, J. Chen, X. Song, and R. Ward, "Deep sentence embedding using long short-term memory networks: Analysis and application to information retrieval," *IEEE/ACM Transactions on Audio, Speech, and Language Processing*, vol. 24, no. 4, pp. 694–707,

2016. (cited on page 30)

101. K. S. Kwak, S. Ullah, and N. Ullah, "An overview of ieee 802.15. 6 standard," in *2010 3rd International Symposium on Applied Sciences in Biomedical and Communication Technologies (ISABEL 2010)*. IEEE, 2010, pp. 1–6. (cited on page 33)

102. A. Zhang, D. B. Smith, D. Miniutti, L. W. Hanlen, D. Rodda, and B. Gilbert, "Performance of piconet co-existence schemes in wireless body area networks," in *Wireless Communications and Networking Conference (WCNC), 2010 IEEE*. IEEE, 2010, pp. 1–6. [Online]. Available: https://doi.org/10.1109%2Fwcnc.2010.5506746 (cited on pages 34 and 47)

103. J. B. Rosen, "Existence and uniqueness of equilibrium points for concave n-person games," *Econometrica*, vol. 33, no. 3, pp. 520–534, 1965. [Online]. Available: http://www.jstor.org/stable/1911749 (cited on pages 37 and 147)

104. C. U. Saraydar, N. B. Mandayam, and D. J. Goodman, "Efficient power control via pricing in wireless data networks," *IEEE Transactions on Communications*, vol. 50, no. 2, pp. 291–303, Feb 2002. (cited on page 39)

105. M. Slater, "Lagrange multipliers revisited," in *Traces and emergence of nonlinear programming*. Springer, 2014, pp. 293–306. (cited on page 45)

106. D. Davenport, N. Seidl, J. Moss, M. Patel, A. Batra, J. Ho, S. Hosur, J. Roh, T. Schmidl, O. Omeni *et al.*, "Medwin physical layer proposal documentation," *IEEE Document P*, vol. 802, pp. 15–09, 2009. (cited on pages 50, 79, 84, and 109)

107. G. Bianchi, "Performance analysis of the ieee 802.11 distributed coordination function," *IEEE Journal on Selected Areas in Communications*, vol. 18, no. 3, pp. 535–547, March 2000. (cited on page 58)

108. Y. Yang and D. Smith, "Wireless body area networks: Energy-efficient, provably socially-efficient, transmit power control," in *IEEE International Conference on Communications*. IEEE, may 2017, pp. 1–6. [Online]. Available: http://ieeexplore.ieee.org/document/7997347/ (cited on pages 66 and 81)

109. D. Smith, M. Portmann, W. L. Tan, and W. Tushar, "Multi-source–destination distributed wireless networks: Pareto-efficient dynamic power control game with rapid convergence," *Vehicular Technology, IEEE Transactions on*, vol. 63, no. 6, pp. 2744–2754, 2014. (cited on page 67)

110. D. Monderer and L. S. Shapley, "Potential games," *Games and Economic Behavior*, vol. 14, no. 1, pp. 124 – 143, 1996. [Online]. Available: http://www.sciencedirect.com/science/article/pii/S0899825696900445 (cited on page 72)

111. Q. D. Lã, Y. H. Chew, and B.-H. Soong, "Potential games," in *Potential Game Theory*. Springer International Publishing, 2016, pp. 23–69. [Online]. Available: https://doi.org/10.1007%2F978-3-319-30869-2_2 (cited on page 73)

112. M. Voorneveld, "Best-response potential games," *Economics Letters*, vol. 66, no. 3, pp. 289 – 295, 2000. [Online]. Available: http://www.sciencedirect.com/science/article/pii/S0165176599001962 (cited on page 73)

113. T. Ui, "Discrete Concavity for Potential Games," *International Game Theory Review*, vol. 10, no. 01, pp. 137–143, mar 2008. [Online]. Available: https://doi.org/10.1142%2Fs0219198908001820 (cited on page 74)

114. M. Ghazvini, N. Movahhedinia, and K. Jamshidi, "GCW: A game theoretic contention window adjustment approach for IEEE 802.11 WLANs," *Wireless Personal Communications*, vol. 83, no. 2, pp. 1101–1130, mar 2015. [Online]. Available: https://doi.org/10.1007%2Fs11277-015-2441-z (cited on page 76)

115. Z. Han, Ed., *Game theory in wireless and communication networks: theory, models, and applications*. Cambridge, UK ; New York: Cambridge University Press, 2012, oCLC: ocn699759838. (cited on page 78)

116. F. Xia, J. Li, R. Hao, X. Kong, and R. Gao, "Service differentiated and adaptive CSMA/CA over IEEE 802.15.4 for cyber-physical systems," *The Scientific World Journal*, vol. 2013, pp. 1–12, 2013. [Online]. Available: https://doi.org/10.1155%2F2013%2F947808 (cited on page 79)

117. A. Astrin *et al.*, "Ieee standard for local and metropolitan area networks part 15.6: Wireless body area networks: Ieee std 802.15. 6-2012," *The document is available at IEEE Xplore*, 2012. (cited on pages 79 and 80)

118. D. Smith, L. Hanlen, D. Rodda, B. Gilbert, J. Dong, and V. Chaganti, "Body area network radio channel measurement set," 2016. [Online]. Available: https://data.csiro.au/collections/#collection/CIcsiro:18350v1 (cited on pages 80 and 126)

119. J. Dong and D. Smith, "Coexistence and interference mitigation for wireless body area networks: Improvements using on-body opportunistic

relaying," *arXiv preprint arXiv:1305.6992*, 2013. (cited on page 80)

120. A. Svensson, "An introduction to adaptive qam modulation schemes for known and predicted channels," *Proceedings of the IEEE*, vol. 95, no. 12, pp. 2322–2336, 2007. (cited on page 93)

121. L. Dong, G. Xu, and H. Ling, "Prediction of fast fading mobile radio channels in wideband communication systems," in *GLOBECOM'01. IEEE Global Telecommunications Conference (Cat. No. 01CH37270)*, vol. 6. IEEE, 2001, pp. 3287–3291. (cited on page 94)

122. M. Chen and M. Viberg, "Long-range channel prediction based on non-stationary parametric modeling," *IEEE Transactions on Signal Processing*, vol. 57, no. 2, pp. 622–634, 2009. (cited on page 94)

123. H. Ye, G. Y. Li, and B.-H. Juang, "Power of deep learning for channel estimation and signal detection in ofdm systems," *IEEE Wireless Communications Letters*, vol. 7, no. 1, pp. 114–117, 2017. (cited on page 94)

124. R. Jozefowicz, W. Zaremba, and I. Sutskever, "An empirical exploration of recurrent network architectures," in *International Conference on Machine Learning*, 2015, pp. 2342–2350. (cited on page 94)

125. I. Sutskever, O. Vinyals, and Q. V. Le, "Sequence to sequence learning with neural networks," in *Advances in neural information processing systems*, 2014, pp. 3104–3112. (cited on pages 94 and 145)

126. S. Hochreiter, Y. Bengio, P. Frasconi, J. Schmidhuber *et al.*, "Gradient flow in recurrent nets: the difficulty of learning long-term dependencies," 2001. (cited on page 95)

127. S. Ioffe and C. Szegedy, "Batch normalization: Accelerating deep network training by reducing internal covariate shift," in *ICML*, 2015. (cited on page 98)

128. A. C. Wilson, R. Roelofs, M. Stern, N. Srebro, and B. Recht, "The marginal value of adaptive gradient methods in machine learning," in *Advances in Neural Information Processing Systems*, 2017, pp. 4148–4158. (cited on page 101)

129. D. P. Kingma and J. Ba, "Adam: A method for stochastic optimization," *CoRR*, vol. abs/1412.6980, 2015. (cited on page 101)

130. X. Glorot and Y. Bengio, "Understanding the difficulty of training deep feedforward neural networks," in *AISTATS*, 2010. (cited on page 102)

131. A. Aguiar and A. Wolisz, "Channel prediction heuristics for adaptive modulation in WLAN," in *Vehicular Technology Conference, 2007. VTC2007-Spring. IEEE 65th*. IEEE, 2007, pp. 1091–1095. (cited on pages xxi, 105, and 117)

132. T. Eyceoz, S. Hu, A. Duee-Hallen, and H. Hallen, "Adaptive prediction, tracking and power adjustment for frequency non-selective fast fading channels," in *Communication Theory Mini-Conference, 1999*. IEEE, 1999, pp. 1–5. (cited on pages xxi, 105, and 117)

133. A. Boulis, D. Smith, D. Miniutti, L. Libman, and Y. Tselishchev, "Challenges in body area networks for healthcare: The MAC," *IEEE Communications Magazine*, vol. 50, no. 5, 2012. (cited on page 105)

134. B. Yu, H. Yin, and Z. Zhu, "Spatio-temporal graph convolutional networks: a deep learning framework for traffic forecasting," in *Proceedings*

of the 27th International Joint Conference on Artificial Intelligence, 2018, pp. 3634–3640. (cited on page 112)

135. S.-Y. Shih, F.-K. Sun, and H.-y. Lee, "Temporal pattern attention for multivariate time series forecasting," *Machine Learning*, vol. 108, no. 8-9, pp. 1421–1441, 2019. (cited on page 112)

136. G. Lai, W.-C. Chang, Y. Yang, and H. Liu, "Modeling long-and short-term temporal patterns with deep neural networks," in *The 41st International ACM SIGIR Conference on Research & Development in Information Retrieval*, 2018, pp. 95–104. (cited on page 112)

137. A. Vaswani, N. Shazeer, N. Parmar, J. Uszkoreit, L. Jones, A. N. Gomez, Ł. Kaiser, and I. Polosukhin, "Attention is all you need," in *Advances in neural information processing systems*, 2017, pp. 5998–6008. (cited on page 113)

138. K. He and J. Sun, "Convolutional neural networks at constrained time cost," in *Proceedings of the IEEE conference on computer vision and pattern recognition*, 2015, pp. 5353–5360. (cited on page 113)

139. K. Cho, B. Van Merriënboer, C. Gulcehre, D. Bahdanau, F. Bougares, H. Schwenk, and Y. Bengio, "Learning phrase representations using rnn encoder-decoder for statistical machine translation," *arXiv preprint arXiv:1406.1078*, 2014. (cited on page 114)

140. S. D. Van, S. Cotton, and D. Smith, "Channel deviation-based power control in body area networks," *IEEE journal of biomedical and health informatics*, vol. 22, no. 3, pp. 785–798, 2017. (cited on pages xxi, 115, and 117)

141. Y. Yang and D. Smith, "Robust wireless body area networks coexistence: A game theoretic approach to time-division mac," *arXiv preprint arXiv:1808.10094*, 2018. (cited on page 116)

142. S. Shimly, D. Smith, and S. Movassaghi, "Wide-sense-stationarity of everyday wireless channels for body-to-body networks," in *2018 IEEE International Conference on Communications (ICC)*. IEEE, 2018, pp. 1–6. (cited on pages 125 and 126)

143. R. S. Nickerson, "Null hypothesis significance testing: a review of an old and continuing controversy." *Psychological methods*, vol. 5, no. 2, p. 241, 2000. (cited on page 125)

144. D. Smith, D. Miniutti, T. Lamahewa, and L. Hanlen, "Propagation models for body-area networks: A survey and new outlook," *IEEE Antennas and Propagation Magazine*, vol. 55, no. 5, pp. 97–117, 2013. (cited on page 125)

145. V. Chaganti, L. Hanlen, and D. Smith, "Are narrowband wireless on-body networks wide-sense stationary?" *IEEE Transactions on Wireless Communications*, vol. 13, no. 5, pp. 2432–2442, 2014. (cited on pages 126 and 129)

146. L. M. Lix, J. C. Keselman, and H. Keselman, "Consequences of assumption violations revisited: A quantitative review of alternatives to the one-way analysis of variance f test," *Review of educational research*, vol. 66, no. 4, pp. 579–619, 1996. (cited on page 129)

147. B. Neyshabur, S. Bhojanapalli, D. McAllester, and N. Srebro, "Exploring generalization in deep learning," in *Advances in neural information*

processing systems, 2017, pp. 5947–5956. (cited on page 130)

148. D. W. Marquardt, "An algorithm for least-squares estimation of nonlinear parameters," *Journal of the society for Industrial and Applied Mathematics*, vol. 11, no. 2, pp. 431–441, 1963. (cited on page 133)

149. T. N. Kipf and M. Welling, "Semi-supervised classification with graph convolutional networks," *arXiv preprint arXiv:1609.02907*, 2016. (cited on page 145)